FLOATING BREAKWATERS
Literature Review

by

E.C. Bouwmeester

and

H.M. van der Breggen

Delft University of Technology
Department of Civil Engineering
Hydraulic Engineering Group
March 1984

TABLE OF CONTENTS

LIST OF TABLES

LIST OF FIGURES

LIST OF SYMBOLS

ROMAN LETTERS

	DEFINITION	DIMENSION	UNIT
A	: amplitude	L	m
B	: beam	L	m
b_a	: internal damping	TL^{-1}	s/m
b_r	: radiation damping	TL^{-1}	s/m
C_D	: drag coefficient	-	-
C	: hydrodynamic mass coefficient	-	-
C_t	: transmission coefficient	-	-
C_r	: reflection coefficient	-	-
c	: wave speed	LT^{-1}	m/s
c_g	: wave group velocity	LT^{-1}	m/s
D	: draft	L	m
d	: water depth	L	m
E	: modulus of elasticity	$ML^{-1}T^{-2}$	N/mm^2
E	: energy (per unit surface area)	MT^{-2}	N/m
E	: energy of the waves		
E_D	: dissipated energy (per unit surface area)	MT^{-2}	N/m
E_R	: reflected energy (per unit surface area)	MT^{-2}	N/m
F	: force (per unit length)	MT^{-2}	N/m
F_D	: drag force		
F_i	: inertia force		
G	: center to center distance from pipes	L	m
H	: wave height	L	m
H_i	: incident wave height	L	m
H_t	: transmitted wave height	L	m
H_r	: reflected wave height	L	m
h	: freeboard	L	m
h	: the rise of the still water level	L	m
I	: mass moment of inertia per unit length	ML	Ns^2
K	: mooring force constant	-	-
k	: wave number	L^{-1}	1/m
	spring constant	MT^{-2}	N/m
l	: structure length	L	m
L	: wave length	L	m
M	: mass	M	kg
	momentum per unit length	MLT^{-2}	N
M_a	: added mass	M	kg
m	: mass (per unit length)	ML^{-1}	kg/m
m	: mass (per unit surface area)	ML^{-2}	kg/m^2
m_a	: added mass (per unit surface area)	ML^{-2}	kg/m^2
N	: tension force of cable (per unit length)	MT^{-2}	N/m
	the number of tires in volume ByO	-	-
n	: defines the sort of motion, n=0 heave	-	-
	bending stiffness (per unit width)	ML^2T^{-2}	Nm
	the number of tires contained in a segment Δx ; $n=N(\Delta x/B)$	-	-
P	: power	ML^2T^{-3}	W
	porosity coefficient	-	-
P_i	: incident power	ML^3T^{-3}	W
P_t	: transmitted power	ML^3T^{-3}	W

P_r	: reflected power	ML^3T^{-3}	W
p	: pressure	$ML^{-1}T^{-2}$	N/m^2
p^+	: dynamic pressure	$ML^{-1}T^{-2}$	N/m^2
Q	: cost factor	-	-
R	: offset length	L	m
S	: total area of the raft	L^2	m^2
s	: elevation above the bottom	L	m
T	: wave period	T	s
T_n	: natural wave period	T	s
$\vec{u}$	: velocity of a water particle	LT^{-1}	m/s
u	: velocity of a water particle in x-dir.	LT^{-1}	m/s
v	: velocity of a water particle in y-dir.	LT^{-1}	m/s
w	: velocity of a water particle in z-dir.	LT^{-1}	m/s
W	: absorption width	L	m
W^{max}	: maximum absorption width	L	m
x	: horizontal coordinate direction	L	m
y	: horizontal coordinate direction	L	m
z	: vertical coordinate direction (+ up)	L	m
Z	: bottom displacement of the raft measured from its equilibrium position (+ up)	L	m

GREEK LETTERS

β	: fraction of energy that can be used	-	-
γ_w	: unit weight of water	$ML^{-2}T^{-2}$	kg/m^3
γ_b	: unit weight of the breakwater	$ML^{-2}T^{-2}$	kg/m^3
γ_s	: unit weight of the submerged breakwater	$ML^{-2}T^{-2}$	kg/m^3
ξ	: the horizontal displacement of the breakwater from equilibrium position	L	m
θ	: polar coordinate	-	rad
	angle	-	rad
ρ	: density of water	ML^{-3}	kg/m^3
η	: water displacement from z=0 (+ up)	L	m
ϕ	: velocity potential	L^2T^{-1}	m^2/s
ν	: kinematic viscosity	L^2T^{-1}	m^2/s
ω	: circular frequency	T^{-1}	rad/s

Chapter I

INTRODUCTION

Floating breakwaters used for the protection of marine facilities were proposed in the early part of this century. However, no extensive exploitation of the concept was attempted until the second world war, when a floating breakwater was constructed for use in the Normandy invasion. Unfortunately this breakwater was completely destroyed in a severe storm shortly before the invasion. This unfortunate experience with floating breakwaters has not been benefical to its reputation. For decades there was very little incentive for developing floating breakwaters. In the early seventies, floating breakwaters were again in the scope of engineers. The major stimulus for this development has been the increasing demand for pleasure boat marina facilities. In some parts of the U.S.A. most sites suitable for harbor development are already used. The remaining sites available for potential harbor development are generally in areas where the water depth is too high for traditional techniques of marine construction.

Costs are very important in the construction of a breakwater. The cost of a rubble mound breakwater rises rapidly with increasing water depth, whereas the cost of a floating breakwater is relatively insensitive to water depth and bottom conditions. But construction cost is not the only criterium to be taken in consideration. The expected life-time of the structure and the yearly maintenace costs are equally important.

Advantages of floating breakwaters without doubt are:

1. Transportability.
2. Little or no interference with marine ecosystems.
3. Costs are relatively insensitive to water depth and bottom conditions.

On the other hand floating breakwaters are highly tuned to both frequency and direction. Also their extreme event survival has to be taken in consideration. Users must be aware that when applying a floating breakwater, there is always some energy transmitted past the structure. Acceptance and tolerance of the level of the transmitted wave depends on the purpose of the floating breakwater.

So far, only the application for marina facilities is mentioned. Let us now direct our attention to possible applications in open sea conditions. Offshore activities and interest are increasing since the early seventies. Important are the construction of oil platforms, pipe-laying activities and the proposed construction of power plants off-

shore. All these activities could benefit from a temporary protection during construction or operation.

The purpose of this report is to find out which floating breakwaters can be utilized in open sea conditions and what can be expected of them. Since every breakwater interferes with the energy of the waves, it is logical that a probable power generation function of floating breakwaters is also investigated.

This report is a global review of the literature about floating breakwaters and energy devices. It is not complete, but the most important types are investigated systematically. In this review the following points are taken in consideration:

1. Description of the breakwater.
2. Wave attenuation performance.
3. Mooring characteristics.
4. Transportability.
5. Power generation.
6. Costs.

The chapters dealing with floating breakwaters will subsequently deal with these points. Finally, conclusions are drawn. As stated by all authors, floating breakwaters have the advantage of being flexible unlike other breakwater types. However, transporting these uncommon structures will impose a great deal of problems on the operators. Because of the complexity of the transport problem, the reader will find in the sections 'transportability' only a superficial look at the transport facilities. This information is not taken from the papers, because information is lacking on this point.

Wave energy utilization has interested inventors for years. A scientific approach of the problem was only initiated as a result of the oil crises of 1973. Therefore it is not surprising that only a limited number of publications from only a few authors are available. The information contained in these papers is often incomplete. Also contradictionary information, especially on the resource potential of wave energy, is presented. Whenever this occured, it is explicitly mentioned. When reading about wave energy one must keep in mind that wave energy is a newly discovered field of scientific research, and a lot of what has been reported is still preliminary.

Chapter II

THEORETICAL BACKGROUND OF FLOATING BREAKWATERS

2.1 SUMMARY OF LINEAR WAVE THEORY

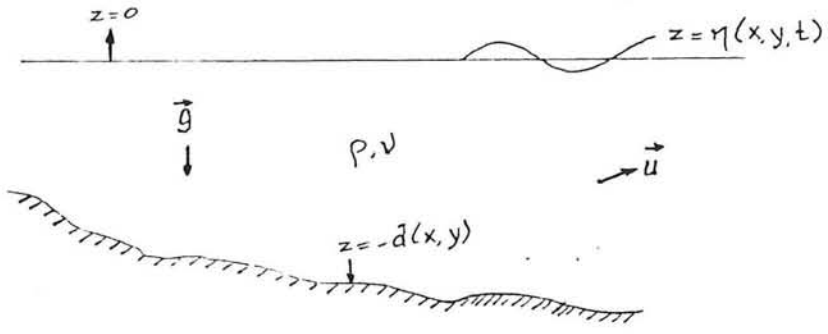

Figure 1: Definition sketch.

For convenience a summary of linear wave theory is presented in this section. In the remainder of this chapter the reader will be refered to these equations when theoretical problems are discussed.

Notation.

space coordinates		: x,y,z
	x,y	: horizontal coordinates.
	z	: vertical coordinate measured from the still water surface (+ up).
time		: t
	(x,y,t)	: height of the water surface above z = 0.
	$\vec{u}$=(u,v,w)	: water particle velocities.
	p	: pressure
	ρ	: density of water.
	ν	: kinematic viscosity.
	g	: acceleration of gravity.
	ϕ	: velocity potential.

2.1.1 Short wave theory

Generally, a short wave theory problem can be defined using the Laplace equation and appropriate initial and boundary conditions.

In the space filled with water the Laplace equation has to be satisfied:

$$\nabla^2 = 0 \qquad (2.1)$$

Kinematic boundary condition: $w = \eta_t + u\eta_x + v\eta_y$ (2.2)

Dynamic boundary condition : $\phi_t + p/\rho + \frac{1}{2} v^2 \Big]_{z=\eta} + g\eta = c$ (2.3)

See figure 2.

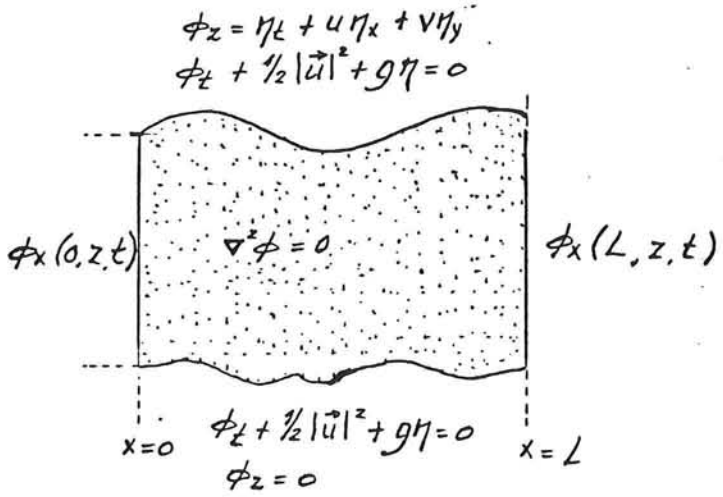

Figure 2: General short wave problem.

Usually these equations are presented in a simplified form. The simplifying assumptions can be summerized as:

1. Rigid bottom : $\phi_n = 0$ at $z = -d(x,y)$. (2.4)

2. Free surface : $p = 0$ at $z = \eta(x,y,t)$. (2.5)

Linearization of the free surface conditions leads to:

$w\big]_{z=0} = \eta_t$ (kinematic boundary condition) (2.6)

$\phi_t + g\eta = 0$ (dynamic boundary condition) (2.7)

(2.6) + (2.7) gives:

$\phi_t + g\phi_z = 0$ for $z=0$. (2.8)

Substitution of a sinusoidal wave in (2.8) leads to the well known short wave equations.

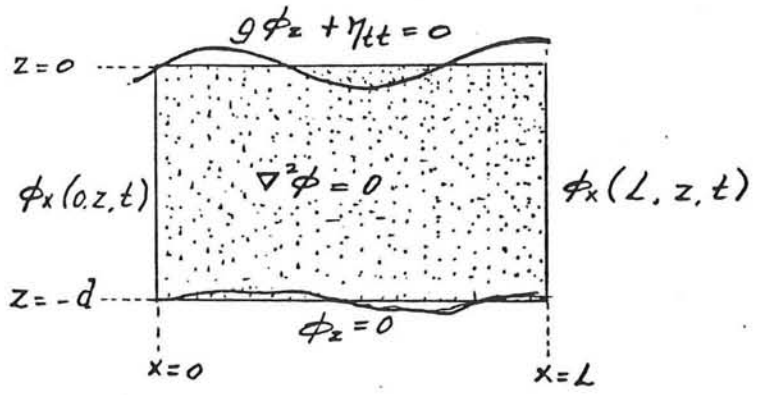

Figure 3: Linearized short wave problem.

2.2 INTRODUCTION TO WAVE ATTENUATION

Wave attenuation can be achieved by:

a. reflection
b. interference
c. dissipation (turbulence, friction)
d. absorption (non-elastic deformation of the structure)

In general a good reflector has to stay relatively motionless. Such a breakwater must be able to withstand large wave forces and the associated mooring forces.

Wave attenuation through interference is most effective in monochromatic waves, and is usually not efficient in field conditions.

The following parameters are used to describe the damping characteristics:

P_i , H_i : power, respectively the height of the incident wave.
P_t , H_t : power, respectively the height of the transmitted wave.
P_r , H_r : power, respectively the height of the reflected wave.
C_t : transmission coefficient= $\sqrt{P_t/P_i}$ (= H_t/H_i for monochromatic waves).
C_r : reflection coefficient= $\sqrt{P_r/P_i}$
L : wave length.
d : water depth.
B : beam of the structure (in the direction of the wave propagation).
D : draft of the structure.

For no energy loss the wave attenuation process of the breakwater is governed by:

$$\tfrac{1}{8}\rho g H_i^2 = \tfrac{1}{8}\rho g H_t^2 + \tfrac{1}{8}\rho g H_r^2 \qquad (2.9)$$

$$H_i^2 = H_t^2 + H_r^2 \qquad (2.10)$$

$$1 = C_t^2 + C_r^2 \qquad (2.11)$$

2.3 BASIC BREAKWATER GROUPS

It is possible to divide flcating breakwaters into two major groups:

1. Rigid floating breakwaters.
   All the parts of the structure remain in the same position to each other. So the relative motion of one part to another part of the structure is zero.

2. Flexible floating breakwaters.
   The position of one part tc another part of the structure may vary (each wave period). So relative motions are possible.

This division is made because the features of these breakwater groups and their theoretical analysis are different.

Rigid breakwaters can achieve wave attenuation mainly through reflection (except the pcint absorber). Flexible breakwaters attenuate waves mainly through dissipation or absorption.

The theoretical analysis of a rigid body is less complicated than that of a flexible body, since the latter involves more unknown parameters: the position of each part of the structure and the forces between the parts, both as a function of time, and the interaction between water and breakwater is more complicated.

In this report, the rigid breakwaters are discussed first, after that the flexible breakwaters are discussed.

One can find the discussions of energy devices among those of the floating breakwaters, because they are in fact wave attenuatcrs which in addition generate power. If no energy is needed, one can change this type in merely a breakwater, so that the construction ccsts will decrease.

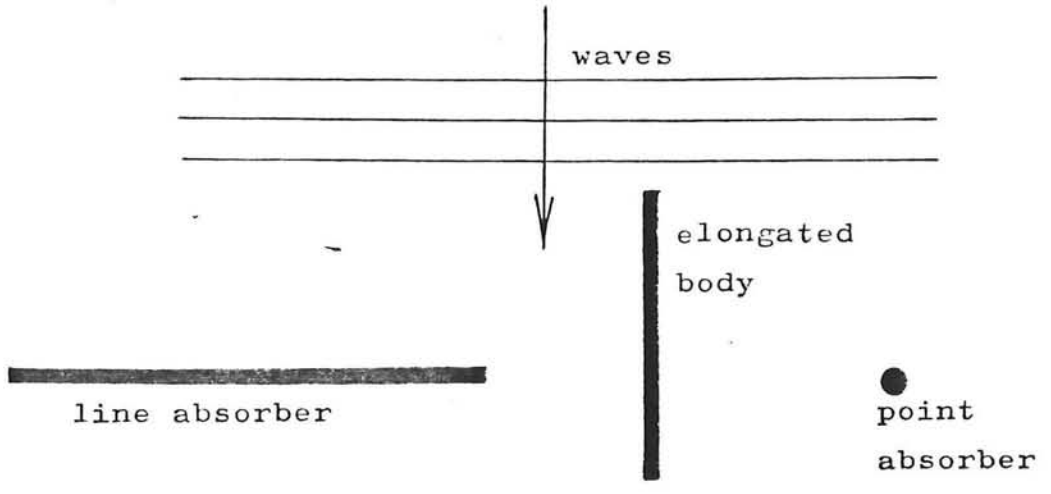

Figure 4: Definition plan sketch, line absorbers, elongated bodies and point absorbers.

All the energy devices are based on absorption of wave energy. Three major groups can be distinguished:

1. Line absorbers
   Line absorbers have the largest size in the direction perpendicular to the wave propagation. Their design concept is: a wave camb represents a certain power per meter, so the broader the structure, the more power can be extracted. The beam of the structure (length in the direction of the wave propagation) is relatively small.

2. Elongated bodies
   An elongated body has the largest size in the direction of the wave propagation. Mooring forces compared to that of the Line absorbers are much smaller for the same energy extraction. The energy extraction rate is reasonably high because of diffraction.

3. Point absorbers
   Point absorbers are converters consisting of a long vertical pipe in which a water column resonates. Tests indicated a satisfactory extraction rate. They are already in use as navigational buoys in Japan. But it's also possible (and proposed) to couple four absorbers together for larger scale applications (several kilowatts).

From each of these groups, one type will be discussed: Salter's duck, Cockerell raft and the WATG (wave activated turbine generator) respectively.

2.4 DIMENSIONAL CONSIDERATIONS FOR RIGID STRUCTURES

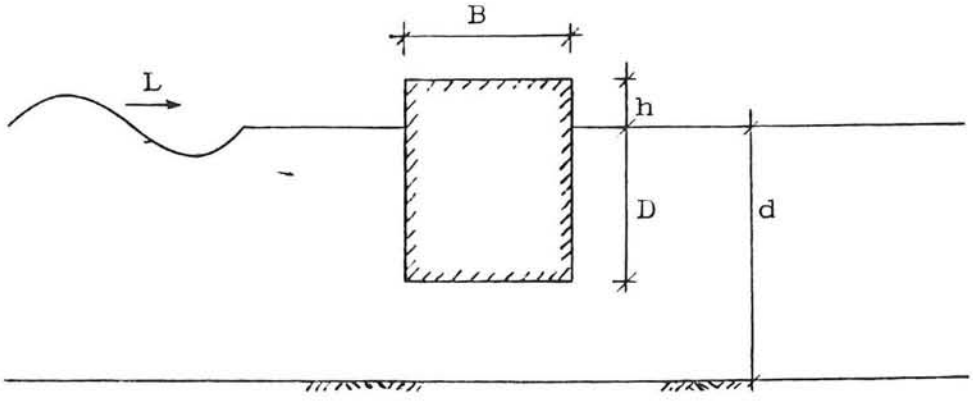

Figure 5: Defenition sketch of a rigid breakwater.

The transmission coefficient is given by:

$$C_t = H_t / H_i = f_1(H_i, L, B, D, d, h, \gamma_s, \gamma_w, \gamma_h) \qquad (2.12)$$

$$C_t = f_2(H_i/L,\ L/B,\ D/L,\ d/L,\ h/L,\ \gamma_w/\gamma_b,\ \gamma_s/\gamma_w) \quad (2.13)$$

where :

γ_w : unit weight of water.
γ_b : unit weight of the breakwater.
γ_s : unit weight of the submerged breakwater.
L : wave length.

the other variables are shown in figure 5. When there is no wave breaking over the structure, the value of $\Delta h + |\eta_i + \eta_r|_{max}$ is significant instead of h, where:

η_i : instantanious elevation of the incident wave.
η_r : instantanious elevation of the reflected wave.
Δh : rise in still water level = $\frac{\pi H_i^2}{4L}$ coth kd.

For a given breakwater system γ_w/γ_b and γ_s/γ_w are constant. For deep water waves ($d > L/2$) h and D (if D not to small, see 2.5.4) become unimportant and hence the expression can be reduced to

$$C_t = f_3(H_i/L,\ L/B) = f\ (H_i/L,\ T_n/T) \quad (2.14)$$

Where:

T_n : natural period of oscillation
T : period of incident waves

The same is valid for C_r.

The horizontal component of the mooring force is expressed as:

$$F = \phi_1\ (H_i, H_r,\ L,\ B,\ D,\ d,\ \gamma_s,\ \gamma_w,\ \gamma_b) \quad (2.15)$$

$$F D / \gamma_w H_i^2 L = \phi_2\ (H_i/L,\ H_r/H_i,\ L/B,\ D/d,\ \gamma_s/\gamma_w,\ \gamma_w/\gamma_b) \quad (2.16)$$

For deep water and for values of $D \approx L/2$ and constant γ_s/γ_w and γ_w/γ_b (2.16) can be written as:

$$F D / \gamma_w H_i^2 L = \phi_3\ (H_i/L,\ H_r/H_i,\ L/B) \quad (2.17)$$

2.5 TRANSMISSION COEFFICIENT OF FIXED, RIGID STRUCTURES

Specially in deep water, the restriction "fixed" is very unrealistic. The influence of the natural period of oscillation of the breakwater and the influence of the breakwater motions on the wave attenuation may not be neglected. The restricton "rigid" can be realistic in many cases. Three simple formulas for C_t prediction and a kinetic energy distribution after Ippen will be discussed subsequently.

2.5.1 Macagno (1953)

assumptions:
- the structure is rigid.
- the structure is fixed.
- water will not overtop the barrier.
- linear wave theory

$$C_t = \frac{1}{\sqrt{1 + \left[\frac{\pi B}{L_i} \frac{\sinh (2\pi d/L_i)}{\cosh (2\pi (d-D)/L_i)}\right]^2}} \qquad (2.18)$$

See fig. 6.

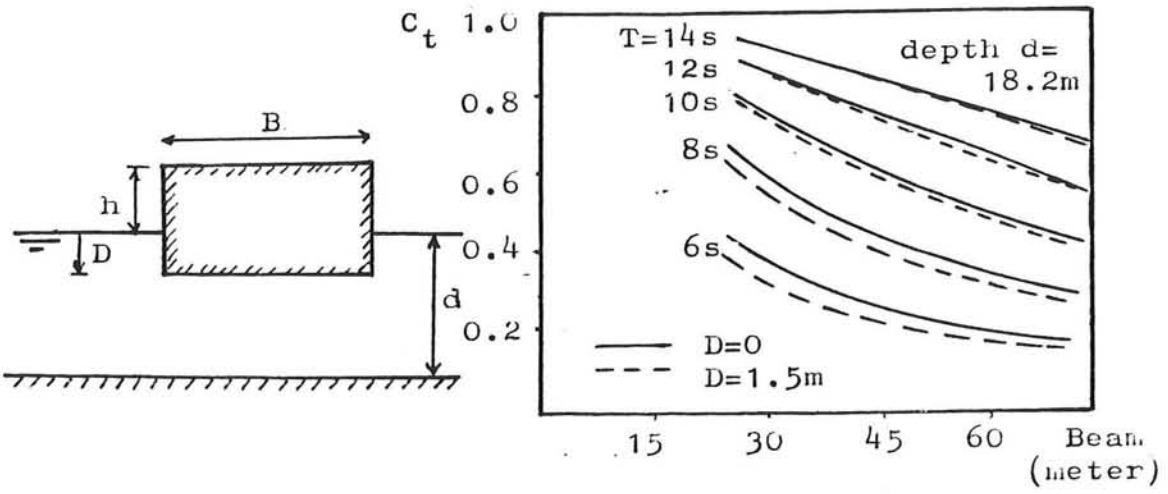

Figure 6: Macagno: definition sketch and theoretical transmission coefficient.

2.5.2 Ursell (1974)

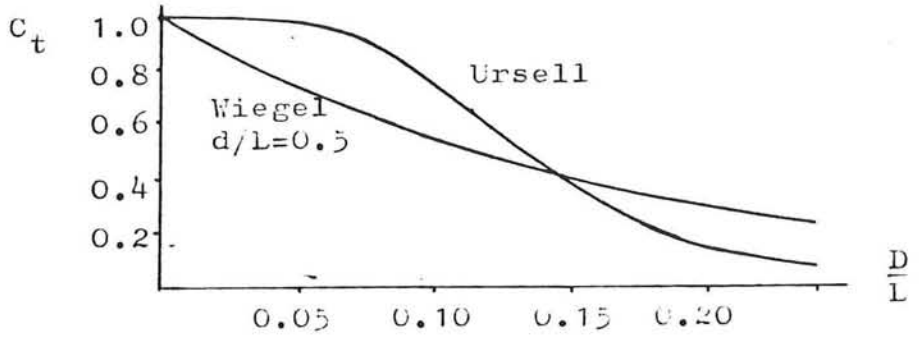

Figure 7: Transmission coefficient in deep water as a function of the draft relative to wave length (Ursell, Wiegel).

Ursell developed a theory, based on potential theory for partial transmission and partial reflection of waves in deep water with a barrier extending from the water surface to a depth D, such that:

$$C_t = \frac{K_1(2\pi D/L_i)}{\sqrt{\pi^2 I_1^2(2\pi D/L_i) + K_1^2(2\pi D/L_i)}} \qquad (2.19)$$

Where $I_1(2\pi D/L_i)$ and $K_1(2\pi D/L_i)$ are modified Bessel functions. Ursell assumed a fixed, rigid and thin barrier. See fig. 7.

2.5.3 Wiegel (1959)

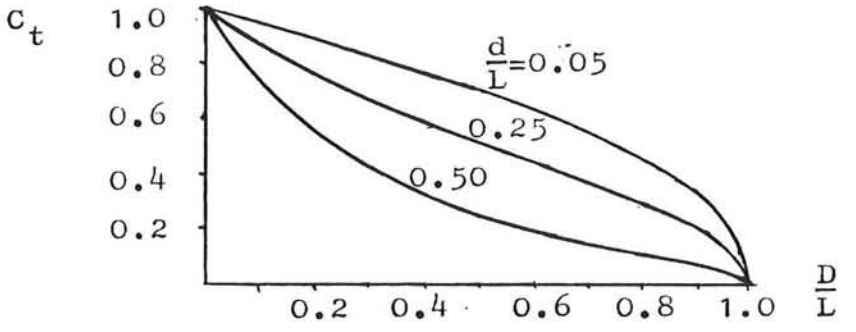

Figure 8: Power transmission theory of Wiegel.

Wiegel developed a linear theory (the so-called "power transmission theory") to predict the wave heights transmitted past a rigid, vertical, thin barrier extending from above the water surface to a depth, D.

Wiegel assumed that the power transmitted by a wave between the bottom of the vertical barrier and the channel bottom, will be the power transmitted past the structure, if the structure would not be there.

$$C_t = \left[\frac{2k(d-D) + \sinh 2k(d-D)}{\sinh 2kd + 2kd} \right]^{\frac{1}{2}} \qquad (2.20)$$

See figures 7 and 8.

2.5.4 Ippen (1966)

Ippen described the kinetic energy distribution, according to linear wave theory. The percentage of kinetic energy within an oscillatory wave between the bottom and an arbitrary elevation, s, above the bottom, is then given by:

$$\%\ \text{kin. energy between bottom and s} = \frac{\sinh 2ks}{\sinh 2kd} * 100\% \qquad (2.21)$$

where:

k : the wave number.
s : elevation above the bottom.

When the distance between elevation s and the water surface is "D", (2.21) can be written as:

$$\% \text{ kin. energy above elevation D} = \frac{\sinh 2k(d-D)}{\sinh 2kd} * 100\% \qquad (2.22)$$

See figure 9. Taking the square root of (2.22), yields a formula which equals the formula of Wiegel (2.20) when d becomes infinite.

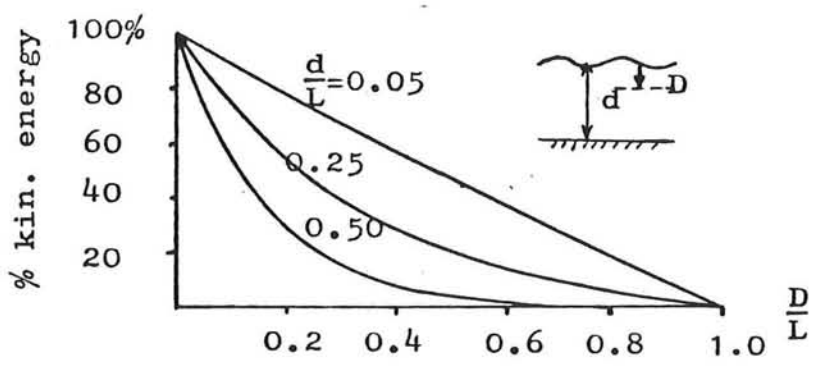

Figure 9: Percentage of kinetic energy between the bottom and an elevation with distance D to water the surface, of the total kinetic energy.

The formula of Ippen shows that a reflecting surface in the upper part of the water will reflect more energy in case of deep water waves than shallow water waves. For example: the upper 1/5 part contains 71.5% of the total kinetic energy if d/L=0.5 (deep water), but only 21.8% if d/L=0.05 (shallow water).

2.6 THE EFFECT OF BREAKWATER MOTIONS ON THE WAVE ATTENUATION PERFORMANCE

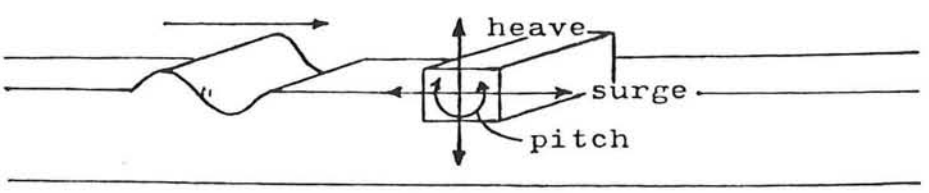

To get a better understanding of the influence of breakwater motions on the transmission coefficient, A.A. Sutko and E.L. Haden did experimental work with a 0.10m square breakwater in a laboratory wave tank. They could restrict one or more motions of the breakwater. Their purpose was to establish the effect of surge, heave and pitch on the performance of a floating breakwater. They concluded that:

1. Surge is the floating breakwater motion contributing the most to wave transmission.

2. In test with only one beakwater motion allowed, surge gave by far the highest wave transmission. Pitch gave a slightly higher transmission than heave.

3. In tests with two breakwater motions allowed, surge + heave, and pitch + surge, gave considerable more wave transmission than pitch + heave.

4. Adding either heave or pitch to surge results in less wave transmission than surge by itself.

5. In tests with only one breakwater motion allowed, there was little difference in wave reflection for surge, heave or pitch. In two motion tests, pitch + heave gave more reflection than pitch + surge or surge + heave.

6. In tests with only one breakwater motion allowed, energy dissipation was highest for pitch and heave. For the two motion tests, there was little difference in energy dissipation for any of the combinations.

7. When the breakwater is held rigid or allowed to either pitch or heave, the transmitted wave is less than that would be formed by the energy passing beneath its base.

2.7 TRANSMISSION COEFFICIENT OF NON-FIXED, RIGID STRUCTURES

As indicated in the previous section, the relation between wave attenuation performance and breakwater motion is evident. Since the floating breakwater is assumed to be non-fixed in the next models, the results will be more reliable. The most simple approximation, is the formula of Carr. The other three approximaticns are computer models, which can take more parameters intc account. They are able to give a reliable prediction of wave attenuation in non-dissipative systems.

2.7.1 Carr (1951)

Carr assumed: - shallow water
- hydrostatic pressure distribution
- linear damping
- only horizontal breakwater motions

$$C_t = \frac{1}{\sqrt{1 + \left[\frac{\pi m g}{\gamma_w L d}\right]^2 * \left[\left(\frac{T}{T_n}\right)^2 - 1\right]^2}} \qquad (2.23)$$

where:

T_n : natural period of the breakwater
T : period of the waves
m : mass per unit length of the breakwater
γ_w : unit weight of water

2.7.2 Computermodel of Stiassnie (1980)

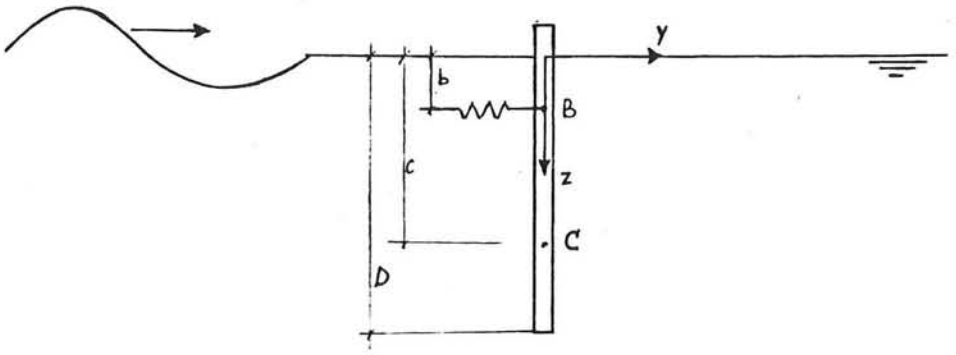

Figure 10: Floating vertical thin plate permitting development of a simple analytical expression of floating breakwater response (after Stiassnie, 1980).

Stiassnie developed a simple mathematical model, based on the solution of the two-dimensional problem of a floating plate as shown in figure 10. Stiassnie assumed in addition to the linear wave assumptions an infinite water depth.

The input parameters are L_i , H_i , γ_{water} , g, D, c (=location center of mass), m (mass per unit length), I_c (mass moment of inertia), k (spring constant) and b (see figure 10).

Stiassnie investigated the influence of the mass parameter. For this he took k=0, and plotted C_t as a function of D/L for various values of the relative beam B/L (see figure 11).

He concluded that the distribution of the mass of the breakwater is much more important than the magnitude of the mass. For example: B/L=0.01, D/L=0.7 so that C_t =0.5. Two proposals to improve the wave attenuation are:

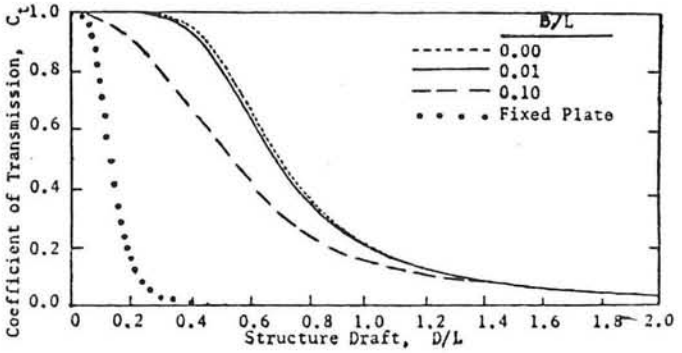

Figure 11: Effect of mass parameter on coefficient of transmission for floating breakwater, k=0 (after Stiassnie).

A: increase the beam with a factor 10 (10 times more mass).
B: double the draft (only two times more mass).

In figure 11 can be seen that "A" leads to C_t=0.31 (improvement 35%) and "B" leads to C_t=0.08 (improvement 83%). This may be remarkable, but one must nct forget that a rigid, fixed (k=0) breakwater has been assumed, so that case "B" leads to too optimistic results.

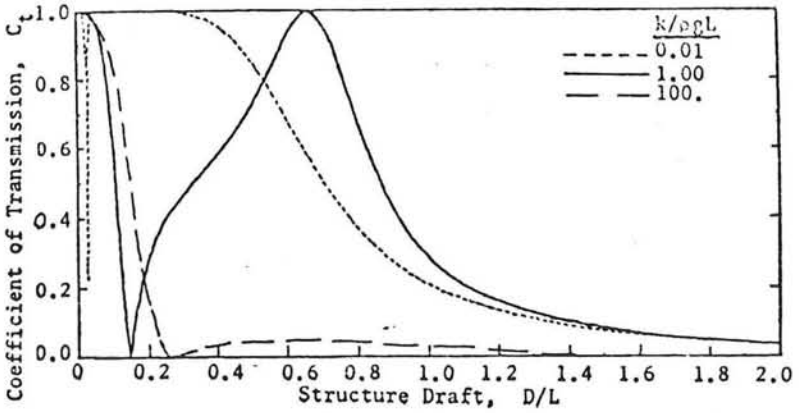

Figure 12: Effect of mooring stiffness parameter on coefficient of transmission, B=0 (after Stiassnie, 1980).

Stiassnie also investigated the influence of the mooring stiffness for B=0. Remarkable are the sharp peaks caused by resonance (see D/L=0.03 in fig. 12). The mass-spring system can cause C_t=0 as well as C_t=1 (see $k/\rho gL$=1).

2.7.3 Computermodel of Adee, Martin, Richey and Christensen.(1976)

The computermodel of Adee, Martin, Richey and Christensen is based on an existing program to predict the behavior of ships in waves.

Assumptions:
- -In this two-dimensional model all equations may be linearized and the breakwater may be treated as a linear system.
- -Infinite waterdepth.

The input variables are: ω (circular frequency), the body contour, mooring spring constants, hydrodynamic spring constant of the floating body and the physical properties of the body (mass, mass moment of inertia, position of gravity). The calculations may be seperated into three parts:

a. Formulation of the equations of motion.
b. Solution for the waves diffracted by a rigidly restrained breakwater.
c. Summation of the components a. and b. to obtain the total transmitted wave.

See figure 13.

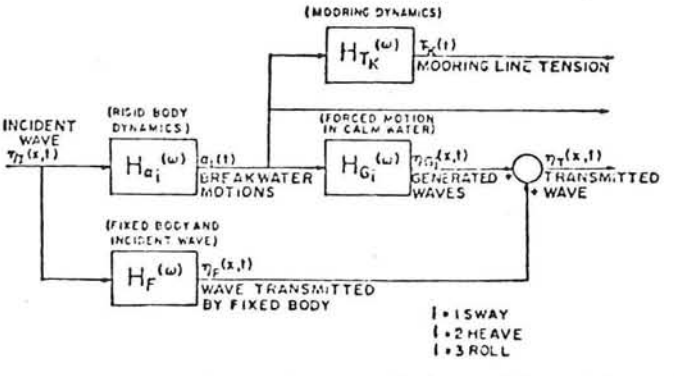

Figure 13: Linear system describing floating breakwater performance (after Adee, Richey and Christensen, 1976).

The output variables of the model are: transmitted wave, motions of the structure (heave, sway, roll), mooring forces and hydrodynamic coefficients. The effectiveness of the model in evaluating the performance of floating breakwaters was determined by comparing the theoretical prediction with a physical model. See figure 14.

Adee, Richey and Christensen concluded that the linearized, non-viscous, deep water theory is able to predict qualitatively the wave transmission performance. The quantitative results are within approximately 20% of the experimental measurements. Larger discrepancies occur primarily in short waves where too much transmission was predicted.

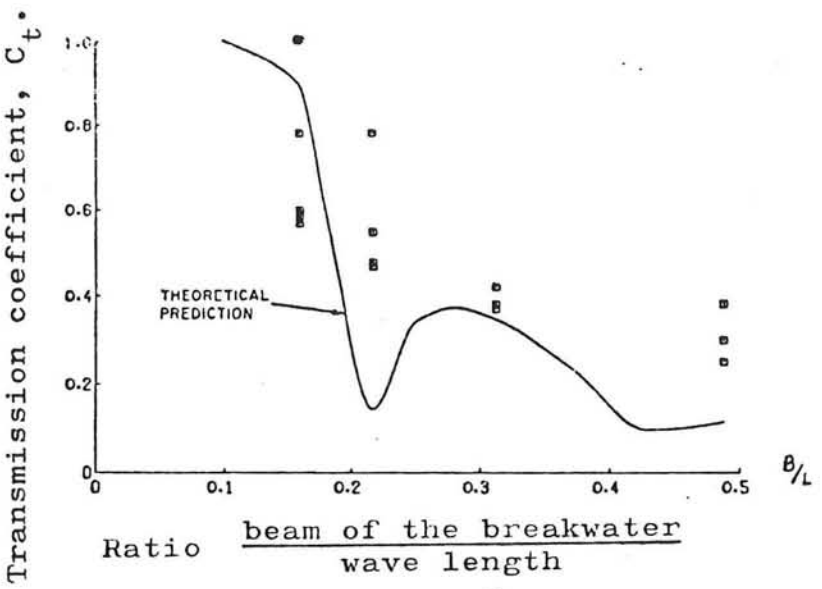

Figure 14: Comparison of the linear theoretical model by Adee, Richey and Christensen, with experimental data by Davidson (1971).

The infinite depth assumption does not appear to desgrade the results, as long as the section draft is less than half the actuel water depth, and the wave lengths are less than five times the actual water depth. Although nonlinear effects may be present in the performance of the breakwater, they are not of major importance to wave transmission, which justifies neglection of viscous roll damping.

2.7.4 Computermodel of Yamamoto, Yoshida and Ijima (ca 1980)

Assumptions:
- -small breakwater motions.
- -linear theory is valid.

The cross-sectional shape of the flcating object, the bottom configuration, and the mooring arrangements may be arbitrary. A great advantage of this model is that more general and rather complicated problems, such as multiple floating objects can be easily analyzed with only a slight modification of the flow and boundary conditions. The accuracy of this model appeared to be very good for structures of simple geometry.

Using this computermodel, the influence of the mooring on the transmission coefficient is investigated. See figure 15.

The "open spring" mooring worsened the results due to the undesirable rolling motion generated by the waves. The best results were achieved with the "cross-spring" mooring for the highest spring constant. According to this computer model a stiff mooring system results in the best wave attenuation performance. (In case of scrap-tire floating breakwaters, best results were achieved with a slack mooring line.)

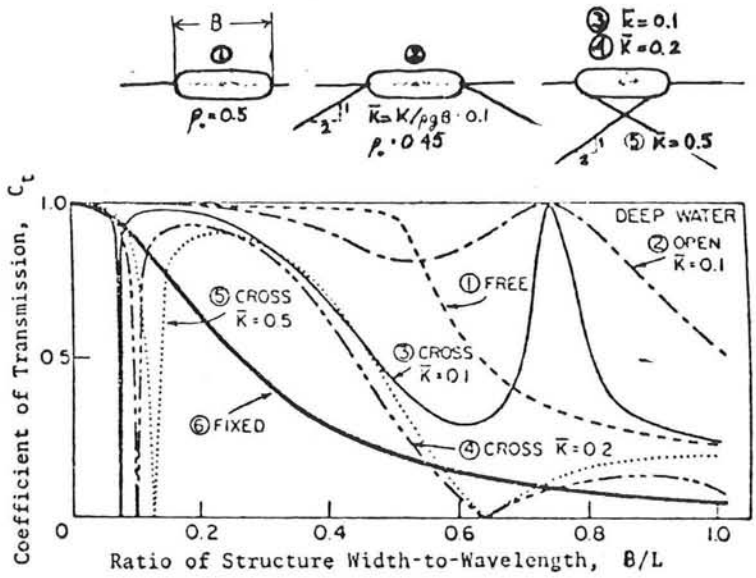

Figure 15: Calculated transmission coefficients for floating structure with various mooring conditions (after Yamamoto, Yoshida, and Ijima, 1980).

2.8 BREAKWATER MOTION PREDICTION OF RIGID STRUCTURES

Ofuya (1968) made calculations to predict the sway motion, the heaving motion and the rolling motion of the A-frame breakwater, but his calculations can also be used for other rigid structures.

Ofuya expressed the equation of sway motion as:

$$M\ddot{x} = \text{external forces} = F_{px} + F_{ix} + F_{dx} + F_{rx} \qquad (2.24)$$

Where:

- M : mass of block
- $\ddot{x}$: $\frac{d^2x}{dt^2}$
- F_{px} : hcr. component of force due to wave pressure.
- F_{ix} : inertial force in the direction of sway-motion.
- F_{dx} : drag force in the direction of the sway-motion.
- F_{rx} : restoring force of the elastic mooring line.

assumptions:

F_{px} is caused by waterpressure varying linear with depth.
F_{ix} is linear with the average fluid particle acceleration.
F_{dx} is linear with the square of the relative body velocity.
F_{rx} is linear with x.

For heaving motion Ofuya wrote:

$$M\ddot{Z} = \text{external forces} = F_{pz} + F_{iz} + F_{rd} + F_{wd} + F_{rz} - W_1 \qquad (2.25)$$

Where:

- F_{pz} : pressure force
- F_{iz} : inertial force in the heaving direction.
- F_{rd} : viscuous drag in the heaving direction.
- F_{wd} : drag force due to wave generation.

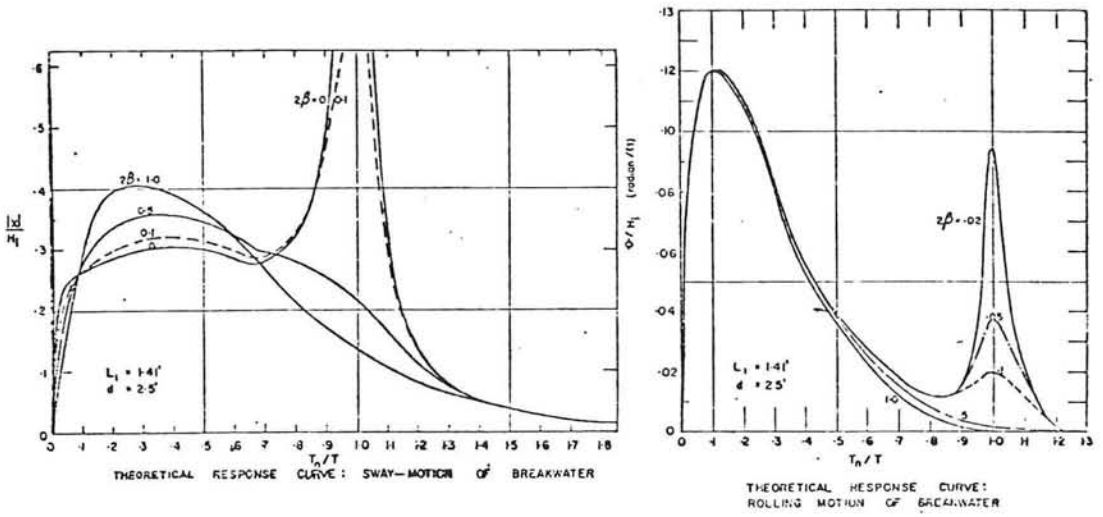

Figure 16: Theoretical response of breakwater motion.

F_{rz} : restoring force of the mooring line.
W_1 : weight of the breakwater.

This gives a solution similar to that of the sway-motion.

The equation of rolling motion can be expressed as:

$$I\ddot{\theta} = M_{i\theta} + M_{d\theta} + M_{r\theta} + M_{b\theta} + M_{ip} \qquad (2.26)$$

Where:

θ : angular motion of breakwater about its center of mass.
$M_{i\theta}$: moments caused by inertial forces.
$M_{d\theta}$: damping moment caused by wave generation of breakwater.
$M_{r\theta}$: restoring moment of mooring-line.
$M_{b\theta}$: restoring moment due to displacement of the center of buoyancy of immersed body.
M_{ip} : moment due to wave pressure forces.

Ofuya assumed that:

$M_{i\theta}$ is linear with $(\ddot{\phi}-\ddot{\theta})$ where ϕ is the angular motion of the diplaced fluid, about the center of mass of breakwater, and is linear with I_θ (added mass of inertia).
$M_{d\theta}$ $=N_\theta(\dot{\phi}-\dot{\theta})$. Also linear damping is assumed; N_θ is a damping factor
$M_{r\theta}$ $= -kD_1\theta$. A linear mooring system is assumed. (D_1= moment arm of the mooring-line about the watersurface).
$M_{b\theta}$ $= -W_1(\overline{GM})$. Where $\overline{GM}$ is the metacentric height

2.9 REDUCTION OF BREAKWATER MOTION BY AN OFFSET CONFIGURATION

Reduction of breakwater motion can be achieved by changing the mooring system or by changing the configuration of the breakwater. The latter is the design concept of the offset breakwater (see chapter XI).

To compare the forces on a simple rigid wall with those on the offset breakwater, the next simplified analysis can be made using the following assumptions:

1. The walls are fixed in position.
2. Still water conditions are present on the lee side.
3. The forces on the offset-wall are not effected by end conditions at each segment.
4. Transilatory waves approach the wall with crests parallel to the wall and form standing waves.
5. The waves do not break.
6. The pressure distribution at the wall is based on the Sainflou method.
7. The pressure distribution is the same as for a wall that penetrates to the bottom, but it acts only for the depth of penetration of the wall.

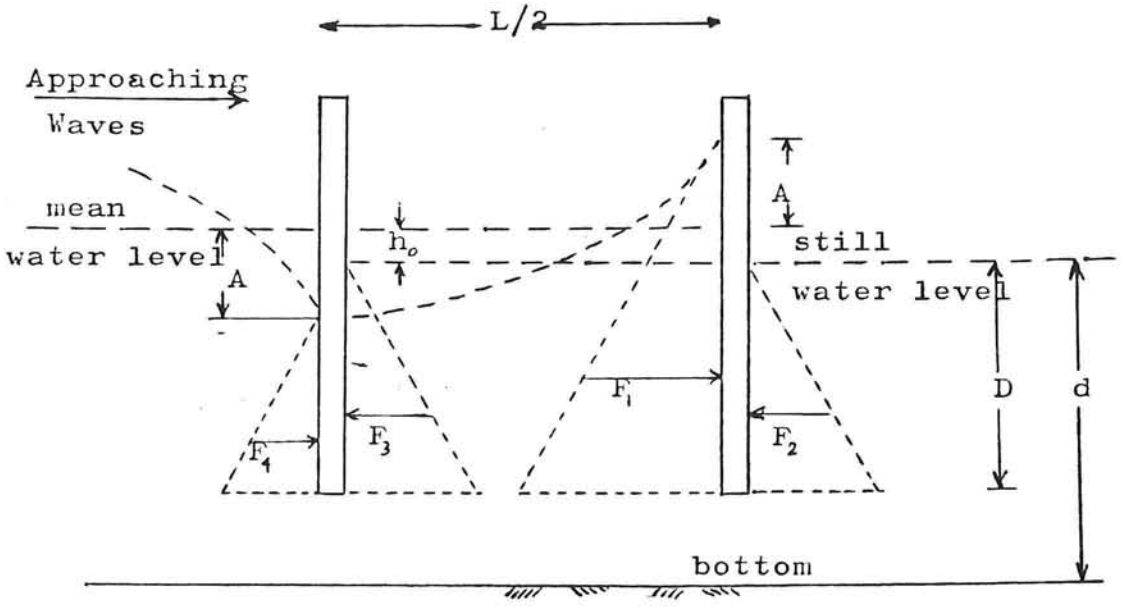

Figure 17: Diagram of forces acting on a offset breakwater configuration. Wave trough at first reflecting surface, crest at second surface.

Let F_1 , F_2 , F_3 and F_4 be forces per unit length (see fig. 17) then the total force for a width of one unit length of each offset wall (two units of length total) is F_o and is given by:

$$F_o = F_1 + F_4 - F_1 - F_3 \qquad (2.27)$$

$$F = \frac{(D+h_o+A)^2\,(\gamma d+P_1)}{2\,(d+h_o+A)} + \frac{(D+h_o-A)\,(\gamma d-P_1)}{2\,(d+h_o-A)} - \frac{\gamma D^2}{2} - \frac{\gamma D^2}{2} \qquad (2.28)$$

$$= \frac{\gamma A^2}{2}\left[\frac{\left(\frac{D}{A}+\frac{h_o}{A}+1\right)^2\left(\frac{d}{A}+\frac{P_1}{A\gamma}\right)}{\left(\frac{d}{A}+\frac{h_o}{A}+1\right)} + \frac{\left(\frac{D}{A}+\frac{h_o}{A}-1\right)^2\left(\frac{d}{A}-\frac{P_1}{\gamma A}\right)}{\left(\frac{d}{A}+\frac{h_o}{A}-1\right)} - 2\left(\frac{D}{A}\right)^2\right] \qquad (2.29)$$

where:

$h_o = (\pi A^2/L)*\coth\,(2\pi d/L)$.
A = amplitude of incident wave.
d = depth of water.
L = wave length.
$P_1 = A\gamma/(\cosh\,(2\pi d/L))$
γ = specific weight of water.

On a simple rigid wall, also for a width of two units of length is:

$$F_R = 2F_1 - 2F_2 \qquad (2.30)$$

$$= \frac{\gamma A^2}{2}\left[2\,\frac{\left(\frac{D}{A}+\frac{h_o}{A}+1\right)^2\left(\frac{d}{A}+\frac{P_1}{A\gamma}\right)}{\left(\frac{d}{A}+\frac{h_o}{A}+1\right)} - 2\left(\frac{D}{A}\right)^2\right]$$

The ratio of F_o/F_R is a measure of the reduction in force on an offset wall configuration compared with a simple rigid wall. See figure 18. The figures indicate that for the given wave and water depth conditions the force on the offset wall is approximately 1/4 to 1/5 of that on a simple rigid wall.

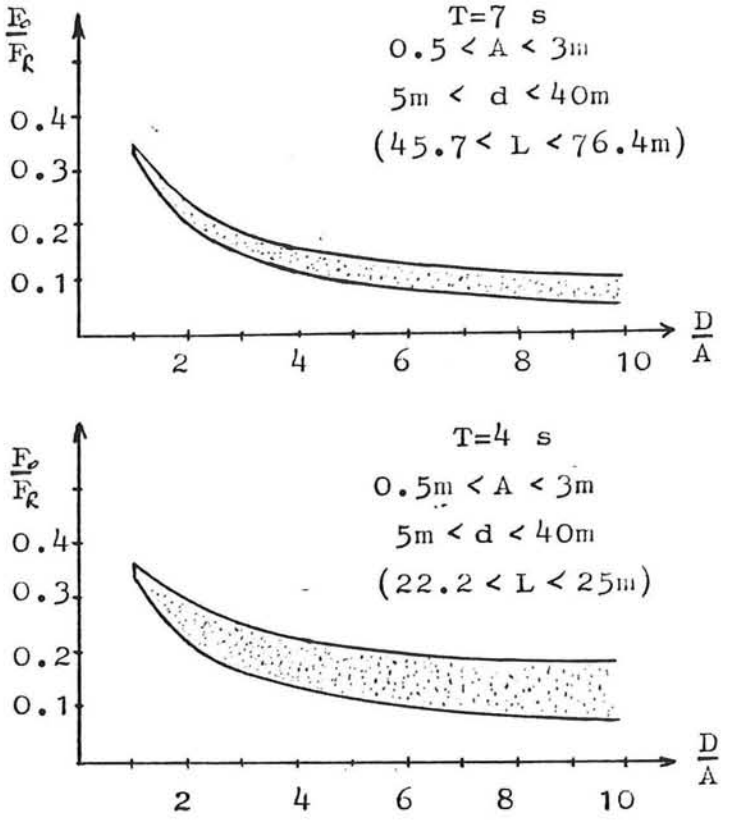

Figure 18: Ratio of mooring forces on a fixed simple rigid wall to fixed offset wall configuration.

2.10 ABSTRACT OF MODELS FOR WAVE ATTENUATION PREDICTION

MODELS:	Nacagno	Ursell	Wiegel	Carr	Stiassnie	Adee et al.	Yamamoto et al.
REQUIRED DATA FOR	R	I	G	I	D		
C_t PREDICTION	FIXED		NON-FIXED				
				c	c	c	
of the breakwater:							
beam (B)	X	≈0		≈0			
draft (D)	X	X	X		X		
body contour						X	X
weight per unit length			X	X	X	X	?
center of gravity					X	X	?
mass moment of inertia					X	X	?
hydrodynamic spring constant						X	
natural period			X				
circumstances:			1				2
water depth (d)	X	∞	X	X	∞	∞	X
wave length	X	X	X	X	X	X	X
wave height					X		?
mooring:							
spring constant					X	X	X
location of mooring line attachment					X		X

c computer model
1) shallow water
2) bottom configuration

2.11 DIMENSIONAL CONSIDERATIONS FOR A FLEXIBLE BREAKWATER

For a certain type of breakwater it is possible to express the transmitted wave H_t as a function of the following variables:

$$H_t = f(H, L, B, \phi, G, l, m, k, \mathcal{E}, d, \gamma, \nu, g) \qquad (2.31)$$

The following parameters have been deleted for stated reasons:

l/ϕ : only two dimensional problems are considered. (no diffraction).

$\frac{k\zeta}{mg}$: is the ratio of mooring system static restoring and ought not to be changed during the experiment.

ζ/H : assumed to be of little importance fcr small values.

$\frac{B\phi}{mg}$: is the ratio of the displaced mass to the mass of the breakwater itself and ought to be changed during the experiment.

Re : the value is assumed large enough to ensure a Re-independent behavior.

By eliminating dimensionless groups the following relation is obtained:

$$C_t = f(L/B , H/L , D/d , B/D) \qquad (2.32)$$

The mooring force relationship can be expressed as:

$$F = (H_i, H_t, L, B, \phi, G, l, m, K, \zeta, d, \gamma, \nu, g) \qquad (2.33)$$

Or dimensionless:

$$F/(\gamma H^2) = f(L/B , H/L , D/d , B/d) \qquad (2.34)$$

2.12 GLOBAL ANALYSES OF FLOATING MATS

The analyses of a floating slab under different wave conditions is a difficult problem. Especially the damping mechanism and the interaction of the structure with the waves are not fully understood. The damping mechanism seems to be a combined effect of reflection, resonance and absorption through deflection of the structure.

Only a few analyses have been carried out in the past. The remainder of this section will primarily deal with a model made by Stoker et al. (1953). Then attention will be paid to tests concerning floating slabs.

Mathemat:cal analyses of the action of shallow water waves on a rigid freely floating slab and an elastic freely floating slab were carried out by Stoker, Fleishman and Welickzer.

2.12.1 Formulation of the problem

Stoker first formulates the exact problem. See figure 2 . Stoker used the linearized wave theory to determine the velocity potential at the free surface. Under an immersed body the value of the velocity potential is determined by the continuity equation. The exact formulation of the problem would require the determination cf a harmonic function $\phi(x,y,z;t)$ in the space between $z = -d(x,y)$ and $z = \eta$, which

satisfies the conditions (2.2) and (2.3) at the upper surface (see section 2.1). Additional conditions where immersed bodies occur would be necessary to determine p, which provides "coupling" between the water on one hand and the immersed body on the other. Finally, appropriate initial conditions would be needed. All this becomes too complicated and therefore an approximate theory was used.

2.12.2 The approximate theory used by Stoker et al.

The symplifying assumptions can be summerized as:

1. Two dimensional.
2. Vertical accelerations negligible.
3. Friction negligible.
4. Small Froude numbers.

These assumptions lead to:

$$u_t = -g\eta_x \quad \text{(equation of motion)} \tag{2.35}$$

$$(ud)_x = -\eta_t \quad \text{(equation of continuity)} \tag{2.36}$$

Elimation of η leads to the well-known dynamic wave equation:

$$\phi_{xx} - \frac{1}{c^2}\phi_{tt} = 0 \qquad |x| > l \tag{2.37}$$

with: $c = \sqrt{(gd)}$

This equation is valid under the free surface. The equation of conservation of mass describes the problem under the raft:

$$\eta_t = -\bar{d}\,\phi_{xx} \qquad |x| < l \tag{2.38}$$

Solutions of the problem for some simple cases are discussed in the next section.

2.12.3 Solutions for the long wave approximations

For a slab fixed at $\eta=0$, extending from x=-l to x=+l, Stoker et al presented an expression for ϕ and η using the above presented theory.
Stoker assumed ϕ_x, ϕ_t to be continuous. Considering only simple harmonic waves:

$$\phi(x,t) = \varphi(x)\exp(i\omega t) \quad |x|>l \tag{2.39}$$

$$\eta(x,t) = v(x)\exp(i\omega t) \quad |x|<l \tag{2.40}$$

(2.37) + (2.38) becomes:

$$\frac{d^2\varphi}{dx^2} + \frac{\omega^2}{gd}\varphi = 0 \qquad |x| > l \qquad (2.41^a)$$

$$\frac{d^2\varphi}{dx^2} + \frac{i\omega}{d} v = 0 \qquad |x| < l \qquad (2.41^b)$$

If the board is rigid then $\eta(x,t)=0$ and $v(x,t)=0$. From equation 2.41^b it follows that $\varphi_{xx}=0$. The velocity potential under the board seems to be a linear function of x. Then it follows that the velocity under the board is given by:

$$\varphi(x) = C_1 x + C_2 \qquad |x| < l \qquad (2.41^c)$$

From the transmission condition H_r and H_t can be solved to obtain:

$$C_r = \left|\frac{H_r}{H_i}\right| = \frac{\Theta\pi}{\sqrt{1+\Theta^2\pi^2}} \qquad (2.42)$$

$$C_t = \left|\frac{H_t}{H_i}\right| = \frac{1}{\sqrt{1+\Theta^2\pi^2}} \qquad (2.43)$$

$$C_r^2 + C_t^2 = 1$$

$$\Theta = 2l/L$$

In table 1 values for C_t and C_r are given as a function of $2l/L$.

Table 1.

Transmission and reflection coefficients as a function of $2l/L$ (after Stoker).

$2l/L$	C_t	C_r
0.5	0.54	0.85
1.0	0.30	0.95
2.0	0.157	0.986

In case of a freely floating board the details of the calculations are more complicated. They can be found in the paper

by Fleishman (1953). Fleishman's calculations are in agreement with the feeling that a fixed board should damp waves more succesfully than a movable one.

Next, Stoker et al considered a floating elastic beam. The beam extends from x=-l to x=0, and is assumed once more to sink slightly below the water when in equilibrium. The same equation as for the floating slab can be used. To describe the transverse oscillations of the beam, the well known linearized deflection equation was used:

$$EI\eta_{xxxx} + m\eta_{tt} = p^{+} \qquad (2.44)$$

where:

EI : bending stiffness of the beam
m : mass per unit area
η : breakwater displacement from z=0 (+ up)
p^{+} : dynamic pressure

The weight of the beam and the contribution of the hydrostatic pressure in p were ignored. Combination of equation (2.44) and (2.38) gives:

$$\frac{d^4\varphi}{dx^4} + \frac{\rho g - m\omega^2}{EI}\frac{d^2\varphi}{dx^2} + \frac{\omega^2\rho}{EId}\varphi = 0 \qquad -l < x < 0 \qquad (2.45)$$

Prediction of the reflection and the transmission coefficients, using equation (2.45) gave rise to very tedious calculations of which two important conclusions can be drawn.

First it was found that an elastic freely floating slab of finite length can achieve a high reflection coefficient. However, a slight change of slab length produces an entirely different value of reflection coefficient.

Secondly it was found that a beam of finite length can be more effective as a breakwater than a beam of infinite length. This wave attenuation performance is a result of multiple reflection that takes place at the end of the beam. That such a proces might well be sensitive to small changes in the parameters, cannot be wondered at.
A study of the results of the mathematical study by Stoker et al suggests that a thin lightweight plastic sheet would be ineffective as a breakwater. However, this is in contradiction with various wave experiments.

To evaluate floating mats, Jones reanalyzed the data of tests conducted on thin membranes. He presented the transmission coefficient C_t as a function of relative water depth, L/d, for several wave steepnesses. The Figures 19 to 22 present Jones reanalyses of four different materials.

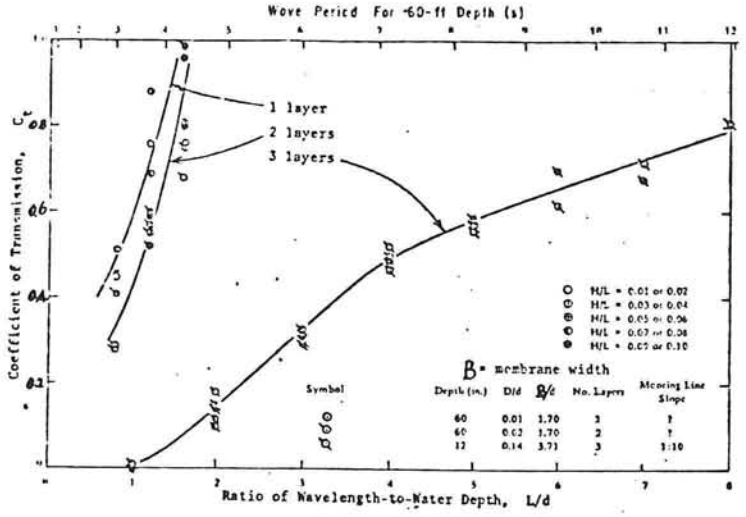

Figure 19: Effect of relative water depth, L/d, and incident wave steepness, H/L, on transmission coefficients, C_t for a woven fabric of plastic fibers.

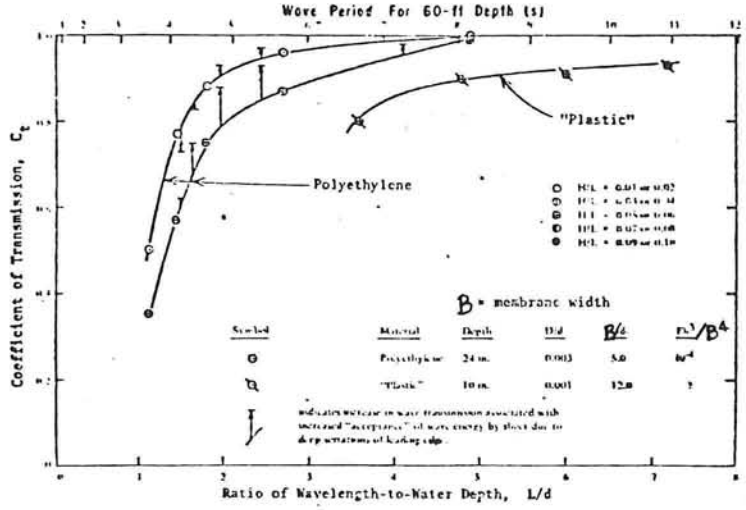

Figure 20: Effect of relative water depth, L/d, and incident wave steepness, H/L, on transmission coefficients, C_t for thin impervious sheets of plastic or polyethylene.

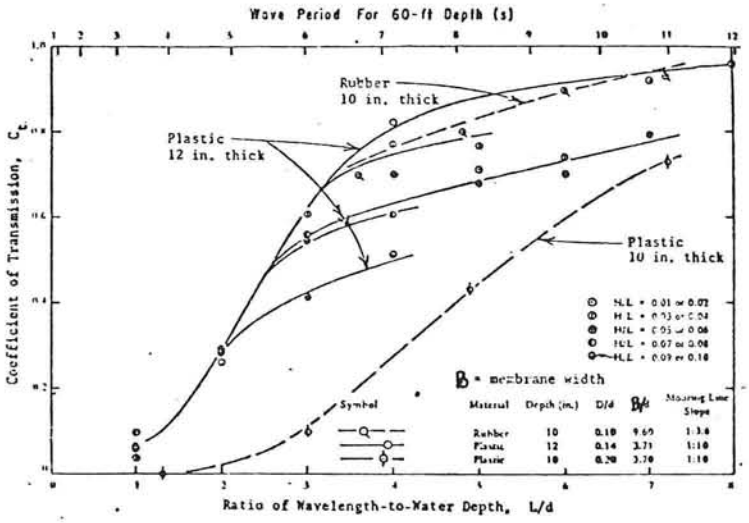

Figure 21: Effect of relative water depth, L/d, and incident wave steepness, H/L, on transmission coefficients, C_t for sponge blankets of varicus thicknesses.

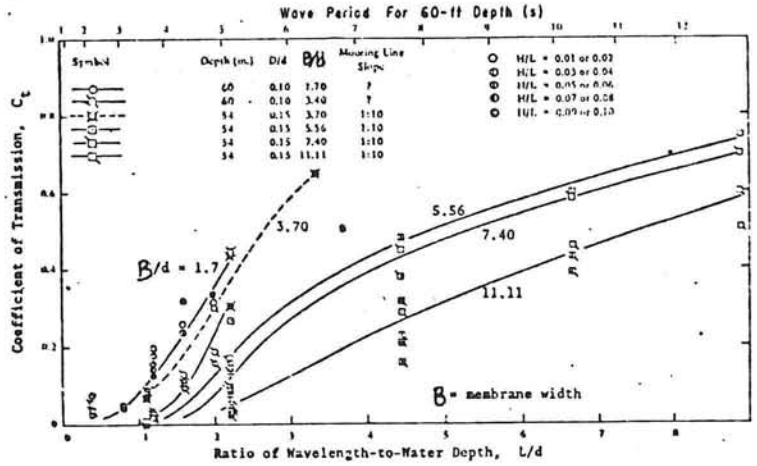

Figure 22: Effect of relative water depth, L/d, and incident wave steepness, H/L, on transmission coefficients, C_t for a corrugated blanket of woven plastic fabric.

2.13 DISSIPATION

Dissipation can be achieved in many ways. When there is a local small water depth, the waves will break (this process will start when H/L=0.6, if the bottom is hard, otherwise they will break later). The energy will be dissipated through turbulence. Another possibility of dissipation is the use of porous walled structures.

Dissipation can also be achieved by friction. Normally, friction will not dominate, but in cases of resonance, when high velocities are achieved, friction may dominate ; this happens in case of the tethered-float breakwater.

Unfortunately, the amount of dissipation or turbulence is difficult to predict or to describe in a model.

2.13.1 Analytical model of drag dissipation

The analytical model of Seymour and Hanes (1979) is made for the tethered float breakwater which is shown in chapter XIX. The model considers only drag dissipation, because preliminary laboratory measurements suggested that scatter and reflection are minor contributors to the reduction of wave energy. They defined the drag power in frequency space for a single float as:

$$P_D(f) = F_D(f) \cdot U_r(f) = 1/2 \rho A C_D [\, U_r(f) \,]^3 \qquad (2.46)$$

where:

$P_D(f)$: drag power of the float in freq. space.
$F_D(f)$: drag force of the float in freq. space.
ρ : fluid density.
C_D : empirically determined drag coefficient.
$U_r(f)$: relative velocity between float and fluid particle.

taking average values: $\overline{U_r^3} = S_r^{3/2}$

$$P_{D,\,total} = \int_0^{\infty} P_D(f)\, df \cong C_1 \sum_{n=0}^{N} [\, S_r(n\Delta f) \,]^{3/2} \qquad (2.47)$$

where: S_r : the spectrum of relative velocities.
C_1 : $1/2 \rho A C_D$

Wave power per unit length:

$$P_W(f) = (1/2) \rho g S_\eta Cn(f) \qquad (2.48)$$

where: $Cn(f)$: the group velocity
$S_\eta(f)$: the spectrum of surface elevation. The ratio of the dissipative power to the incident wave power is the energy reduction factor per row.

$$\varepsilon = \frac{C_2 \sum_{n=0}^{N} [\, S_r(n\Delta f) \,]^{3/2}}{\sum_{n=0}^{N} S_\eta\, Ch(n\Delta f)} \qquad C_2 = AC_D/gl \qquad (2.49)$$

where, l', is the width of the considered wave crest. When the distance between two floats is d^*, d^* + diameter of the float can be taken for l. Unfortunately, "S_r" is unknown, but it is possible to approximate S_r. The linearized equation of motion is:

$$(C_M M_w + M_s)\ddot{x} + C_1 U_o (\dot{x} - u) + g(M_w - M_s)(x/A) = (1 + C_M) M_w \dot{u} \qquad (2.50)$$

where:

x : horizontal position of the sphere.
u : horizontal water motion.
M_s : float mass.
M_w : mass of displaced water.
C_M : added mass coefficient
U_o : characteristic velocity $= \frac{3}{3\sqrt{2}} \sigma_{RV}$
σ_{RV} : standard deviation of the relative velocity.
A : effective tether length.

(2.50) is solved by Seymour. Knowing the motions, it was possible to find $S_r(f)$. By specifying a spectrum and knowing $S_r(f)$, it was possible, using (2.47), to find the drag power

$P_{D,total}$. Finally, knowing $P_{D,total}$, it was possible to predict the wave attenuation. Some results are given in chapter X

2.13.2 Semi-theoretical model to predict wave attenuation of floating tire breakwaters

Harms worked out design criteria for FTB [WW2 may 1979]. Using linear wave theory and deep water conditions he derived a semi-theoretical model for determining C_t. The power required to propel a tire (of negligigble mass) at velocity u(t) unidirectionally through a viscous fluid at rest is:

$$\dot{E} = |F_D u| + |F_i u| \qquad (2.51)$$

where

$F_D = C_D * 1/2\, \rho u^2 A$
$F_i = C_m M_f \dot{u}$
C_D : drag coefficient
C_m : hydrodynamic mass coefficient
M_f : hydrodynamic mass

This basic relationship is assumed to be applicable if the tire is fixed and u(t) represents an unsteady flow. Further it will be assumed that the power represents the rate at which the energy is dissipated within the structure. The rate of energy dissipation within segment Δx of the breakwater is assumed to be proportional to the number of tires, n, contained in that segment

$$n = N\ (\Delta x/B) \qquad (2.52)$$

where:

N : the number of tires contained in the volume $By\phi$

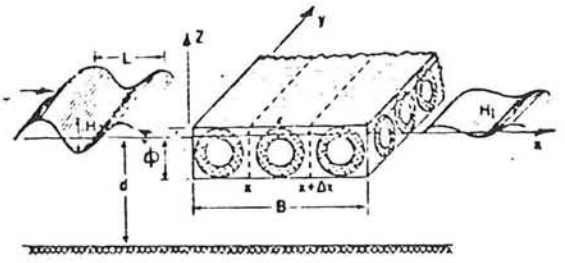

Figure 23: Definition sketch (after Harms).

Another important parameter is the porosity, P, defined as:

$$P = \frac{By\phi}{N\phi^3} \sim \frac{\text{volume of breakwater}}{\text{volume of tires}} \qquad (2.53)$$

To calculate the time average rate of energy dissipation, Harms assumed that the velocity, u, varies sinussoidally with time. Harms then found that

$$\overline{\Delta \dot{E}_D(x)} = (C_1 u_m^3 + C_2 u_m \dot{u}) \cdot \frac{\Delta x}{B} \qquad (2.54)$$

in which

$$C_1 = 2\gamma C_D y B/(3\pi g P)$$
$$C_2 = \gamma C_m y B \phi/(2\pi g P)$$

An energy flux balance within segment Δx indicates that

$$\overline{\Delta \dot{E}_W} = \overline{-\Delta \dot{E}_D} \qquad (2.55)$$

where

$$\overline{\Delta \dot{E}_W} = 1/8 \rho g c_g B \left[\frac{dH^2}{dx}\right] \frac{\Delta x}{B} \qquad (2.56)$$

The variation of $H(x)$ can be obtained from the aforementioned relation. This is not easy since the flow field is not purely wave-induced. Within the structure the flow field is even more complex (wave breaking, air-entrainment, surging, etc.), which cannot be accounted for in the most sophisticated wave theories. Therefore, deep water conditions and linear wave theory are used.

Because the theory is based upon deep water conditions, the influence of D/d is not accounted for. The relative draft, D/d, may be of importance in shallow water. This parameter must certainly be considered as the rigidity of the breakwater (in the direction of wave propagation) increases. This may be demonstrated by considering the Goodyear-Breakwater and the PT-Breakwater.

1. For the Goodyear-Breakwater an increase of D/d from 0.16-0.33 causes a decrease of C_t that is typically less than 0.1.

2. For the PT-Breakwater an increase of D/d from 0.22-0.51 is associated with a decrease of C_t by as much of 0.4, depending upon L/B.

It is obvious that the influence of the relative draft on wave attenuation increases with increasing stiffness of the breakwater. The breakwater then attenuates waves more and more through reflection, which process is mainly governed by the relative draft.

In addition to linear wave theory and deep water conditions the following assumptions are used:

- $D \ll L$
- $F_D \sim H^2$ (local wave energy density)
- $\hat{u}^3 = \pi^2 g H_i H^2/(2TL)$
- $\phi/H_i \approx C_D/C_m$

Using eq. (2.54) and (2.56) in the energy flux balance and integrating across the beam of the breakwater, Harms obtained:

$$C_t = \exp\left[\frac{-20\pi}{3}\,\frac{C_D}{P}\,\frac{\frac{H}{L}}{\frac{L}{B}}\right] \qquad (2.57)$$

in which:

C_D : drag coefficient
P : porosity coefficient

For H/L = 0.04:

$$C_t = \exp\left[-0.84\,\frac{\frac{C_D}{P}}{\frac{L}{B}}\right] \qquad (2.58)$$

In which:

$C_D/P = 0.69$ for the Goodyear-FTB
$C_D/P = 1.22$ for the PT-FTB

The appropriate value of C_D was determined from eq. (2.58) by matching the measured transmission coefficient C_{t1}, occuring at L/B=1, with the theoretical value. This resulted in

$$C_D = -1.19P(\ln C_{t1}) \qquad (2.59)$$

For the Goodyear-Breakwater with P=0.87 and C_{t1}=0.56, this results in C_D=0.60. For the PT-Breakwater with P=0.53 and C_{t1}=0.36, the corresponding value is C_D=0.65. Since the value of C_D does not differ significantly from one structure to the other, the transmission performance is exponentially governed by the inverse of the porosity parameter P if both H/L and L/B are constant.

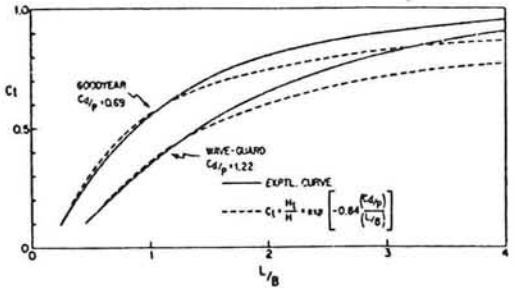

Figure 24: Theoretical transmission curve for scrap-tire breakwaters (after Harms).

In the region where the breakwater provides significant wave protection, typically L/B<2, the theoretical values differed from the measured by less then 10%. For larger values of L/B the theoretical curve is consistantly lower than the experi-

mental curve. But even there the difference does not exceed 15%. This behavior can be anticipated from the theoretical formulation itself. The sway motion of the breakwater is assumed to be significantly small, which is only valid for short waves (say $L/B<<1$). The in-phase surge motion of the breakwater decreases the relative velocity between breakwater components and fluid. The level of energy dissipation, due to these components, should be reduced. The model was found to be sufficient precise for engineering applications.

CERC, the Coastal Engineering Research Center, also published design curves for FTB. These were in good agreement with those published by Harms. However, differences did occur. Especially the wave transmission design curves show moderate differences. These are mainly due to scale effects.

Mooring forces

Harms empirically derived design curves for the PT-Breakwaters and the Goodyear-Breakwater. These curves are shown in figure 25 .

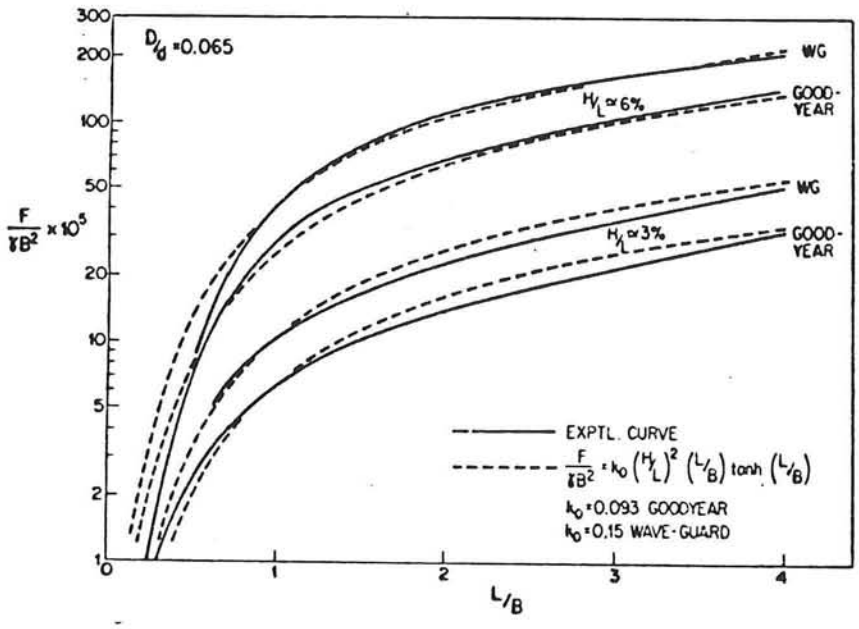

Figure 25: Mooring force design curves (after Harms).

For $D/d=0.065$, $H/L=0.03-0.06$ and $L/B>0.8$, the peak mooring force F per unit length of the breakwater can be determined from:

$$\frac{F}{\gamma H^2} = K_o \left(\frac{L}{B}\right) \tanh\left(\frac{L}{B}\right) \qquad (2.60)$$

with:

$K_o = 0.093$ Goodyear-Breakwater
$K_o = 0.15$ PT-Breakwater

Because of the greater wave attenuation capacity of the PT-Breakwater, the mooring forces are larger than those experienced with the Goodyear-Breakwater. But for a desired wave attenuation the peak mooring force of the PT-Breakwater may be smaller than the value found for the Goodyear, because the desired beam for the Goodyear-Breakwater is greater than the beam of the equivalent PT-Breakwater.

2.14 ABSORPTION

The amount of energy in a wave train is so large, that attempts to take the energy into the system structure, may result in large stresses, strains and fatigue failures. But it is the only way to generate (wave)energy, and it is surely possible. For example, "the nodding duck" which has been studied by Salter in Britain, has an efficiency of 90% at resonance, and the efficiency is still above 50% over a wide band of frequencies. Although the power transported by the waves reaches 70 kW/m at the coast of Scotland and the Hebrides, which would permit an anual production of 620 MWh/m (at 100% eff.), it is still uncertain that such a device can be economically feasible.

2.15 ABSORPTION OF WAVE ENERGY BY ELONGATED BODIES

2.15.1 Introduction

Very important for the absorption of wave energy by elongated bodies is that the capture width is broader than their own beam. In particular Newman investigated this in theory. In practice, the results are a little disappointing due to the non-linear effects.

After discussing the theory of Newman, theories for two different rafts will be discussed: the continuous flexible rafts and the articulated rafts (with, say one to six hinges). In the "Theory by Newman" the articulated rafts will be dicussed too.

2.15.2 Theory by Newman

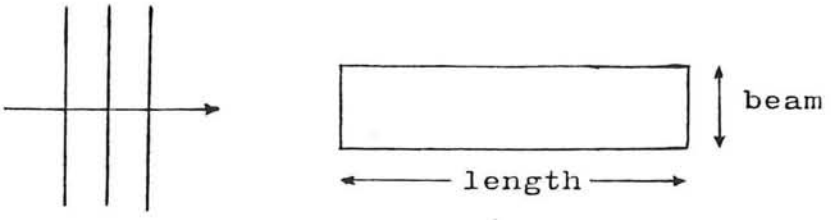

If the absorbing device is two-dimensional, the efficiency of absorption can be defined as the ratio of energy extracted from the incident waves per unit width. The device can only be considered as two-dimensional if the beam is large relative to other scales, including the wave length. When the beam is relative small, the absorbed wave energy is

more than available in the incident waves with a width equal to the beam of the device. Seemingly, more than 100% efficiency is achieved. The energy that can be absorbed equals the available energy in the so-called "absorption width W".

In general, a three dimensional device can be designed to focus the incident waves, and to absorb their energy over a width substantially greater than its own beam. Maximum W is equal to $3L/2\pi$ (L is the wave length). An elongated body with small beam-length ratio, is one of the most promising types of wave absorbers. The forces required to moore such a vessel are relatively small, compared with the two-dimensional configuration, besides, energy can be absorbed along the length of the structure with oscillations of reasonable magnitude, due to diffraction. A further advantage is that with the flexible or articulated body, energy can be extracted by the opposing relative motion between different elements, while the body as a whole is free to respond to the total force and moment of the incident waves. In this case the mooring force is necessarily only to restrain the vessel in a given mean position.
An example of such a raft is the Cockerell raft (several articulated elements).

Newman assumed in his theory:

1. amplitudes of the incident waves and the motions of the absorbing body are small.
2. linearization is justified.
3. axisymmetric body.
4. body length is substantially larger than the beam and the draft (slender body approximation).
5. regular waves.
6. infinite water depth.

For the absorption width was found:

* for axisymmetric motions (such as heave) $W^{max} = L/2\pi$.
* for lateral motions $W^{max} = L/\pi$.
* superposed: $W^{max} = 3L/2\pi$ (=0.48 L).

In the long wave limit ($kl \to 0$):

$$W_n^{max} \simeq \frac{L}{\int_0^{2\pi} \cos^{2n}\theta \, d\theta} \simeq \frac{L}{2\pi} \cdot \frac{2 \cdot 4 \cdots (2n)}{1 \cdot 3 \cdots (2n-1)} \qquad (2.61)$$

where n is a function of the sort of motion (for example if n=0: only heave, if n=1: only pitch). Thus the body shape and dimensions are not important if $l \ll L$, and the beam does not effect W^{max}.
In practice, the vertical body displacement is limited to a maximum value in the order of the incident wave amplitude. This gives a restriction for the absorption width by small l/L. Computations of the absorption width are shown in figure 26 for modes n=0 to 5. In figure 26 the solid curves are for unlimited body displacements and the broken curves correspond to limited body motions.

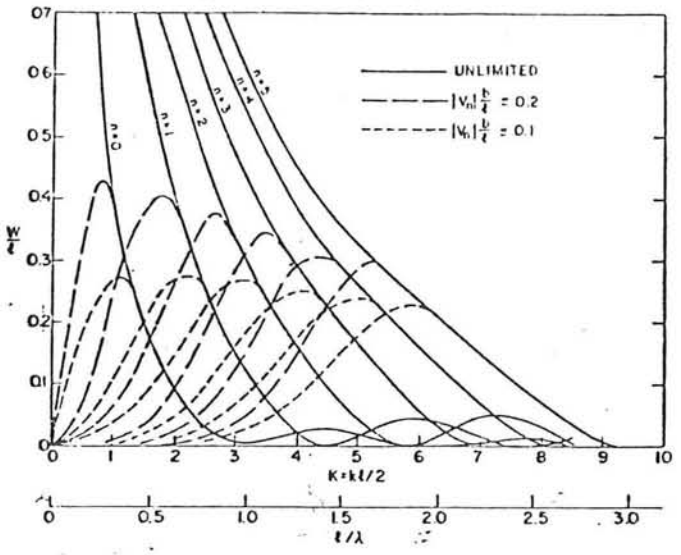

Absorption-width ratios W/l, *for Legendre polynomial modes of optimum magnitude and phase.* ———, *Unlimited body displacement;* ——— *and* ———, *arbitrary limits on the product of the body displacement amplitude* $|v_n|$ *and the beam-length ratio* b/l.

Figure 26: Absorption-width ratios, after Newman.

For a floating body with slack mooring, power can not be extracted from heave and pitch motions, but only from the higher order modes (n>1).

For trigonometric mode shapes (three hinges) and kl>>1:

$$\frac{W^{max}}{\ell} \cong \frac{3}{8}\left(\frac{\pi}{2kl}\right)^{\frac{1}{2}} \qquad (2.62)$$

so, for l>>L the absorption width is proportional to $l^{\frac{1}{2}}$.

With possible exception of its short wave length performance, the relative simple two-hinge configuration appears to be optimum from the engineering standpoint. A greater number of hinges would improve the performance for shorter wave lengths, but probably not to a sufficient extent to offset the increased mechanical complexity. A raft with two hinges can absorb twice as much energy as a raft with only one hinge. When the hinges have the same distance to the middle of the raft, the hinge position is relatively unimportant, unless the hinges are located close to the body ends. The optimum configuration appears to be that where the three segments are about the same length, thus each raft length is approximately 1/3 l.

The optimum body length is approximately equal to the average wave length of the seaway, typically in the range of 100 to 200 m. The optimum beam length appears to be in the range of 0.1 to 0.2 L. The draft was not important in these approximate analysis. For this reason, and also to refine the computations, a more complete analysis using a three-dimensional numerical scheme may be needed.

2.15.3 Theory of a continuous flexible raft by Farley

A long slender floating beam, sufficiently flexible to follow the waves is considered as a wave power converter. Tensioned cables apply longitudinal compression forces to the beam, encouraging buckling, which enhances the wave induced vertical oscillations. The oscillations active pumps incorporated in the structure. The raft is designed so that the phase velocity of vertical flexural waves is equal to the velocity of the sea waves at the design frequency, and at the same the time oscillations of the beam resonate with the waves. As a result a travelling wave is excited with an amplitude larger than that of the sea wave, and travels down the beam with a phase delay of about 90°. The raft radiates a secondary wave, strongly collymated in the forward direction, which tends to cancel the original wave. The backward radiation is small.

preliminary of raft motion.

Let the mass per unit area be m1 and assume that the raft is compressed in the direction of its length by a force N per unit length (this can be provided for example by cables under tension joining the two ends, probably at the sides of the structure). The incident wave is assumed to propagate along the axis of the raft (x-axis), and is given by the instantaneous height of the water surface above mean sea level, $\eta = A\exp(i\omega t - ikx)$. The vertical displacement "Z" of an element of the raft above its equilibrium then satisfies:

inertial force = buoyancy force + force caused by buckling + elastic force of the construction + damping force.

$$m\frac{\partial^2 Z}{\partial t^2} - \rho g(\eta - Z) - N\frac{\partial^2 Z}{\partial x^2} - n\frac{\partial^4 Z}{\partial x^4} - mg(b_a + b_r)\frac{\partial Z}{\partial t} \qquad (2.63)$$

where:

- N : compression force per unit length, applied by tensioned cables.
- Z : vertical displacement of the raft.
- n : EI per unit width.
- ρ : spec. mass of the fluid (water).
- b_a : internal damping.
- b_r : radiation damping.
- m = m1 + m2 = mass per unit raft + added mass (due to water moving with the raft).

The last three are functions of frequency. The solution of equation (2.63) is:

$$Z = \eta / d(F + i\omega b) \qquad (2.64)$$

where:

- $d = m/\rho$
- $b = b_a + b_r$
- $F = F(\omega,k) = 1/d - \omega^2/g - (N/mg)k^2 + (n/mg)k^4$
- $k = 2\pi/L$

The amplitude of the raft will be infinite when both the damping and F are zero. When F is very small, only damping will stop the raft from excessive amplitude. So, small F seems to be important for good absorption results.

The static stability can be checked by observing F(0,k). So w=0, but k≠0. The minimum of F will just reach zero if:

$$\left.\begin{array}{l} F(0,k)=0 \\ \frac{\partial F}{\partial k}=0 \end{array}\right\} \rightarrow \begin{array}{l} T = 2\rho g k_{min}^{-2} \\ n = \rho g k_{min}^{-4} \end{array} \qquad (2.65)$$

If the raft is excited by a water wave $\omega^2/g=k$ (deep water), the resonances are determined by:

$$F = F(\sqrt{gk},k) = 1/d - k - l_1 k^2 + l_2^3 k^4 = 0 \qquad (2.66)$$

Where $l_1 = T/mg$ and $l_2 = (n/mg)^{1/3}$

The work done by the raft per unit area per second determines the power output per unit area:

P_{out} = internal damping force * velocity

$$= m * g * b_a * \left(\frac{\partial Z}{\partial t}\right)^2 = m * g * b_a * \omega^2 * Z^2 \qquad (2.67)$$

$$= \frac{(1/2)\rho g A^2 \omega^2}{d[F^2 + \omega^2 (b_r + b_a)^2]} \qquad (2.68)$$

According to Farly, the maximum output is obtained if the power take off is adjusted so that $b_a = b_r$. The input power is:

$$P_{in} = \frac{1/4\, \rho g^2 A^2 W}{\omega} \qquad \text{where: } A = \text{amplitude}, \; W = \text{effective width} \qquad (2.69)$$

Since $P_{in} = P_{out} * S_t$, where S_t is the total area of the raft:

$$W = \frac{S_t \cdot k^{3/2} \varrho^{1/2}}{d(F^2 + k\varrho)} \qquad \text{where } \varrho = \varrho_f (b_r + b_a)^2 \qquad (2.70)$$

Figure 27 shows a typical power output function W as a function of the wave period for several values of the compression foce N. A broad response is obtained covering a range of 7 to 15 seconds. The influence of N is clear: tension can improve the effective width, and thus the power output. If N and d ($=m/\rho$) are constant, then the effective width is only dependent on S_t. So, if S_t is doubled (no matter the length or the width of the construction is doubled) then W is doubled too. This in contrast with a articulated raft, where, under certain circumstances W is proportional to $l^{\frac{1}{2}}$.

The effect of changing the effective depth of the raft is that for deeper rafts the maximum effective width moves to longer wave periods and the response gets broader.

It can be seen in figure 28 that the continuous flexible raft with traveling wave has a superior absorption width to the hinged raft. This is because the radiation from all elements is in phase in the forward direction. For the same reason a smaller raft motion raft motion is needed.

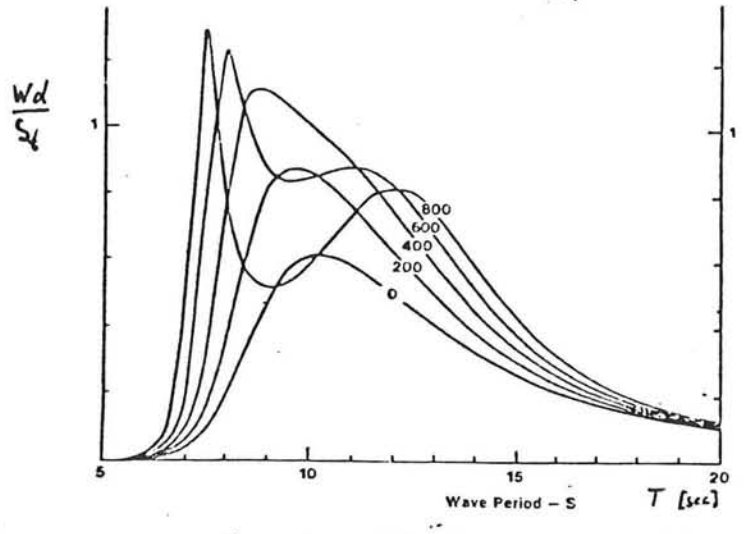

Absorption width W vs. *wave period from equation 2.66a* Wd/S_1 *is plotted for various values of thrust N in t/m width. Static stability limit N=820 t/m. d=20 m,* k_3 = $0.04\ m^{-1}$, $n=1.6$ GNm

Figure 27: Absorption-width, after Farley.

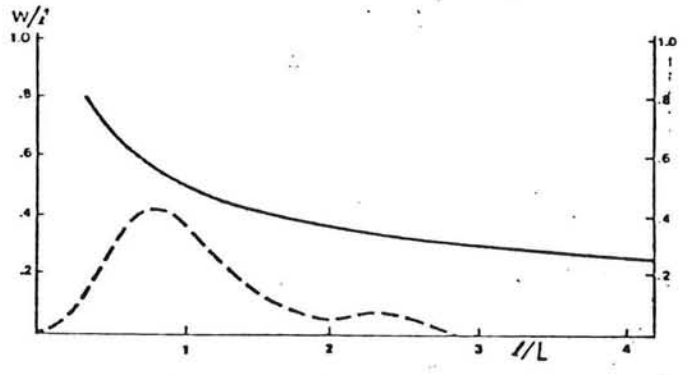

Absorption width W from wave scattering theory, at resonance with optimum damping, plotted against raft length l.

——flexible raft,--- articulated raft

Figure 28: Absorption-width of flexible and articulated raft (after Farley).

2.15.4 Theory of the articulated raft by P. Haren and C.C. Mei

The theory of Haren and Mei is a shallow water theory, where:

$$kd \ll 1 \tag{2.71}$$

$$kl = O(1) \tag{2.72}$$

$$k = \omega/c = \omega/\sqrt{gd} \tag{2.73}$$

$$p = Re(P\exp(-i\omega t)),\ P = i\rho\omega\phi. \tag{2.74}$$

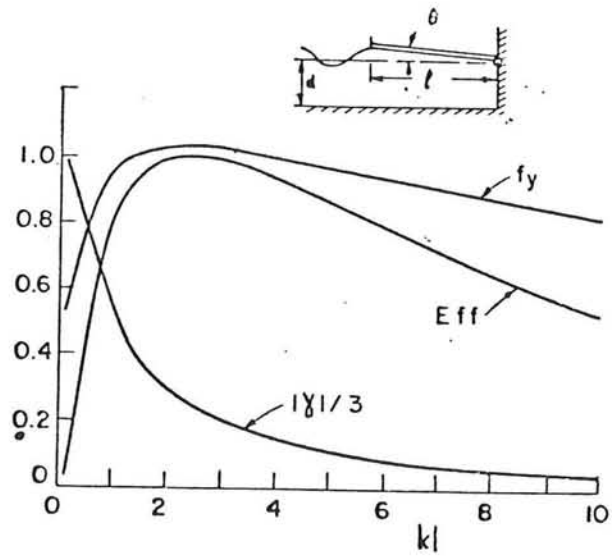

Figure 29: Raft hinged to a sea wall or to another infintely long raft, D/l= 0.01, d/l= 0.1, extraction rate α= 0.278, f_y is normalized vertical force at the hinge, $|\gamma| = |2\theta l/H|$.

Under the free surface, the velocity potential is governed by:

$$\phi_{xx} + k^2 \phi = 0 \qquad (2.75)$$

The velocity potential under the raft is governed by:

$$[\,(d-D)\,\phi_x\,]_x = i\omega Z \qquad (2.76)$$

where:

Z : amplitude of the bottom displacement from equilibrium position.
ρ : velocity potential.
D : common draft.

The total pressure on the bottom of the body is:

$$P_{total} = i\rho\omega\phi - \rho g Z + \rho g D \qquad (2.77)$$

(= dyn. pressure - added hydrostatic pressure + hydrostatic pressure at equilibrium).

At the edges of the raft, continuity of the mass flux and the dynamic pressure is required i.e.:

$$\phi|_+ = \phi|_- \qquad \text{all edges} \qquad (2.78)$$

$$d\,\phi_x|_+ = (d-D)\,\phi_x|_- \qquad \text{at the bow} \qquad (2.79)$$

$$(d-D)\,\phi_x|_+ = d\,\phi_x|_- \qquad \text{at the stern} \qquad (2.80)$$

$$\phi_x|_+ = \phi_x|_- \qquad \text{between two rafts} \qquad (2.81)$$

First they considered a two-dimensional raft, hinged to a vertical wall (see set-up depicted in fig. 29). The solution does not change if the raft is hinged to another stationary horizontal raft of infinite length, since for both there is no flux at x=l: u(l)= 0.

Since P is known, the dynamic momentum about the hinge can be :defined

$$M = -\int_0^{\ell} P(x) * (1-x)\ dx. \qquad (2.82)$$

Let "I" be the momentum of inertia of the raft about x=1. Assume that the effect of the energy absorber is to exert a damping force proportional to the angular velocity of the raft. If α is the damping rate, then:

$$I\ddot{\theta} = \alpha\dot{\theta} + M \qquad (2.83)$$

$$-\omega^2 I\theta = i\omega\alpha\theta + M \qquad (2.84)$$

The maximum efficiency can be obtained when the raft resonates, then the energy extraction is equal to the radiation damping.

The results are shown in fig. 29. When the draft (and hence inertia) is ignored, optimum efficiency can be obtained when $(1/k)^2 = 20/3$, thus $1/L = \sqrt{15}/3\pi = 0.4$. Haren has shown that a lower but flatter efficiency curve may be achieved by slightly increasing α. Haren and Mei extended the theory for more rafts (all of finite length). In this extended theory they involved also the costs, to calculate the optimum raft configuration. They considered the following optimality criteria, for each of which optimizations will be performed on l_i (length of raft i) and α_i (damping at hing i), keeping fixed: N (number of rafts), d (water-depth) and D (draft):

I. line spectrum ($k=k_p$).
II. rectangular spectrum ($k1 < k < 2*k1$).
III. double peak spectrum.

all for:

a. best efficiency with fixed total length (no costs involved).
b. best profit (price penalty on increasing raft length).

Category I: drastic simplification of single peak spectrum.
Category II: wave ranges from 4s to 8s were choosen, which is typical of North Atlantic conditions.
Category III: typical for North Sea conditions.

ad a. It is necessary to impose a constraint on the length of the rafts, otherwise one of the rafts would become infinitely long.
ad b. Assume that the cost of the device is proportional to the length l. So the cost of the device is (c*l), where "c" is the cost per unit width. Assume that the life-time of the raft is 20 years and the interest is 8%. Then the annual cost will be 0.1*c*l. The annual benefit is:

$$\text{benefit} = x * E_0 * \beta * \langle \text{eff} \rangle \qquad (2.85)$$

where:

x = price per kWh.
E = incoming wave energy
β = fraction of the generated energy

that can be used.

<eff> = efficiency off the conversion.

profit = (benefit) - (variable cost)

= ($xE_0\beta$<eff>) - (0.1 * c * 1)

Deviding by the maximum possible income (xE_c 3):

profit index = <eff> - Q1 (2.86)

Where Q is called the "cost factor".

Table 2.

Optimum design by criteria Ia and Ib.

Optimum designs by criteria Ia

$L_0 = d = 30$ ft; $T_p = 5.52$ s; $A = 1$ ft; $\ell = 450$ ft; $A_p = 171$ ft; $K_p d \frac{\ell}{L} = 1.1$

	3 rafts	4 rafts	5 rafts
l_1	1.828 (54.8 ft)	1.8226	1.8242
l_2	5.708 (171.2 ft)	5.9899	5.8295
l_3	7.464 (224 ft)	4.8379	4.9256
l_4		2.3502	1.5385
l_5			0.8823
α_2	0.6704(1.125×10^6 lb)	0.667	0.6497
α_3	2.406(4.036×10^6 lb)	1.149	1.078
α_4		0.9793	1.0361
α_5			0.4009
eff(K_p)	0.9667	0.9823	0.9826
$\|r_2\|$	0.6102 (1178 lb/ft²)	0.615	0.601
$\|r_3\|$	0.5725 (1105 lb/ft²)	0.465	0.472
$\|r_4\|$		0.139	0.143
$\|r_5\|$			0.036
$\|\theta_1 - \theta_2\|$	1.07 (0.036 rad)	1.07	1.09
$\|\theta_2 - \theta_3\|$	0.12 (0.003 rad)	0.144	0.148
$\|\theta_3 - \theta_4\|$		0.129	0.126
$\|\theta_4 - \theta_5\|$			0.029
% of energy extracted at node 2	96%	95%	95%

Optimum designs by criterion Ib

$L_0 = d = 30$ ft; $T_p = 5.52$ s; $A = 1$ ft; ℓ = variable; $A_p = 171$ ft; $Q = 0.0025$ ft^{-1} $kd \cdot \frac{\ell}{L} = 1.1$

	3 rafts	4 rafts
l_1	1.60 (48 ft)	1.60
l_2	3.86 (115.8 ft)	3.91
l_3	1.68 (50.4 ft)	1.62
l_4		0.0001
l_T	7.14 (214 ft)	7.13
α_2	0.269 (4.51×10^5 lb)	0.272
α_3	0.473 (7.93×10^5 lb)	0.441
α_4		0.00022
eff(K_p)	0.806	0.813
eff(K_p) $- QL_T$	0.271	0.271
$\|r_2\|$	0.326 (629 lb/ft²)	0.327
$\|r_3\|$	0.248 (480 lb/ft²)	0.244
$\|\theta_1 - \theta_2\|$	1.48 (0.049 rad)	1.47
$\|\theta_2 - \theta_3\|$	0.40 (0.013 rad)	0.41
$\|\theta_3 - \theta_4\|$		0.0002
% of energy extracted at node 2	89%	89%

The tables show very clearly that the device with the highest efficiency is not the one with the best profit. See table 2, 3, and 4. In all cases the most efficient device has the longest raft at the end, and the shortest at the beginning. The device with the best profit has the longest raft somewhere in the middle.

The influence of kd on the efficiency can be seen in figure 30 for case I and II.

Its obvious that the efficiency and the profit will decrease when the cost factor will increase. The profit can be negative as is showed in the table of figure 31.

Haren and Mei selected a sample raft-train with dimensions already optimized according to the shallow water theory and the criterion 1(a) and performed the calculations for arbitrary water depth using the finite element method.

Table 3.

Optimum design by criteria IIa and IIb.

Optimum designs by criterion IIa
$L_0 = d = 30$ ft; $\ell = 450$ ft

	3 rafts	4 rafts	5 rafts
l_1	1.36 (40.8 ft)	1.56	0.88
l_2	5.72 (171.7 ft)	7.08	2.52
l_3	7.92 (237.5 ft)	3.78	4.77
l_4		2.57	4.55
l_5			2.28
α_2	0.317 (5.31×10^5 lb)	0.508	0.0333
α_3	1.550 (2.6×10^6 lb)	1.551	1.613
α_4		0.931	0.177
α_5			0.986
$\langle \text{eff} \rangle$	0.960	0.967	0.983

Optimum designs by criterion IIb
$L_0 = d = 30$ ft; ℓ = variable; $Q = 0.0025$ ft^{-1}

	3 rafts	4 rafts	5 rafts
l_1	1.32 (39.5 ft)	0.89	0.76
l_2	3.67 (110.2 ft)	1.39	1.06
l_3	1.62 (48.7 ft)	2.86	2.43
l_4		1.49	1.32
l_5			0.97
α_2	0.156 (2.61×10^5 lb)	0.069	0.057
α_3	0.391 (6.56×10^5 lb)	0.820	0.475
α_4		0.308	1.153
α_5			0.191
$\langle \text{eff} \rangle$	0.792	0.793	0.795
$\langle \text{eff} \rangle - QL_T$	0.296	0.302	0.304

Table 4.

Optimum design by criteria IIIa and IIIb.

Optimum designs by criterion IIIa
$L_0 = d = 30$ ft; $\ell = 450$ ft

	3 rafts	4 rafts
l_1	0.65 (19.6 ft)	0.43
l_2	6.94 (208.2 ft)	3.63
l_3	7.41 (222.2 ft)	3.49
l_4		7.44
α_2	0.032 (5.35×10^4 lb)	0.0048
α_3	19.5 (3.26×10^7 lb)	1.553
α_4		1.865
$\langle \text{eff} \rangle$	0.864	0.876

Optimum designs by criterion IIIb
$L_0 = d = 30$ ft; ℓ = variable; $Q = 0.0025$ ft^{-1}

	3 rafts	4 rafts
l_1	0.45 (13.6 ft)	0.45
l_2	2.65 (79.4 ft)	1.04
l_3	0.02 (0.6 ft)	0.79
l_4		0.96
α_2	0.0030 (4.85×10^4 lb)	0.0032
α_3	0.39 (5.08×10^6 lb)	1.57
α_4		1.73
$\langle \text{eff} \rangle$	0.564	0.576
$\langle \text{eff} \rangle - QL_T$	0.330	0.333

In figure 32 the curves for efficiency versus k-times the average raft length (is constant; 150m) are presented. The two theories give remarkable close results. The effect of increasing depth does not change the efficiency materially. This observation gives further evidence that for a surface floating body with a shallow draft such as a dock or a platform whose horizontal dimensions are comparable to the wave length, shallow water theory gives a good rough approximation of the performance of the floating object.

The conclusions taken by Haren and Mei are:

1. From a simple shallow water theory two or three rafts are adequate for a train and further addition of rafts does not help materially.

2. The ideal efficiency is comparable or even better than Salter's cam, while the horizontal and the vertical mooring forces are much less.

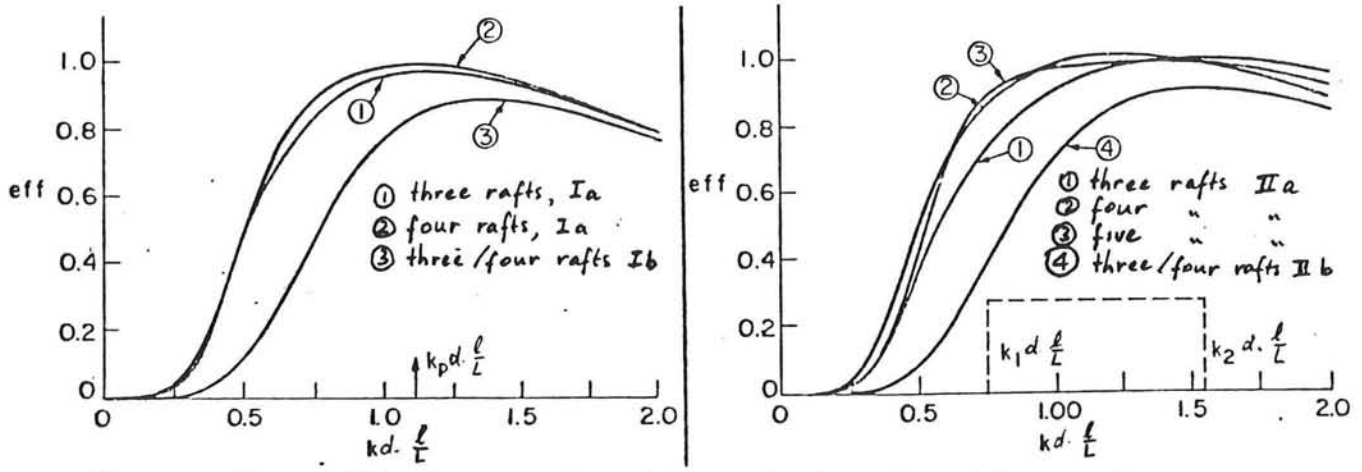

Figure 30: Efficiency of optimum design for line and rectangular spectrum.

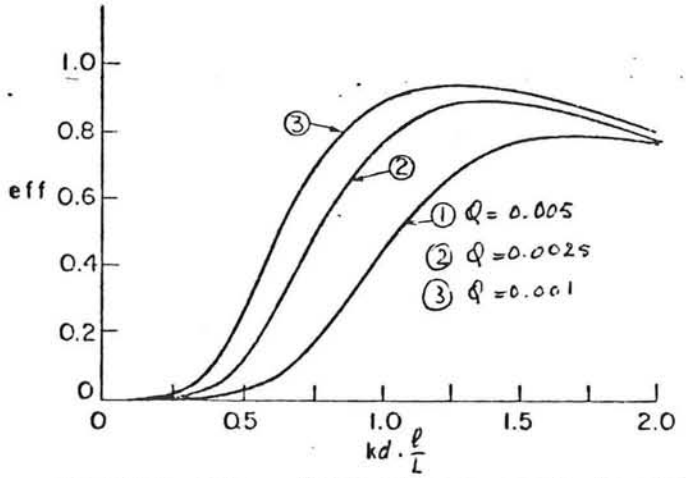

Effect of Q *on the optimum design of three-raft train by Ib*
$L_0 = d = 30$ ft; ℓ_7 = variable; (5.52 s)

	$Q = 0.001$	$Q = 0.0025$	$Q = 0.05$
l_1	1.6875	1.59577	1.48816
l_2	5.68933	3.84635	2.92351
l_3	1.8342	1.69347	1.27941
α_2	0.46582	0.26805	0.17696
α_3	0.69493	0.48378	0.23989
eff (k_p)	0.9045	0.80609	0.64882
eff $- QL_7$	0.62826	0.270922	−0.204942

Figure 31: Effect of cost factor Q on efficiency and optimum design of a three-raft train.

3. For the same wave length, the effect of water depth is weak. This is also found for Salter's cam.

4. For a sample double-peaked spectrum it is most cost-effective to extract energy from the short wave-peak.

In addition, Haren and Mei concluded:

> Clearly the economical considerations made here are the most rudimentary, and additional factors such as cost of energy absorbers, transmission line, local labour, etc., should be involved in a cost-benefit analysis. Not all of these factors can be reliably estimated at present, and future technical and economic development can change these estimates. With these reservations, from the

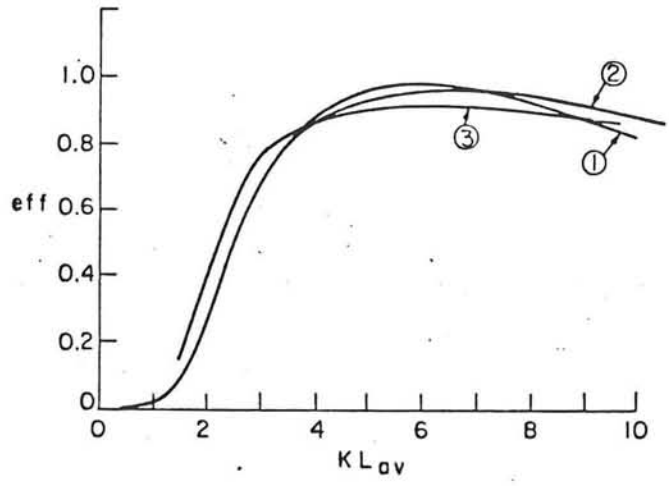

Figure 32: Comparison of efficiency for shallow and deep water theories for the optimal three-raft train. (1) d=30ft, shallow water theory, (2) d=30ft deep water theory, (3) d=120ft deep water.

present study we (Haren and Mei) feel that the raft is problably the best of all designs known to use. Nevertheless, the high cost of construction can render the benefit negative if the objective is to generate electricity. However, one cannot rule out other applications of this power device, such as desalination of water. Further cost reduction is necessary by using three-dimensional arrays of rafts as was orinally proposed by Cockerell and Hagen.

Chapter III

MOORING

There are two main components to a mooring system:
- -anchors.
- -mooring lines.

3.1 ANCHORS

Presently, a range of drag, deadweight and piled equipment is available for anchoring, of which the dimensions are governed by present market requirements.

The dominating parameters which govern the performance of an anchor lie undoubtedly in the soil composition of the sea bed. If the bottom contains rock at or near the surface then the choice becomes very limited to either rock piles or deadweight anchors. The efficiency of all other current means of anchoring is totally dependent on soil conditions and an assessment of anchor holding capacity. Hence, the dimensions of an anchor must be determined for each particular site. An anchor suited for all possible locations does not exist.

The largest size of an individual anchor which currently exists is considerably smaller than required for open sea conditions. Using several smaller anchors instead of a single large one might be possible, but may have economic penalties.

A recently developed anchor (patented by Shell) is shown in figure 33. For penetration of the anchor into the bottom, the water must be pumped out of the cylinder and due to the hydrostatic water pressure, the anchor will penetrate into the soil. This anchor will probably facilitate operation in deep water, unless the seabed is to hard (removal as well as installation of the anchor). The height of the first types reaches from 5 to 10 meters having a diameter of 3.8m. They can resist forces in-horizontal and vertical direction.

3.2 MOORING LINES

There are three categories of mooring lines currently available although stricly speaking only two are widely used for mooring to anchors. These are chain and wire rope.

The third, man made fiber rope, is used extensively for above-water moorings of ships to quays and to single buoy moorings. Sea bed anchoring rarely exists. The properties which man-made fiber ropes have to offer make them worthy of

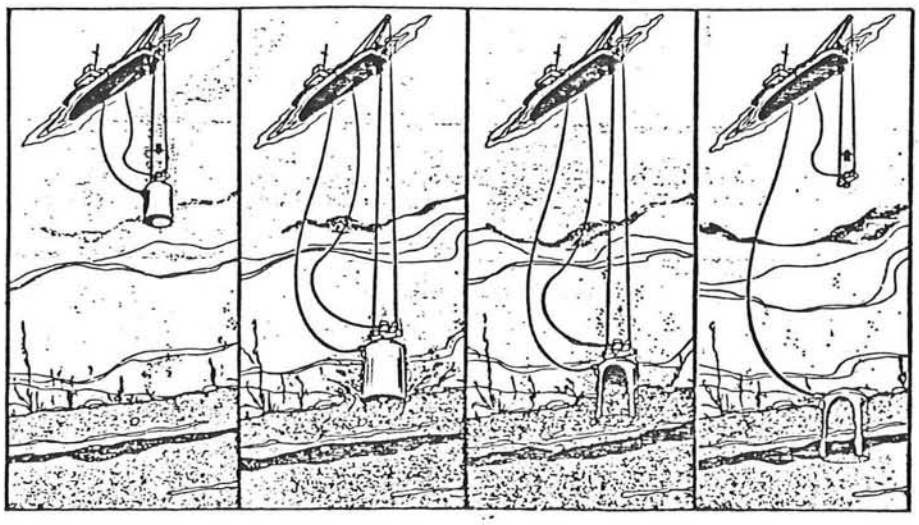

Figure 33: Anchor, developed by Shell, which can penetrate or removed by low or high pressure in a cylinder. (After Technisch Weekblad nr 33/34 1983).

serious consideration. Since the introduction of nylon fiber in 1940 followed by polyester, polypropylene and polyethylene, the use of these fibers has grown dramatically. They are now used almost exclusively instead of the natural fibers hemp, manilla and sisal. They are not susceptible to bio-degradation and the quality of raw material can be carefully controlled. The increased strength offered by man-made fibers allows smaller more manageable sizes. Also their capacity for storing strain energy is relatively high.

Chain is the traditional mooring to anchors and is most widely used throughout the marine industry. However, the offshore industry is tending to use wire ropes instead of chain: the advantages being ease of handling and of saving weight.

The difference in weight per unit length between chain and wire rope is evident. For example:

wire rope: ϕ = 28 mm, F = 506 kN, mass = 328 kg/100m
chain: ϕ = 30 mm, F = 524 kN, mass = 2000 kg/100m

So the weight of the chain is six times more than a comparable wire rope. One consequence of a heavier mooring line is an increase of the required breakwater buoyancy. (For example, this can lead to problems for a floating tire breakwater: a local extra bouyancy would be needed.) Another effect is the influence on the breakwater motion, which will be discussed in the next section.

Although chain can have a life-time of 20 years or more, its life-time can be reduced to only a few years under adverse conditions. The past development has been constrained by handling and storage considerations. With long maintenance free life of increased importance there is scope for a new approach to design.

No mooring line is ideal in all respects, and the final choice will depend upon the accumulation of more detailed knowledge, especially of the load extension characteristics

and the fatigue properties. Other problems include: corrosion fatigue of steel wire ropes, the validly of accelerated testing, failure at terminations and compliant moorings with taut moorings with taut elastic properties.

3.3 INFLUENCE OF THE MOORING SYSTEM ON THE WAVE ATTENUATION PERFORMANCE

The mooring will influence the motion of the breakwater. As can be seen in section 2.6, there is a clear relation between breakwater motion and the wave attenuation performance: the larger the breakwater motion (specially the surge motion), the more wave energy will be transmitted.

3.3.1 Influence of the mooring stiffness

It is tempting to conclude that the breakwater motion will decrease with increasing mooring stiffness, and thus an increase of wave attenuation will take place. However, the situation is more complicated, because the mooring line with the breakwater forms a mass-spring system. This may cause an increase instead of a decrease of wave transmission with increasing mooring stiffness. A clear example is shown in figure 12:

> at $D/L=0.7$, a mooring system with $k/\rho gL=0.01$ results in $C_t=0.45$, while a mooring system with $k/\rho gL=1.00$ results in $C_t=1.0$.

Higher mooring stiffness $\xrightarrow[\text{NO!}]{?}$ Decrease of breakwater motion $\xrightarrow[\text{YES}]{?}$ Decrease of C_t

This report emphasizes breakwaters in deep water. Then, a slack mooring will be evident.

3.3.2 Influence of the mooring line on the wave attenuation performance

First, the influence of the weight of the line will be discussed. A larger weight of the mooring line will increase the natural period T_n of the breakwater.

In shallow water, according to Carr (2.7.1), an increase of T_n might improve as well as worsen the wave attenuation performance.

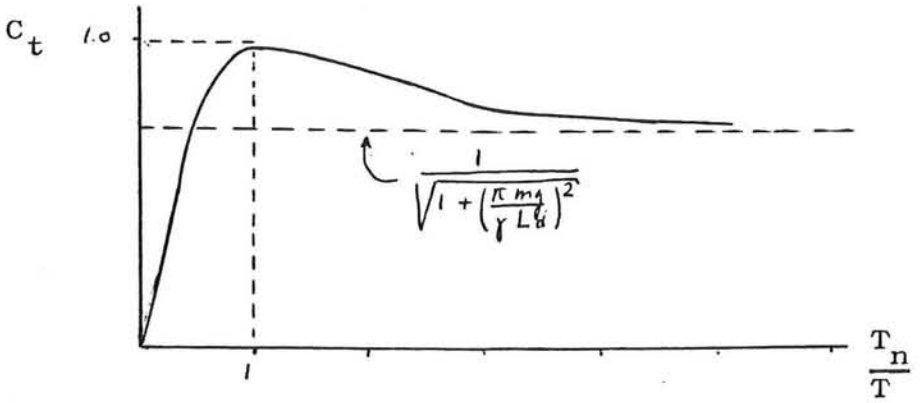

Figure 34: C_t as a function of T_n/T, according to the formula of Carr (shallow water).

As can be seen in figure 34, one must avoid a natural period which equals wave periods of waves which must be attenuated.

In deep water, Stiassnie (2.7.2) investigated the influence of the mass parameter for k=0 (thus slack mooring, which seems to be realistic in deep water). In figure 11 can be seen that an increase of the beam (and thus of the weight) of 10 times, improves the wave attenuation performance for $0.2 < D/L < 1.0$. So, according to this model, a slight improvement may be expected if the weight of the breakwater increases. The attachment of a heavy mooring line will not have exactly the same effect as the increase of the weight of the breakwater. Because the weight ot the mooring line will not have that much influence on the mass of inertia in horizontal direction of the breakwater.

Another effect of the mooring line is the damping caused by turbulence due to the motion of the line in the water. Since a chain will cause more turbulence than a wire rope, a chain is in favour in this aspect.

Chapter IV

WAVE ENERGY

4.1 INTRODUCTION

Wave energy is a derivative of solar energy input to the earth, which is accumulated on open water surfaces by the actions of the wind. The world-wide wave power resources can be related to the distribution of winds. Since early in this century there has been no lack of ideas on how to recover wave energy for useful purposes. In a classic 1892 paper, Stahl presented an exhaustive analysis of mechanical concepts for wave energy conversion. His classification is summarized in figure 35 .

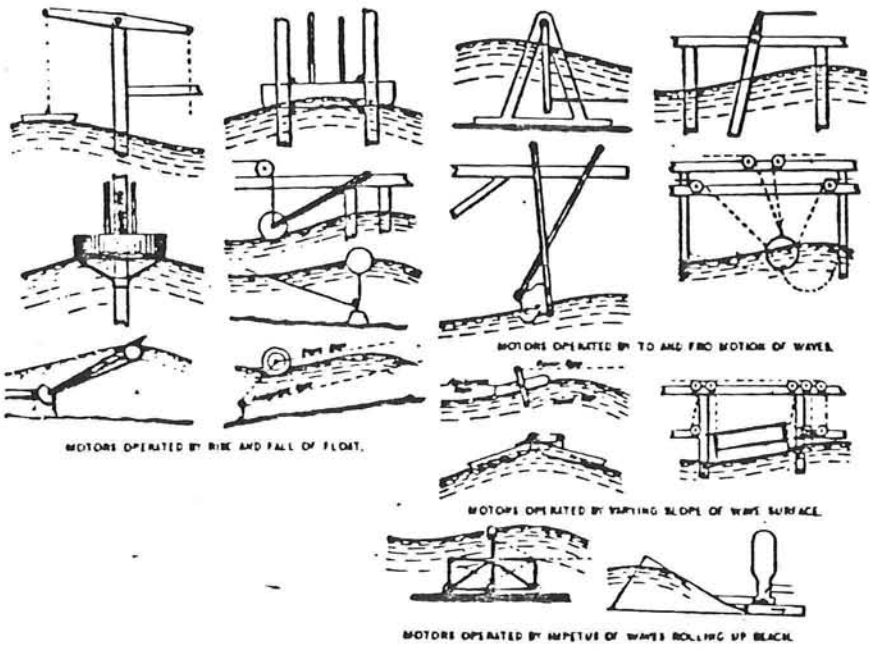

Figure 35: Illustration of the various kinds of devices which can use the motions of waves to develop power (from Stahl, 1892).

Leishman and Scobie estimated that from 1856 to 1973 over 340 British patents were granted on wave-powered generators. Many of these patents show that the concept of conversion is simple but not necessarily straightforward in engineering design and emplantment. A reason for the interest in wave

energy is the challenging potential of wave energy carried within the waves. Using linear wave theory, promising estimates of available wave power can be made. As can be seen in figure 36, energy from waves is available to some degree nearly everywhere at sea, though some regions are more favored than others in this regard.

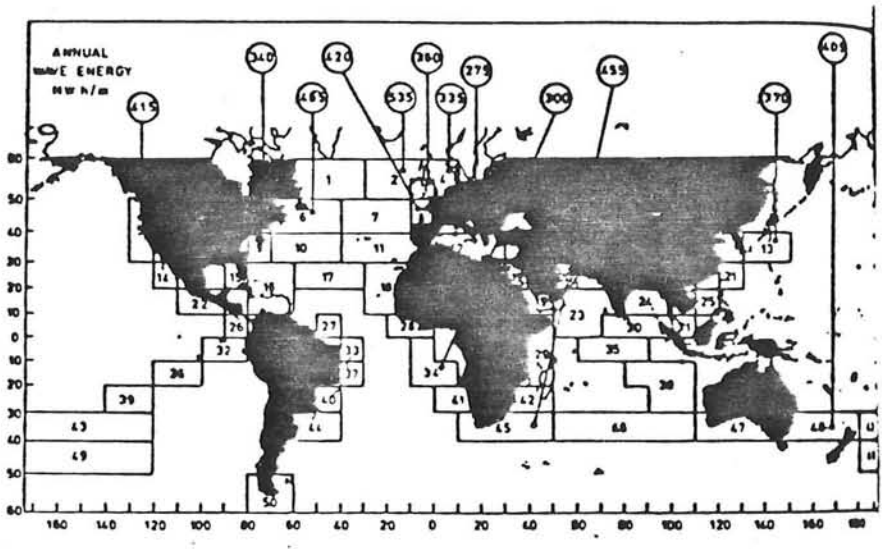

.—Annual wave energy, in megawatt-hours per meter of wave crest length, for various specific areas. (From Leishman and Scobie, 1976.)

Figure 36: Geographical distribution of wave power resources.

Wave energy facilities are most likely to be sited along the coastline, where logistic support can be provided more easily. This has another advantage since most of the nations energy is generated and consumed by coastal states. The highest concentration of energy plants is in the coastal area. For convenience the potential wave power densities for the remote ocean regions are shown in table 5.

Table 5.

Wave power density levels for the remote ocean regions.

[From Connors, Morrison, Mow, and Salter, 1976]

Subregion	Wave power density				
	Average power per midseason month (megawatts per kilometer)				Average of 4 midseason months (megawatts per kilometer)
	May	August	November	February	
A—Far North Atlantic Ocean	30	40	30	30	32.5
B—Mid-North Atlantic Ocean	30	22	50	40	35.5
C—Caribbean	3	3	21	30	14.3
D—West Indian Ocean	3	30	3	3	9.8
E—East Indian Ocean	3	30	3	3	9.8
F—East Pacific Ocean	3	3	12	12	7.5
G—Mid-Pacific Ocean	13	3	22	13	12.8
H—North Pacific Ocean	30	3	60	30	30.8

However, linear wave theory is too much simplified. As everyone knows waves are irregular in size and frequency. Taken into account this feature of waves, indicates that the predicted potential of energy using linear wave theory is an optimistic presentation of wave energy resources. Further this feature of waves complicates the wave energy extraction a lot.

It is clear that long and high waves are the most important energy carriers. So, it seems promising to station wave energy converters at sites where long and high waves frequently occur. However, high waves give rise to complicated construction problems of the converters. The converters have to be capable of withstanding the tremendous forces associated with occasional storm waves. The associated mooring forces have a significant bearing on the feasibility of wave energy converters. On the other hand, converters sited at protected sites must cover a large surface area to extract an amount of energy comparable to that of converters sited at rougher seas. So far research has not given a proper indication of the most suitable site conditions.

Another problem is the lack of wave data for proposed sites, especially measurements of wave directions.

No final conclusions concerning wave energy can be drawn yet, but undisputable features of wave energy are:

1. The potential of wave energy is enormous, but diluted.

2. Wave power is an inexhaustible resource.

3. Wave power cannot provide a guaranteed source of power.

4. Cost of a wave power generating system tend to be high.

4.1.1 The extraction chain

Now the attention will be directed to the energy extraction itself and to the utilization of the extracted energy. The problem of energy extraction is given in the figure below. The number of elements of the conversion chain depends on the scale of the project. Clearly every element of the conversion system introduces losses. So optimum efficiency is gained if the conversion chain is minimized with respect to the number of elements. An advantage of small scale projects is that they enable a more direct energy conversion. Besides, in a distant region, small scale wave energy conversion may be less expensive than conventional energy supply. So, any statement with regard to wave energy conversion depends on both the scale of the project and the site conditions. Generally, large scale extraction is not recommended: first of all, it can not compete with other energy supplies, besides, it imposes large problems on the

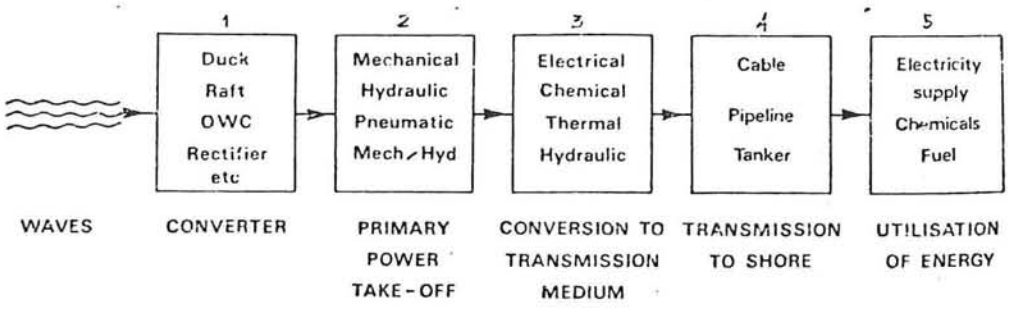

Figure 37: The extraction chain.

design of the conversion chain. A fairly detailed study of this option is presented in the Energy Paper number 42 presented by the department of energy (U.K.) (bibliography nr. 9).

4.2 WAVE ENERGY RECOURCES COMPARED WITH PRESENT ENERGY CONSUMPTION

In order to get an insight in the possible meaning of wave energy it is necessary to investigate its resource potential and the energy consumption. These subjects are judged differently by authors on wave energy. The opinion of Salter (1976) is the most optimistic one. At the "Energy from Oceans Conference", jan. 1976, Salter said:

> Instrument observations of waves in British waters, made by Draper of the British Oceanographic Data Service, indicated that the average power density in the North Atlantic is about 80 kW/m. Work in progress by Mollison and Buneman using more refined techniques suggests that it is actually more than 90 kW/m. The peak supply is in the winter.
>
> Visual observations from around the world have been collected by Lewis, Hogben and Lumb. They show that power densities in open oceans are nearly always greater than 10 kW/m. Draper presents a table which shows that a fetch of 100 km is sufficient to produce large enough waves to be worth harvesting.
>
> North Atlantic waves on a 500km front could produce all the electricity now used in the U.K. If ways can be found of transporting energy from offshore stations to the shore then the world wave power potential is several times the present world demand for all forms of energy.

A less optimistic point of view can be found in "Energy from the Ocean", Science Policy Research Division, Congressional Service, Library of congress, 1978:

The energy in ocean waves is being dissipated and renewed at the continuing rate of about five million megawatts, this is the theoretical extraction limit if wave energy conversion is to be a renewable process. The practical limit however, is much less since wave energy conversion facilities must be located where they can be supported logistically and where they are to be beneficial to not-too-far distant centers of population. In a view of these and other restrictions, a practical limit to wave power would problably not exceed about ten percent of the total renewable power, i.e., about 500,000 megawatts. At this rate, neglecting the efficiency of the conversion devices, the annual worldwide energy production from ocean waves could be about four billion kilowatt-hours. This is small compared with other energy resources. See table 6.

Table 6.

Total estimated ocean resources.

Type	—TOTAL ESTIMATED OCEAN ENERGY RESOURCES			—TOTAL ESTIMATED OCEAN POWER IN MEGAWATTS [Based on 1 yr's utilization]		
	Total potential	Current utilization		Total potential	Megawatts for 30 yr	Current utilization
Ocean thermal Conversion	10,000,000 MW	None.		10,000,000		None
Ocean wave power	500,000 MW	Negligible.		500,000		(1)
Ocean current power	50,000 MW	None.		50,000		None
Ocean tidal power	200,000 MW	248 MW.		200,000		248
Ocean wind power	170,000 MW (United States)	Negligible.	(U.S.)	170,000		(1)
Salinity gradient power	3,540,000 MW	None.		3,540,000		None
Ocean bioconversion	770,000 MW	Negligible.		770,000		(1)
Continental Shelf oil reserves	172,800,000,000 barrels	3,296,000,000 barrels per year.		33,500,000	1,116,000	640,000
Continental Shelf oil resources	520,000,000,000 barrels			101,000,000	3,366,000	
Continental Shelf gas reserves	168,500,000,000,000 ft³	9,532,000,000,000 ft³ per year.		5,600,000	186,000	310,000
Continental Shelf gas resources	2,693,300,000,000,000 ft³			89,000,000	2,966,000	
Offshore geopressured geothermal energy	3,000,000 MW (United States)	None.	(U.S.)	3,000,000	100,000	None
Offshore coal resources	508,300,000,000 tons	33,500,000 tons per year.		499,000,000	16,633,000	32,900
Offshore oil shale resources	1,000,000,000,000 barrels (oil)	None.		194,000,000	6,466,000	None
Offshore tar sands resources	200,000,000,000 barrels (oil)	Do.		38,800,000	1,293,000	None
Offshore uranium resources	29,400,000,000 g U^{235}	Do.		77,200,000	2,573,000	None
				1,056,330,000		983,148

Note: The United States consumes over 6,000,000,000 barrels of oil and about 21,000,000,000,000 ft³ of gas per year.

¹ Negligible.

Note: Total U.S. power capability equals 2,000,000 MW. Total U.S. electrical power capability equals 440,000 Mw. Total world power capability equals 8,200,000 Mw. Projected world power capability needed in year 2000 equals 15,000,000 Mw.

Table 7.

Conversion table: kWh and other units of energy.

Unit	kwh	j	Cal	W-yr	Btu
1 kilowatt-hour (kwh) equals	1	3.60×10^{6}	8.60×10^{5}	0.114	3,410
1 joule (j) equals	2.78×10^{-7}	1	.239	3.17×10^{-8}	9.48×10^{-4}
1 calorie (cal) equals	1.16×10^{-6}	4.18	1	1.33×10^{-7}	3.97×10^{-3}
1 watt-year (w-yr) equals	8.77	3.16×10^{7}	7.54×10^{6}	1	2.99×10^{4}
1 British thermal unit (Btu) equals	2.93×10^{-4}	1054	252	3.21×10^{-5}	1
1 metric ton of coal (=10^{6} g) yields	8,600	3.10×10^{10}	7.40×10^{9}	981	2.93×10^{7}
1 barrel (bbl) of oil (=42 gal) yields	1700	6.12×10^{9}	1.46×10^{9}	194	5.80×10^{6}
1 cubic foot (ft^3) of natural gas yields	.29	1.05×10^{6}	2.52×10^{5}	.033	1,000
1 gram (g) of U^{235} yields	2.30×10^{4}	8.28×10^{10}	1.98×10^{10}	2,620	7.84×10^{7}
1 gram (g) of deuterium yields	6.60×10^{4}	2.38×10^{11}	5.68×10^{10}	7.53×10^{3}	2.25×10^{8}

From: Wilson, Richard & William J. Jones, "Energy, Ecology, and the Environment," Academic Press, Inc., 1974.

Comparing the limit of wave energy conversion to the U.S. annual oil and gas consumption (i.e. 6,000,000,000 bbl oil and 21,000,000,000,000 ft^3 gas):

oil:	$6*10^9$ bbl	* 1700	= 10.2	$* 10^{12}$ kWh
gas:	$21*10^{12}$ ft	* 0.29	= 6.09	$* 10^{12}$ kWh
			16.3	$* 10^{12}$ kWh per year
	Wave energy:		0.004	$* 10^{12}$ kWh per year

So the total wave power at the coastlines all over the world is about 25 % of the U.S. oil and gas consumption.

In the near term, the most available and economically and technically exploitable ocean energy resource is oil and gas from the continental shelves. The offshore oil and gas resource base is very large and the technologies and economics of its development have been demonstrated throughout the world for a number of years.

So, ocean energy from renewable sources will not become a significant source of the world energy supply, but could be of major local importance in particularly favorable areas where the resource potential is significant or where conventional energy systems are not available or feasible.

In the long term, the exploitation of renewable oceanic power sources may rest on their economic competiveness when all internal and external costs of conventional energy sources are properly assessed. The uncertain availabilities and increasing costs of fossil fuels, together with the increasing costs of nuclear power plants, could advance the time when oceanic power achieves local competitive posture.

Chapter V

PONTOON

5.1 INTRODUCTION

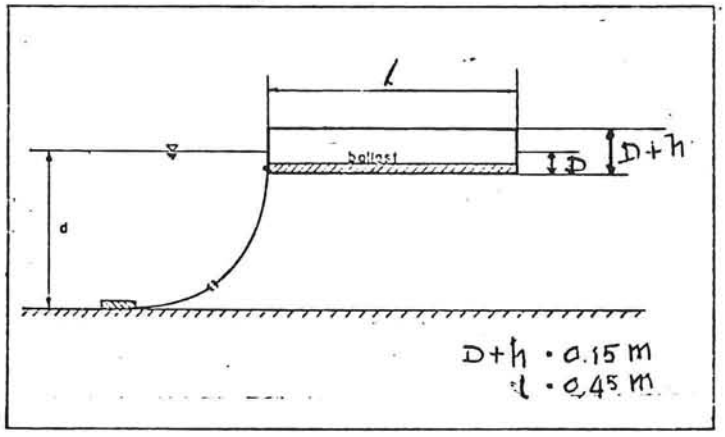

Figure 38: Pontoon breakwater (after Ofuya).

The pontoon, see figure 38 , is a massive structure of rectangular cross-section. Its depth of submergence depends on its mass. The concept of the design is based on the criterion of large mass. The natural period of its heaving motion depends on the mass and the elasticity of the pontoon. The undamped natural period T_n of heaving motion can be written as:

$$T_n = \left[\frac{2[M+M_a]}{F} \right]^{\frac{1}{2}}$$

in which:

M : mass
M_a : added mass in heaving motion
F : restoring force per meter immersion

An increase of mass produces an increase in the natural period of oscillation. But the metacentric height $\overline{GM}$, which determines the stability of the floating body decreases with increasing mass. This feature imposes a limitation on the extent to which the natural period of the pontoon may be increased.

5.2 WAVE ATIENUATION CHARACTERISTICS

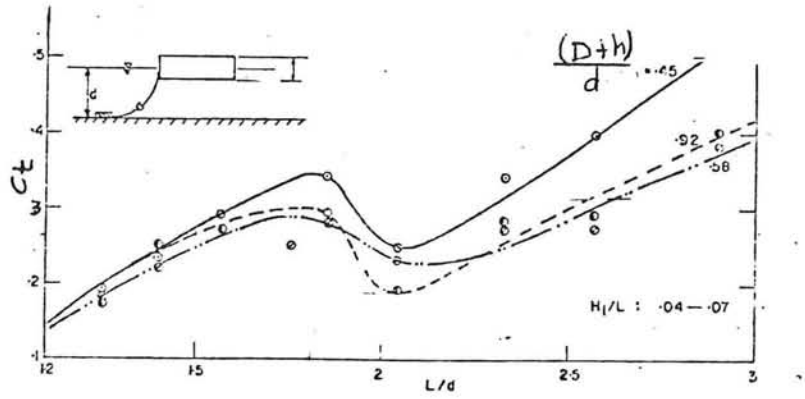

Figure 39: Pontoon breakwater wave attenuation characteristics (after Ofuya).

Figure 39 shows a plot for C_t against L/d for various depths of submersion. The occurence of "kinks" in the wave attenuation curves indicates the contribution of factors other than mass to floating breakwater performance.

Chapter VI

DOUBLE MODULE BREAKWATER

The double module breakwater consists of two massive units of rectangular cross-section which are rigidly connected at intervals. The design attempts to damp waves by wave reflection, turbulence and interference. The design also tries to combine large mass and large radius of gyration.

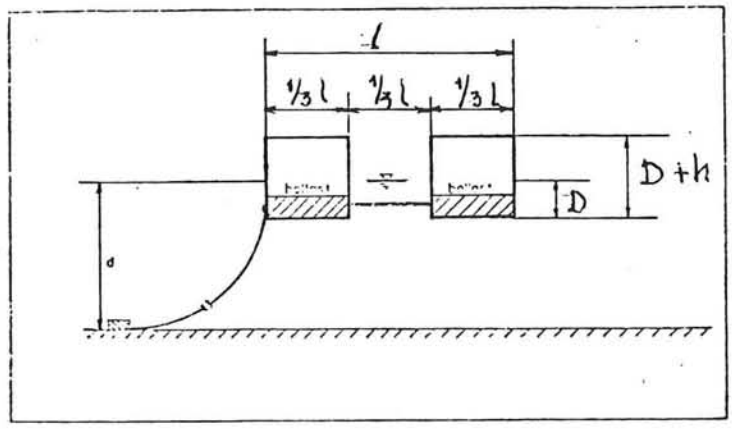

Figure 40: Double module (after Ofuya).

The pontoon and double module can function as floating piers as well as wave dampers. In that case the stability and performance of the structure under various loading conditions, the construction materials, and the choice of ballast would be prime considerations in the design of the pier.

6.0.1 Field experience

The Divisicn of Water and Harbors of the State of Alaska has embarked on an ambitious program of harbor development with the aid of several pontoon type breakwaters. They designed the so called " Alaska Type Floating Breakwater " which had to meet the following demands:

1. Ease of transportation.
2. Ease of assembly at the site.
3. Effective attenuation of a 1m wave.

4. Survival of a 2m wave.

The maximum wave height desired inside the small harbors is defined as 0.15-0.30m. The basic module of this breakwater is given in figure 41 .

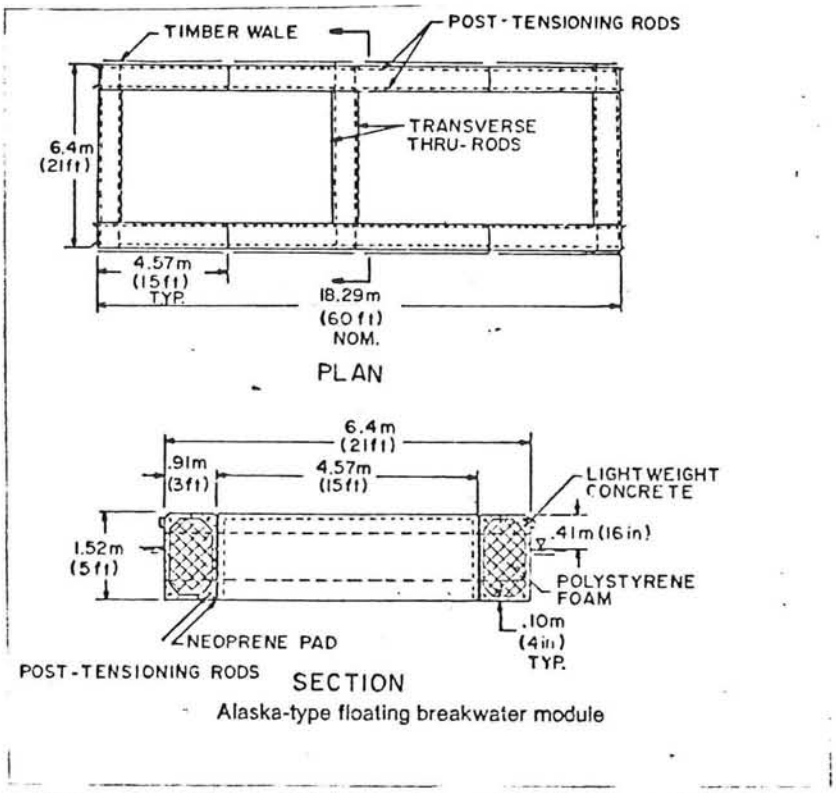

Figure 41: Alaska breakwater module.

The Alaska breakwater is fabricated from reinforced light-weight concrete pieces which are formed over a styrofoam core. Each peace is 4.6*1.5*0.9m with fifteen pieces joined together to form a module. The connections between the modules have been the "Achille's Heel" of floating breakwater design. The current design trend is to posttension the modules to form a continuous structure. Although the initial costs of the breakwater are higher than those of conventional assembling techniques, the final product should be cost effective. The assembly technique was a difficult procedure to carry out in field conditions, towing was also a difficult operation except at very low speed.

Full scale breakwaters have been installed at Tenakee (1972), Sitka (1973) and Ketchican (1980). The Tenakee breakwater has a length of 91m. The Sitka breakwater has a L-configuration and extents for over 279m.

The present locations are protected from the ocean. The prevailing winds at the sites are not directed towards the beam but tend to be parallel to the breakwater. Fetches are of the order of 8km at Tenakee and less than 1.6km at Sitka. The shorter leg at Sitka is open to a longer fetch and there is also a component of ocean swell which comes from that direction. The breakwater at Ketchican has the longest fetch of 14km.

Generally, specification of a realistic wave climate is one of the more perplexing problems facing the designers. At some sites, boat wake loading may be more important than wind generated waves. Users of the Alaska-type breakwater gave the following recommendations:

1. Standardisation of the breakwater dimensions could lead to lower design and fabrication cost.

2. Safety ladders should be provided where the free-board is more than 0.3m.

3. Navigation or radar targets should be placed at more regular intervals than those required by U.S. Coast Guard regulations.

4. Quality control in fabrication.

From the previous facts one can conclude that users of the Alaska type seem to be quite satisfied with the wave attenuation efficiency of the breakwater. The project is seen as an example of what can be accomplished in reducing wave heights within a given budget. In many cases the floating breakwater enhanced or provided additional habitat for birds.

6.1 WAVE ATTENUATION PERFORMANCE

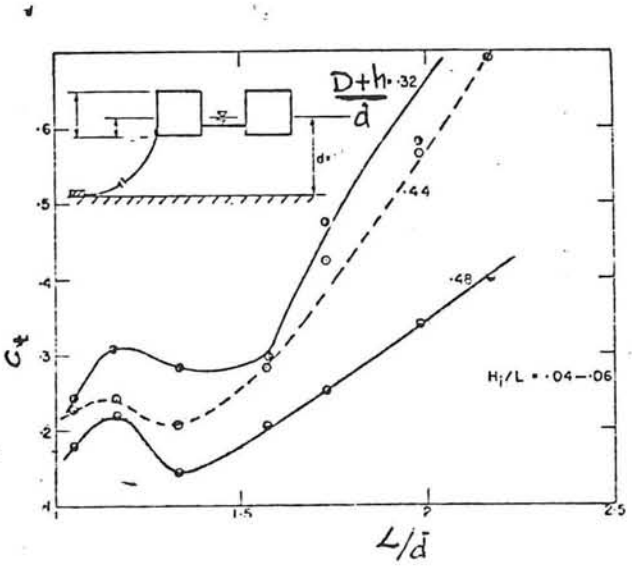

Figure 42: Double module wave attenuation characteristics (after Ofuya).

The figures show that the effectiveness of the breakwater in wave damping increases with increasing mass and slightly decreasing radii of gyration. This trend is similar to that of the pontoon.

6.2 TRANSPORTABILITY

Although ease of transportabilty was explicitly mentioned in the design goals, the use of heavy large concrete blocks did not enhance this feature. It is not surprising that problems were reported when setting out the anchors.

6.3 COST

Cost data of the Alaska breakwater are given in the following table. Note how the storm damage affects the cost of the Ketchican breakwater.

Table 8.

Cost of Alaska-type breakwaters.

Sitka	$ 1580.-/m	(1973)
Tenakee	$ 1400.-/m	(1972)
Ketchican	$ 4600.-/m *	(1980)

* including storm damage

Chapter VII

TWIN CYLINDERS

7.1 INTRODUCTION

The twin cylinder consists essentially of two circular alluminium cylinders rigidly connected at intervals by short pipes. See figure 43 .

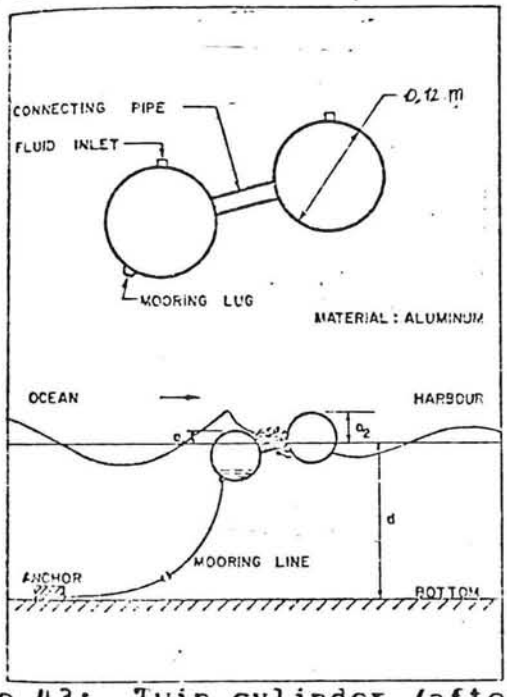

Figure 43: Twin cylinder (after Ofuya).

Its design is an attempt to attenuate wave energy mainly trough forced instability of the incident wave, to produce wave breaking and turbulence in the gap of the cylinder. The optimum depth of submergence a(1)/a(2) has been determined experimentally. For optimum wave attenuation with one cylinder filled, the submergence position had a value of a(1)/a(2)=0.4, and seemed to be independant of the incident wave length. With a filling fluid of higher viscosity and density than water, the oscillation characteristics and hence its wave damping performance, was considerabely increased.

7.2 WAVE ATIENUATION PERFORMANCE

The wave attenuation of the breakwater is discussed as a function of wave steepness, H/L, and the ratio of wave length to water depth, L/d. As exhibited in figure 44 an almost linear relationship exists between C_t and L/d for wave steepnesses in the range of 0.045-0.065.

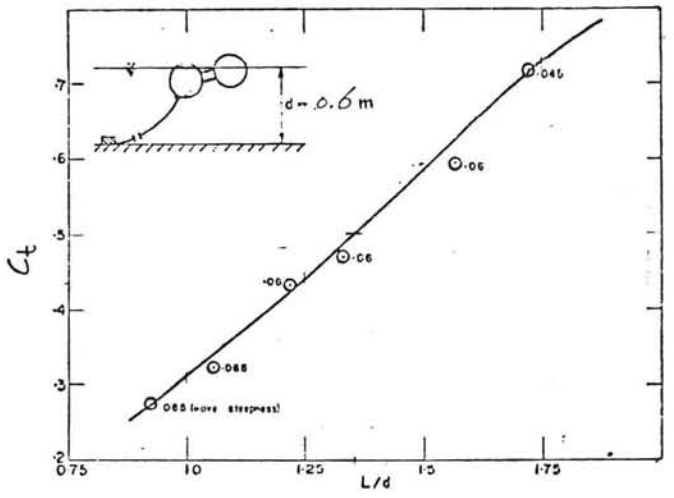

Figure 44: Twin cylinders wave damping characteristics (after Ofuya).

For large values of L/d the structure is an ineffective breakwater. However for L/d<1.3 the twin-cylinder achieves a transmission coefficient less than 0.5. Wave breaking in the gap between the two cylinders appeared to be the most important damping mechanism for small values of L/d. Furthermore the breakwater motions decreased ccnsiderably in the range of L/d in which the structure was found to be an effective breakwater.

Chapter VIII

PARABOLIC BEACHES

8.1 INTRODUCTION

The hinged and floating parabolic beaches are made of wooden beams of parabolic shape:

$$s = \frac{4x^2}{3d}$$

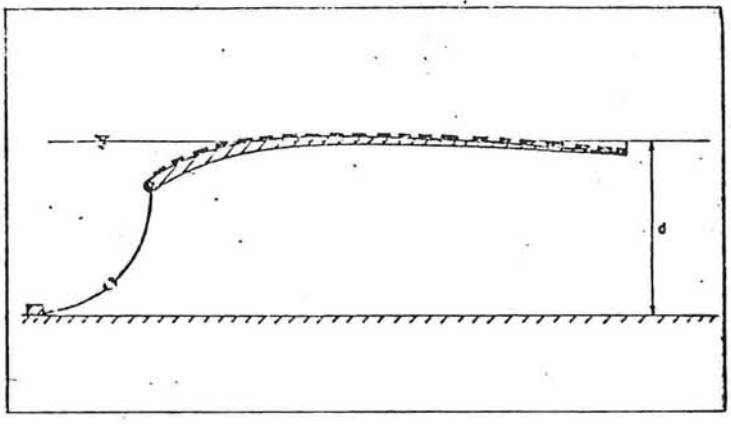

Figure 45: Floating parabolic beach (after Ofuya).

Wooden slats of equal size are laid over the beams. See figure 45 . The design attempts to cause wave damping by forced instability of the incident wave, production of counter currents by the motion of the breakwater, and energy absorption through the deflection of the structure. The performance of the beaches is evaluated in terms of L/d and their porosity. The porosity is defined as the number of slat gaps on the beach surface to the number of slats required to cover the entire surface.

8.2 WAVE ATTENUATION

Experiments showed that a hinged parabolic beach having porosity of 20% or less can effectively attenuate deep water and intermediate water depth waves. A beach having a porosity of 30% to 50%, may be suitable for damping deep water

waves. A beach having a porosity of more than 50% is ineffective as a breakwater.

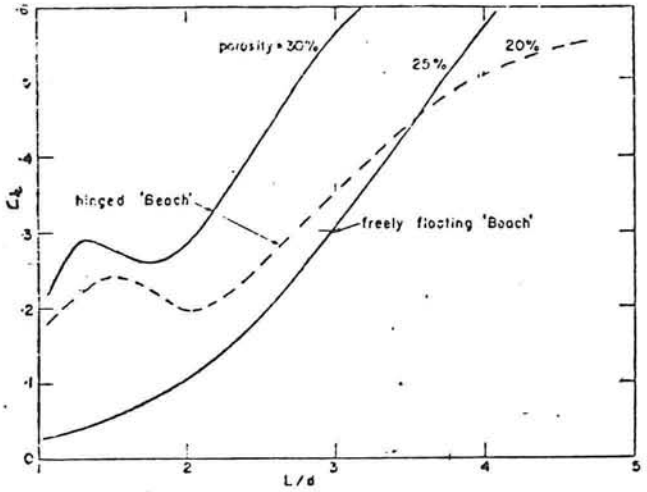

Figure 46: Parabolic beach wave damping characteristics (after Ofuya).

Figure 46 shows that the moored floating beach is more effective than the one hinged to the bottom, especially for deep water conditions. This difference in performance is attributed to the fact that the floating beach is interacting with waves in the region of large kinetic energy concentrations.

8.3 MOORING CHARACTERISTICS

Ofuya states that due to repeated loading and hysteresis of the deflecting wooden structure its energy absorbtion and strength characteristics would decrease with time. A rather large modulus of elasticity would be needed, hence a material other than wood would be required for the construction of the prototype beach. The hinged parabolic beach is referred to as an academical concept. It is hardly surprising that no practical information is available.

Chapter IX

PERFORATED HORIZONTAL PLATE BREAKWATER

9.1 INTRODUCTION

The breakwater has a simple rectangular geometry with perforations on its horizontal plate. Incoming wave energy is dissipated through the perforations. The construction materials are not mentioned by Raman, but the structure is assumed to be made of rigid materials. The research dealt only with the influence of the form of the structure on the wave attenuation. Mooring forces were measured as well.

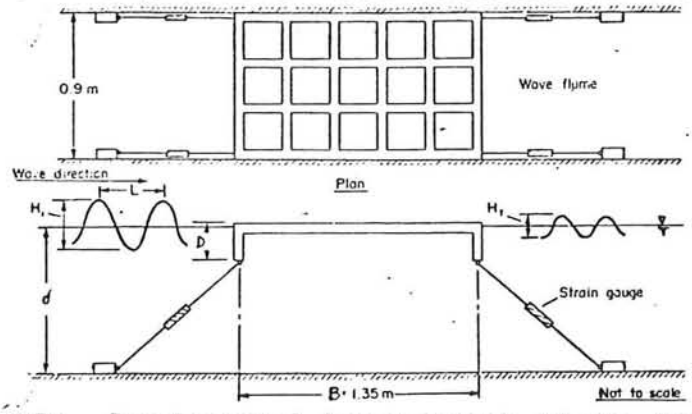

Figure 47: Perforated horizontal plate breakwater (after Raman).

9.2 WAVE ATTENUATION

Experiments were carried out to find the effect of wave steepness, relative length, B/L, and relative draft, D/d, of the breakwater on transmission and reflection coefficients. From figure 48 one can see that C_t decreases with increasing wave steepness. This observation is in agreement with other reported transmission characteristics.
The relative length of the breakwater plays a significant role in the wave attenuation performance. The damping characteristics are compared with those of the PT-1-Module and with the predicted curves by John's theory. See figure 49 . Note that a drop of relative breakwater length from two to one results in a corresponding decrease of C_t from 0.8 to 0.3. The better performance of the Perforated Horizontal Plate Breakwater could be due to its higher plan area ratio. The relative draft, D/d, of the structure has only a minor influence on the wave damping. As the relative water depth, d/L, and the wave steepness increase this effect becomes negligible, as can be seen from figure 50 .

9.3 MOORING CHARACTERISTICS

Figure 51 shows the variation of the dimensional peak mooring force $F/(\rho g L H^2)$ as a function of wave steepness, H/L, for two values of relative draft. The scope, S, had the value 3.75 during all the tests.

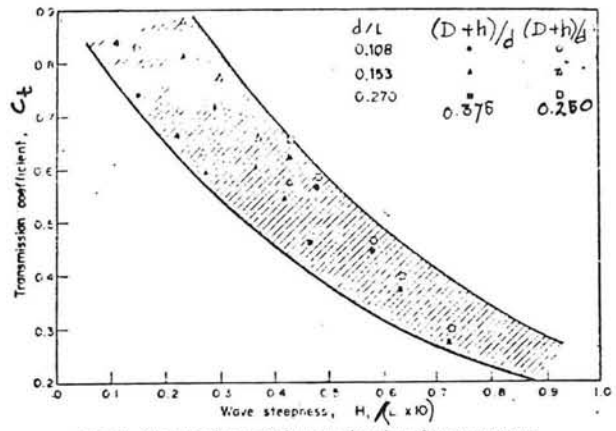

FIG. 4. Transmission coefficient as a function of wave steepness.

Figure 48: C_t as a function of wave steepness.

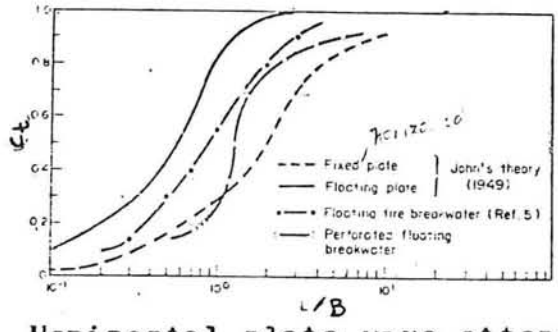

Figure 49: Horizontal plate wave attenuation characteristics compared with other types. (after Raman).

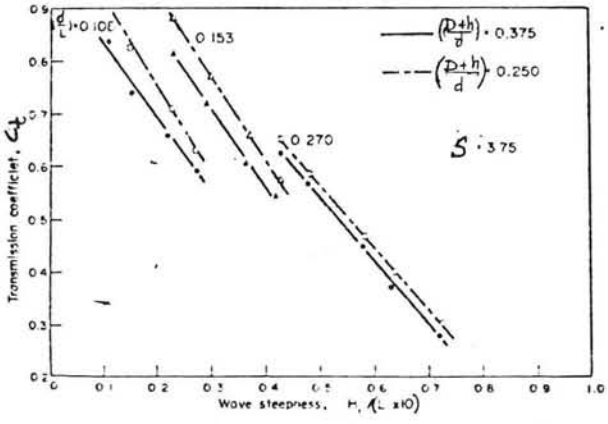

Figure 50: Transmission coefficient as a function of relative draft.

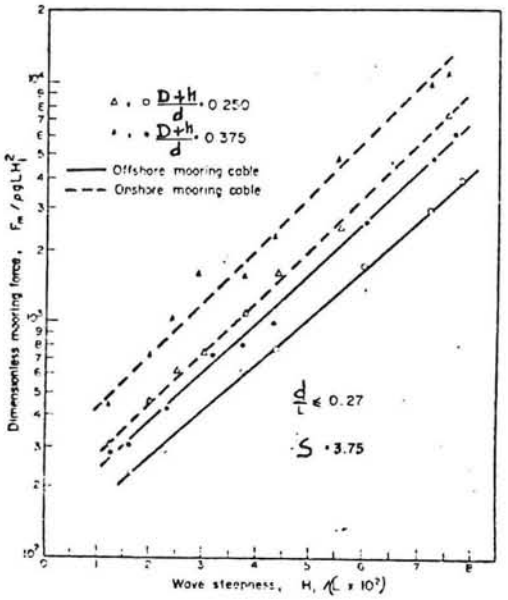

Figure 51: Mooring force characteristics as a function of H/L and D/d.

Comparing figure 50 with figure 51 one sees that the reduction of the transmitted wave height is closely followed by an increase of mooring force. Note that the mooring forces on the onshore side are larger than those on the offshore side.

9.4 TRANSPORTABILITY

Because of the perforations in the plate, towing will be difficult.

Chapter X

A-FRAME BREAKWATER

10.1 INTRODUCTION

Massive, fixed breakwaters present problems of mobility and installation. The first floating breakwaters were designed according to the criterion of large mass, which resulted in rather ponderous structures. Ofuya investigated whether the criteria of large mass could be replaced by that of large moment of inertia involving only small increase of mass. For his investigation, Ofuya made use of the A-frame breakwater which consists essentially of a central thin vertical rigid curtain of wood, and two circular aluminium cylinders symmetrically located about a vertical curtain.

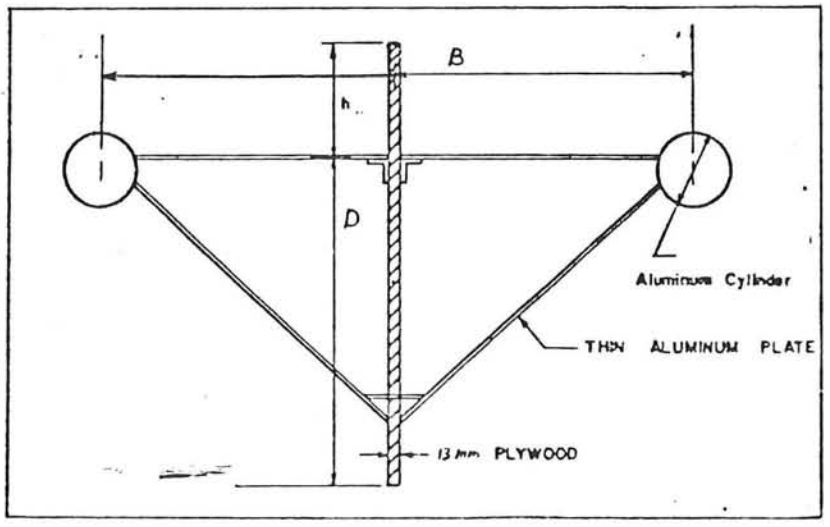

Figure 52: The A-frame configuration.

The cylinders are connected at intervals by thin rods to the vertical board. The depth of the vertical board below the water surface can be varied. The height of the curtain above the water surface is such that wave breaking cannot occur above the curtain. Variation of the cylinder spacing amounts to changes of the radius of gyration of the structure about a lateral axis through its center of gravity. A configuration with more cylinders is also possible.

10.2 WAVE-ATTENUATION CHARACTERISTICS

10.2.1 Influence of mooring line location and of frequency

Two different attachment points of the mooring-line were tested. The method of mooring which caused the largest C_t values was abandoned because the system caused more irregular and jerky breakwater motions. See figure 53.

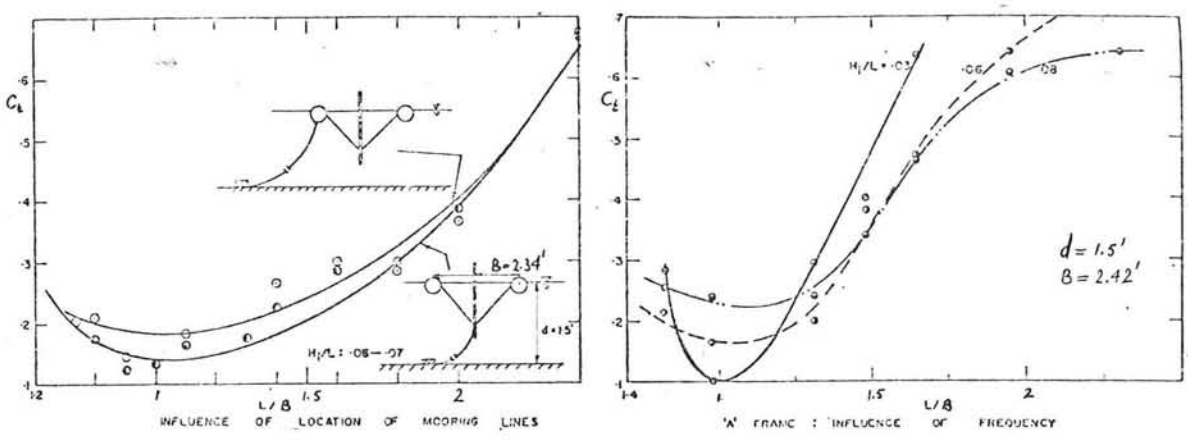

Figure 53: Influence of mooring line location and of frequency.

In fig. 53 can be seen that the optimum of wave attenuation is achieved for L/B=1 (for the given values of d and B). The explanation seems to be obvious: the two cylinders have a distance of one wave length to each other, so the vertical motion of the cylinders are in the same direction, consequently the vertical board remains in a more or less vertical position.

10.2.2 Effect of wave steepness

Figure 54 shows that the general trend is that C_t decreases with increasing wave steepness. For values of L/B between 0.9 and 1.2 deviate from this general trend. This may attributed to wave interference effects. No simple relationships are evident. (See fig. 54).

10.2.3 Effect of depth of vertical curtain

In theory the effect of changes in depth of the vertical curtain will be relatively small in deep water (when a certain depth is achieved), and greater in shallow water. The measurements show that in deep water an increase of D/d=0.23 to D/d=0.34 causes a clear decrease of C_t, an increase to D/d=0.47 has no effect, but in intermediate depth it has effect.

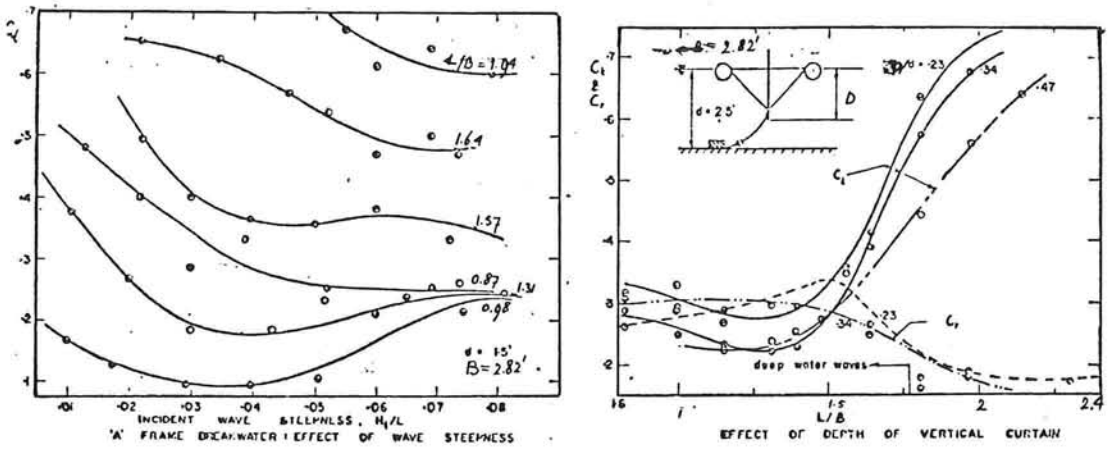

Figure 54: Effect of wave steepness and of depth of the vertical curtain.

10.2.4 Comparison of theory and experiment for C_t and C_r

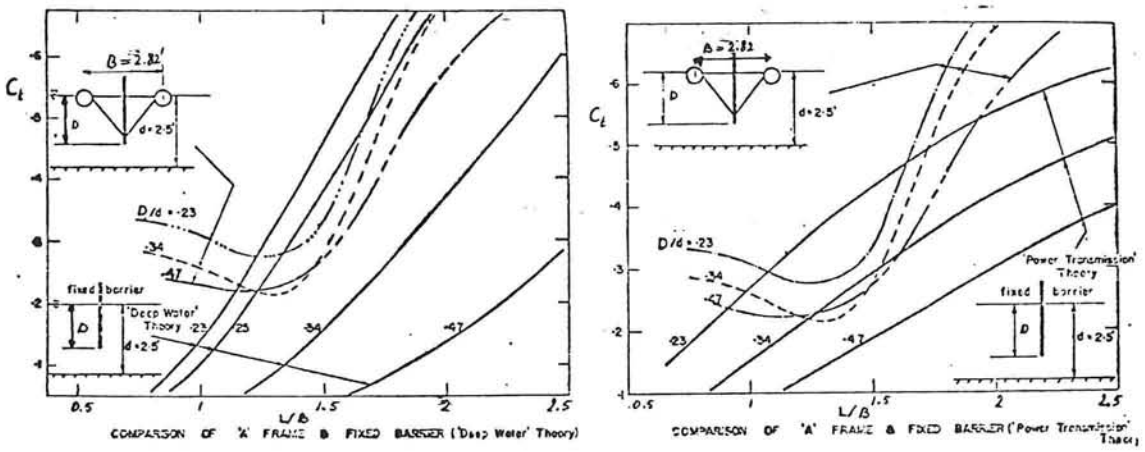

Figure 55: Comparison of theory and experiment for C_t.

Figure 55 shows plots of Ursell's "deep water" theory and Wiegel's "power transmission" theory, for waves transmitted past fixed barriers having equal drafts as the vertical curtain of the A-frame. Experimental results are also shown. The theoretcal values are much more sensitive to changes in D/d than they should be. The Ursell theory is good for D/d=0.25 and L/B > 1.2. But for D/d=0.47, the theoretical figures are much too optimistic.
Figure 56 shows plots of those theories, but now for the reflection coefficients. The reflection seems to be much less than the predicted values. It is obvious that the difference is caused by dissipation. It may be remarked that energy dissipation appears to be caused mainly by partial wave breaking due to the wave steepening effect of the cylinder on the seaward side of the system. So the longer the wave

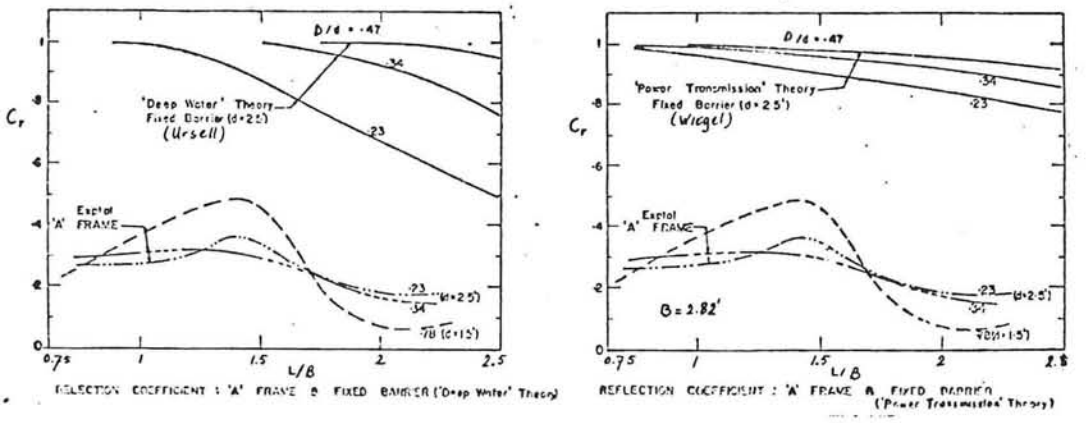

Figure 56: Comparison of theory and experiment for C_r.

length, the less the energy dissipation. There is only a vale at L/B=1.2 which is close to L/B=1 where the optimum of attenuation is achieved. That may be attributed to the one-wave-length distance between the cylinders, so that the vertical board remains more or less in a vertical position.

10.2.5 Four cylinder A-frame

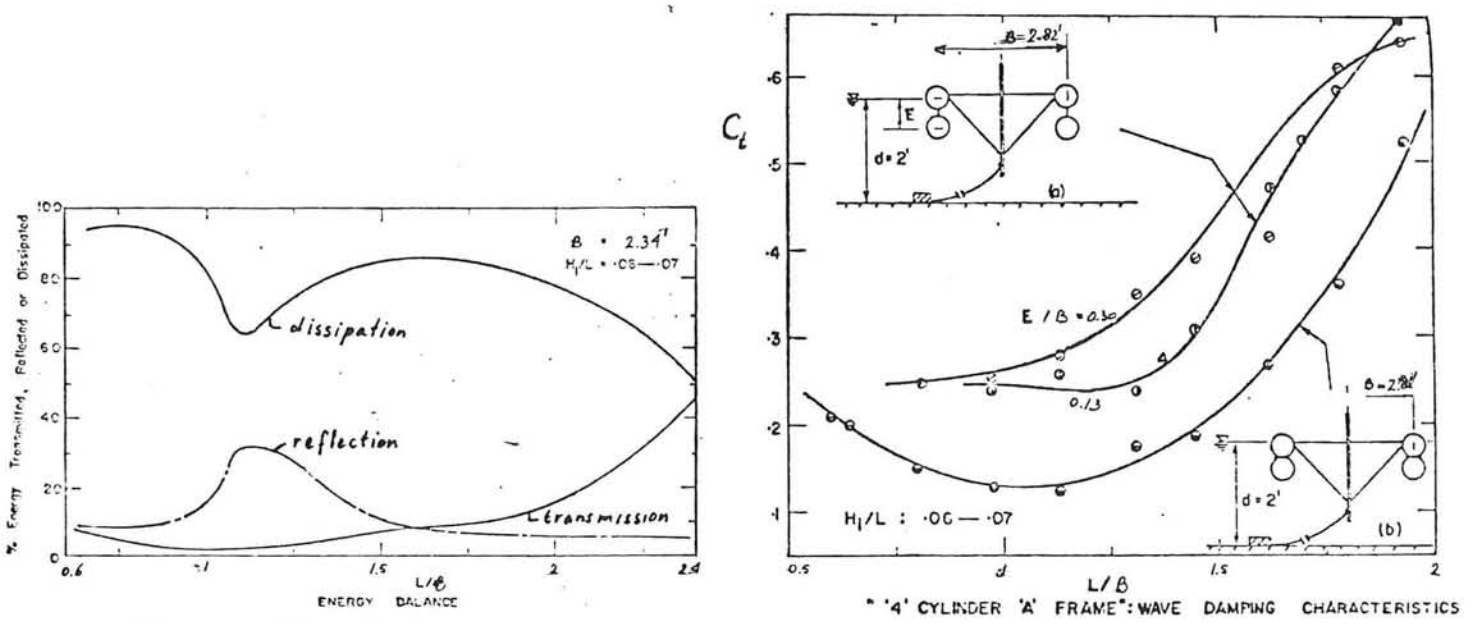

Figure 57: Energy balance and damping characteristics of the 4-cylinder A-frame.

Figure 57 shows the wave attenuation characteristics of both types. Wave damping by chain connected cylinders decreases with decreasing values of E/B. This may be partly attributed

to the fact that, with decreasing values of E/B, both cylinders become more located in regions of large kinetic wave energy concentration. Since both cylinders move independently, the waves generated by the lower cylinder augment those produced by the basic A-frame unit. At certain values of E/B, the structure moved towards the seaward direction and hence the mooring cable remained slack. The seaward movement, which made the measurements of mooring forces difficult, may be attributed partly to the inertial effects of the lower cylinders, or perhaps, to mass transport in the fluid due to finite wave effects. Greater effectiveness may be achieved by welding the cylinders, as shown in figure 57. Unlike the chain connected type, seaward movements did not feature the system. The jet effect of fluid emerging from the lower porous cylinders provides an additional source of energy dissipation.

10.3 MOORING FORCES

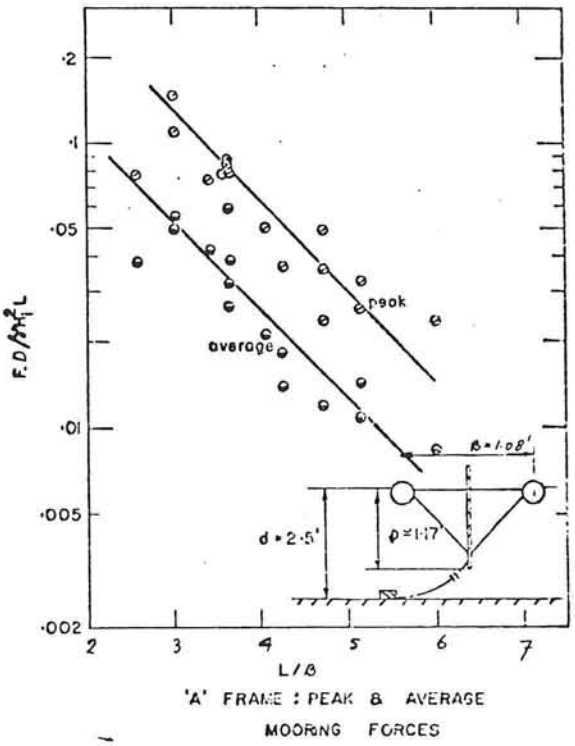

Figure 58: A-frame: peak and average mooring forces.

When L/B decreases, the mooring force will increase exponentially (see fig. 58). The scatter in the results may be partly attributed to the influence of wave reflection, wave steepness, variation of the damping factor, and, in particular to the variation of amplitudes of motion with time. The peak mooring forces are about 1.5 to 2 times the average forces.

10.4 TRANSPORTABILITY

No information about transportability was available, but floating transport does not seem to require much power, considering the cross-section of the A-frame. Since the A-frame is a reflecting breakwater, it is very important that the draft is large enough. If the A-frame breakwater must be used in deep water, we can see in figure 7 that the draft will have to be larger than 0.12 L to obtain C_t between 0.5 and 0.6 (theoretically, after Ursell and Wiegel). This may result in a very large draft, and hence transportation problems.

10.5 COSTS

During 1964 and 1965 an A-frame breakwater was built at Lund, British Columbia, having a total length of 110m. The costs were about $755 for the sections built in 1965. The maintenance costs have ranged between $5 to $10 per meter per year.

Chapter XI

THE OFFSET BREAKWATER

11.1 INTRODUCTION

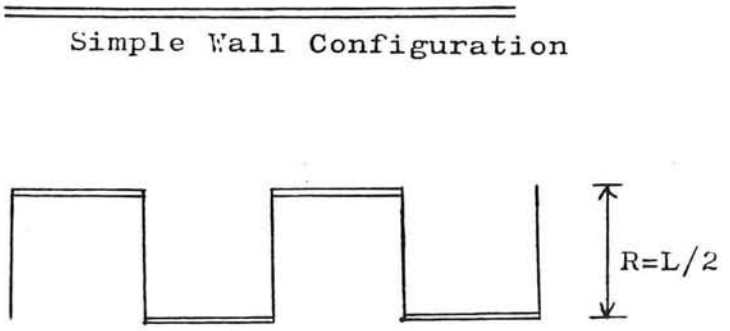

Figure 59: Plan view of breakwater design. Waves approaching from top of the page.

The offset breakwater configuration, being studied at the University of Texas at Austin, incorporates vertical reflecting sufaces oriented normal to the direction of wave propagation, and deplaced from each other one-half a wave length. See figure 59.

The offset configuration has the following design concept:

A simple rigid wall wil reflect more energy if it is penetrating deeper in the water, thus the less energy is transmitted past the structure, but the higher are the forces on the structure. When acted on by large waves, the forces required to hold a rigid wall in a fixed position, are of such a magnitude that it is impossible to anchor the structure so that a rigid wall is simulated. Displacements and rotations of the floating wall will occur. These motions act to generate waves in the lee of the wall, reducing its effectiveness as a breakwater. The offset configuration is supposed to reduce the mooring forces and to increase the wave attenuation performance because of the smaller motions. Unfortunately, in field conditions, the waves differ in wave length, so that the offset is not always one-half wave length. So a test using wind-generated waves is desirable.

The offset configuration has been patented.

11.2 WAVE ATTENUATION CHARCTERISTICS AND MOORING FORCES

11.2.1 Penetration

Generally, transmission coefficients were lowest for the greatest penetration and increased as the relative penetration decreased. When the wave length was twice the offset, differences in wave attenuation performance were very small, See figure 60.

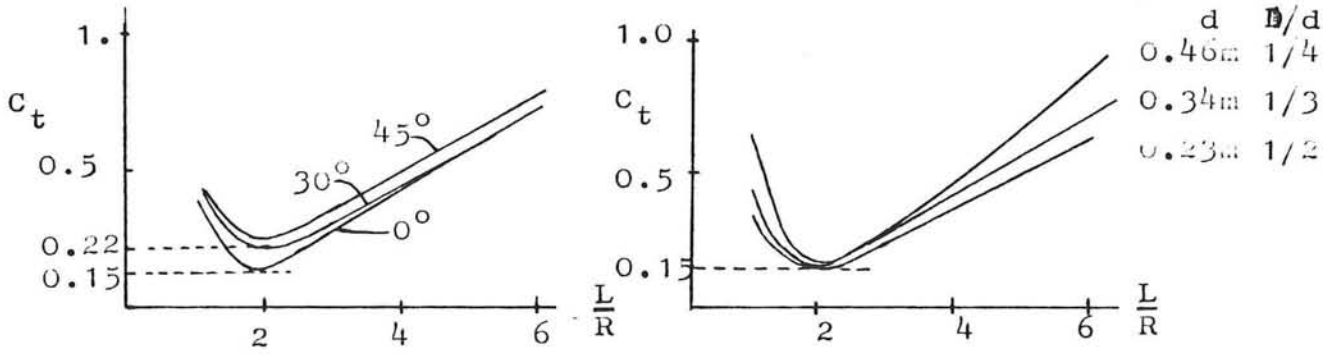

Figure 60: Relative penetration tests (left) and angle of incidence (right).

11.2.2 Anchor attachment

Attaching the mooring cables 1/6 of the model height from the top gave better results than the same distance from the bottom.

11.2.3 Angle of incedence

The long (horizontal) axis of the model was placed at angles of 30 and 45 degrees to the incident wave fronts. See figure 60.

11.2.4 Wind-generated waves

Moore et al wrote:

> Tests on these waves indicate that the offset breakwater is capable of extremely good wave attenuation performance, based on values for measured wave transmission. The situation on the windward side of the breakwater was complicated due to the influence of the reflected waves, but the leeward side was smooth and regular with no interference.

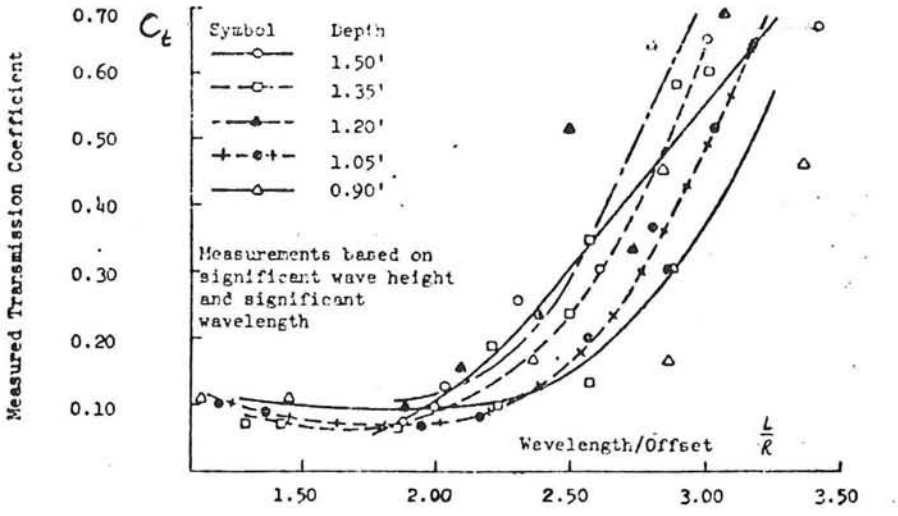

Figure 61: Transmission coefficients for wind generated waves.

When the models were designed, a wave length of one foot was considered the design wave length. Test results showed that for all tests where the value of the significant incident wave length was less than or equal to one foot, the model behaved well. See fig. 61. The minimum values for measured wave transmission coefficients are well below those reported for other floating breakwaters. In addition, this is the only test of floating breakwaters known by the authors (Moore et al.) where wind generated waves were used. The minimum recorded transmission coefficient as listed by the Navel Civil Engineering Laboratory was 0.20 under ideal conditions. There is a significant difference between results when models are tested in regular mechanically-generated waves and this test with wind generated waves. The transmission curve of the offset breakwater is compared with the transmission curve of a rigid wall. See figure 62.
The power transmission theory by Wiegel (2.5.3) was used to determine the curve for the rigid surface. The offset breakwater design agrees very well with the idealized model for all values up to the design wave length. Figure 62 shows that the offset design allows wave lengths up to 1.3 times the design before a transmission coefficient of 0.30 (which is considered acceptable in many cases) is exceeded.

Anchor forces were not measured. But to give an idea of the magnitude, we can use the analysis for F_o / F_R (see section 2.9). For example:

case I: an offset breakwater with a draft of 4 meters, a water depth of 15 meters and waves with a period of 4 seconds and 3.5 meters high, so that the wave length becomes 24.96 meters (offset=12.48m) results in:

$$F_R = 11.19 * \gamma A^2/2$$
$$= 11.19 * (1020 * 9.8) * (1.75)^2/2 \quad N/2m$$
$$= 85.63 \text{ kN/m}$$

$$F_o = 0.25 * F_R = 21.83 \text{ kN/m}$$

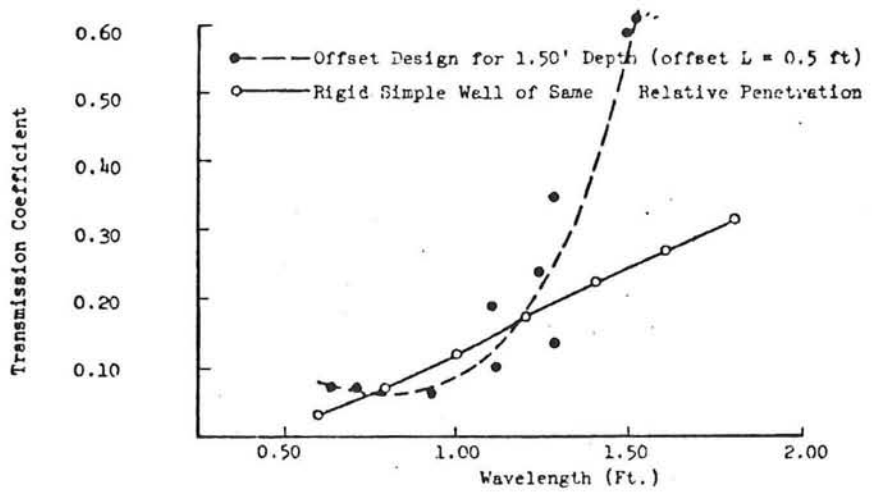

Figure 62: Comparison of the offset design with a rigid simple wall.

<u>case II</u>: as in case I, but now T=2 sec, so that L=6,24. And H=0.90 (max. steepness).

$$F_R = 39.36 * \gamma A^2/2$$
$$= 39.36 * (1020 * 9.8) * (0.45)^2/2 \quad N/2m$$
$$= 19.92 \text{ kN/m}$$

$$F_o = 0.21 F_R = 4.09 \text{ kN/m}$$

In practice the structure can make small movements, which will reduce the mooring forces. So the reported values are upper limits.

As mentioned before, wave attenuation of waves with a wave length of more than 1.3 times the design wave length will be small. This results in a considerable offset length related to the longest waves which have to be attenuated. In open sea, this can lead to an offset of more than 150m. This could be too expensive. The breakwater in case II, will not perform well for waves longer than say 8.5m, but having a small offset length it will be cheaper. There will be a optimum between the values found in case I and II.

11.3 TRANSPORTABILITY

There is no experience with transport but the best way seems to be floating transport. The features of transport are not very promising if the offset breakwater is used for open sea conditions, because of the large dimensions and the irregular shape.

11.4 COSTS

An offset breakwater is never built at full scale, so the costs are unknown. Cost are not very promising, because of the large sizes and the irregular shape of the structure.

Chapter XII

WAVE ACTIVATED TURBINE GENERATCR (POINT ABSORBER)

12.1 INTRODUCTION

This section is restricted to the "wave activated turbine generator" or "WATG". This type has been developed in Japan and is in limited operational use by that country for powering navigational buoys and lighthouses. In these devices, described by Masuda, the air above an internal free surface within a pipe is compressed and drives an air turbine which is coupled to an electric generatcr. Use of navigational buoys containing WATGs has started in 1965 by the Japanese Maritime Agency. Standard off-the-shelf models of the WATG with capacities of 70 watts, 120 watts and 300 units are available since 1974. A 500-Watt device was demonstrated in 1970, and a kilowatt unit was contemplated by Masuda.

The relatively small power output of the WATGs results from their simple and inexpensive construction. The device has a central pipe through a buoy. The waterlevel in the pipe changes as the pipe follows the up and down motion of the wave surface. The water in the pipe serves a piston which compresses the air in a chamber, forcing it through a nozzle at high velocity into a small air turbine. Details of the internal valve mechanism are shown in figure 63.
The U.S. Coast Guard has been examining several ocean energy conversion devices for potential use with aids to navigation. A Japanese-made WATG buoy was tested, located 22.5km east of Cape Henry, Virginia, where the buoy was moored in water having a depth of 22 meters. From Sept. 1973 till Aug. 1974 the power generated by the buoy has been monitored, during this period the average generated power was 5.75W. Sufficient battery charging power was developed to compensate for the power drain typical of most Coast Guard floating aid lanterns.

McCormick et al. performed an experimental study of a pneumatic type wave-energy device using a one tenth scale model in a wave tank at the U.S. Naval Academy. The measurements confirmed that the air velocity for operation of a turbine, which is excited by both the heaving and the sway motion of the buoy, is proportional to the water depth. They also found that there is an optimum length of centerpipe and watercolumn fcr maximum power develcpment; the power is reduced if the length is increased or decreased from this optimum. Furthermore, the wave power actually converted by the pneumatic energy buoy was shown to be proportional to the cube of the water depth, and the optimum design is such that the water mass in the center pipe is approximately two-thirds of the sum of the buoy mass and the added mass.

Additional conclusions from this study are:

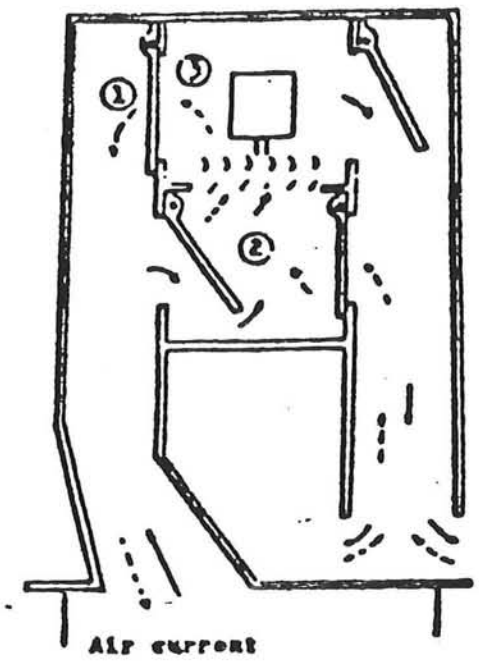

Figure 63: Details of the air valves in the wave activated turbine generator (WATG). (From Masuda, 1971).

1.

The optimum design of the wave-energy converter is one which incorporates a large centerpipe radius and a large area contraction value.

2. The wave period at which the time-averaged peak power per wave occurs can be effectively adjusted by changing the length of the internal column. By making the centerpipe length adjustable, the device can be made suitable for any wave sprectrum encountered.

3. The device is practical for use on offshore structures and, in addition, to supply power to coastal communities.

In another paper, McCormick, et al., considered a preliminary design of a pneumatic wave-energy system for supplying an offshore structure. They concluded that, by coupling four of the proposed fixed pneumatic wave energy converters, a total time averaged power between 2.8 kilowatts and 88 kilowatts per wave can be obtained, if wave heights range from one to five feet having a wave period greater than four seconds. To insure a uniform output to provide power during periods of calm seas, they proposed the power generated to be stored in batteries.

12.2 WAVE ATTENUATION PERFORMANCE

In the literature used for this report, the wave attenuation is not investigated. Although energy will be extracted by the WATG, a smooth water surface behind the WATG is unlikely, due to the cicular wave crests caused by the buoy, which will interfere with the linear wave crests of the incident wave. Much better wave attenuation performance can be expected if the WATG is changed tc a line absorber, or if several bouys, are mored close to each other.

12.3 MOORING

No information about mooring was available in the used literature. Of course, a flexible mooring is needed, due to the vertical motion of the buoy, necessary for energy extraction. Since several WATGs are already put into practice and because of the similarity with normal buoys, the mooring will not be a difficult problem.

12.4 COSTS

As told in the introduction the construction of the WATG is relatively simple and inexpensive. No further information was available.

Chapter XIII

WAVE TRAP

13.1 INTRODUCTION

The system consists of a large thin rather impermeable floating sheet fitted with numerous attachment cords supporting a large thin valve sheet. See figure 64. The most successful membrane-type consists of a floating blanket attached by flexible lines to a second blanket. The bottom sheet is valved for maximum resistance when rising and minimum resistance when falling. So the rising and falling tends to accelerate the large mass of water contained between the sheets.

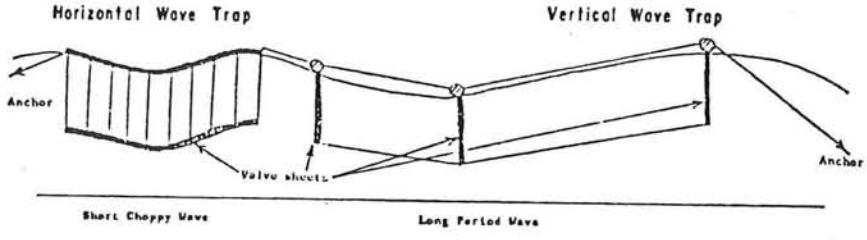

Figure 64: Wave Trap (after Ripken).

13.2 WAVE ATTENUATION

The efficiency of the system was good on the preliminary tests on waves of high steepness because of the large vertical accelerations. Low steepness required a wide trap to achieve a substantial reduction in wave height.
It is stressed that reflection plays a minor role in the wave attenuation process. The energy is dissipated in the structure. This causes large if not fatal internal stresses. Limited duration tests on scale showed that wave heights higher than one feet already caused structural damage.

13.3 MOORING CHARACTERISTICS

The mooring force data are obtained under two dimensional conditions and should be used conservatively. Mooring forces tend to be small since wave forces against the seaward baf-

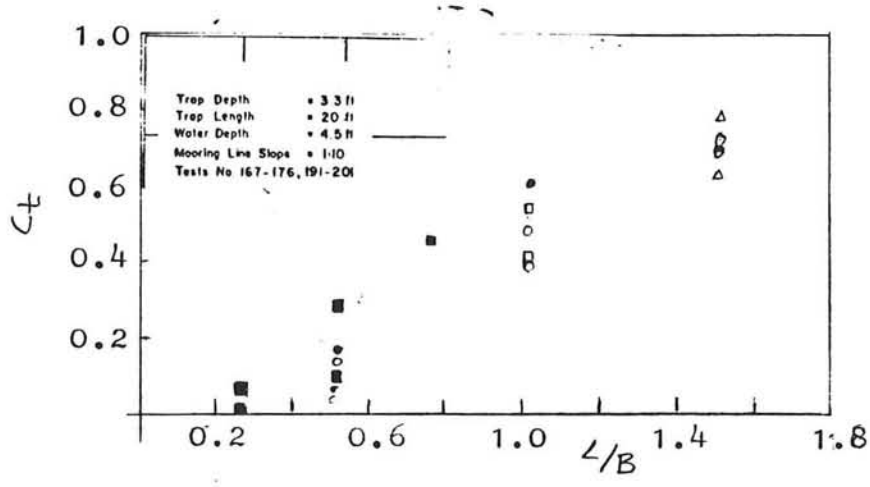

Figure 65: Wave Trap attenuation characteristics (after Ripken).

fle will be balanced by forces on the shoreward baffle. Mooring characteristics and a formula for the mooring forces are given in figure 66.

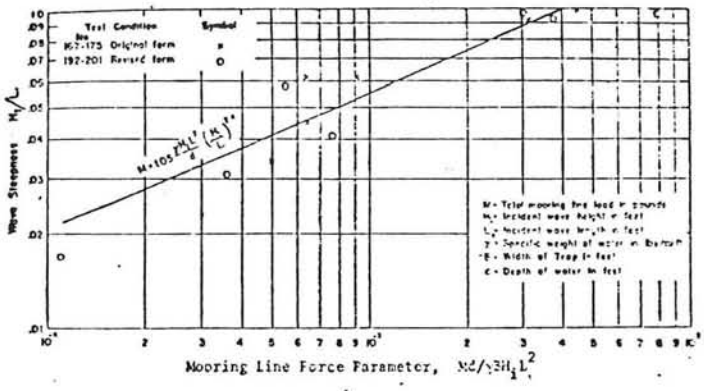

Figure 66: Mooring force characteristics (after Ripken 1960).

Chapter XIV

WAVE BLANKET

14.1 INTRODUCTION

The wave blanket is a design consisting of a permeable blanket floating just below the water surface. The design concept assumes that the orbit and translation velocity of the wave will force a flow through the permeable construction, the resistance should induce energy loss. An analysis of the force mechanism indicates that both viscous and gravity forces may be involved.

The blankets used in Ripkens tests were assembled from sheets of three-dimensional fabric-woven stiff plastics fibres varying 0.36mm to 0.51mm in diameter. The fabric used in wave tests was designated 4-ply "Trilok". The blanket assembly consisted of two sheets of "Trilok" fabric. The upper sheet had a sine wave form, the lower lay flat. See figure 67.

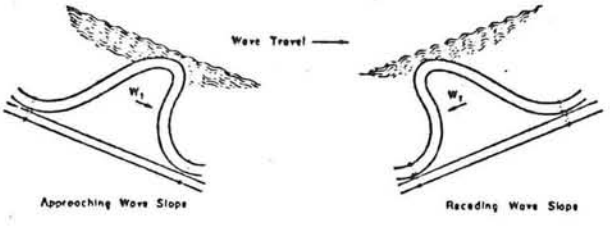

a. Distortion of Wave Blanket under wave action

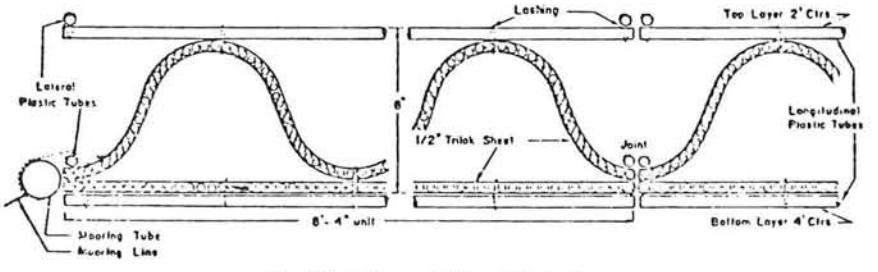

b. Structure of Wave Blanket

Figure 67: Structure of the Wave Blanket (after Ripken).

The two sheets were lashed together with plastic cording to form the unit blanket.

14.2 WAVE ATTENUATION

From Ripkens experiments can be concluded that the wave attenuation performance is not critically dependent on the structure and form of the blanket. A blanket made of a dense sponge gave essentially the same wave attenuation characteristics. The relative breakwater width, L/B, and the blanket thickness proved to be of major importance to the wave damping performance. See figure 68.

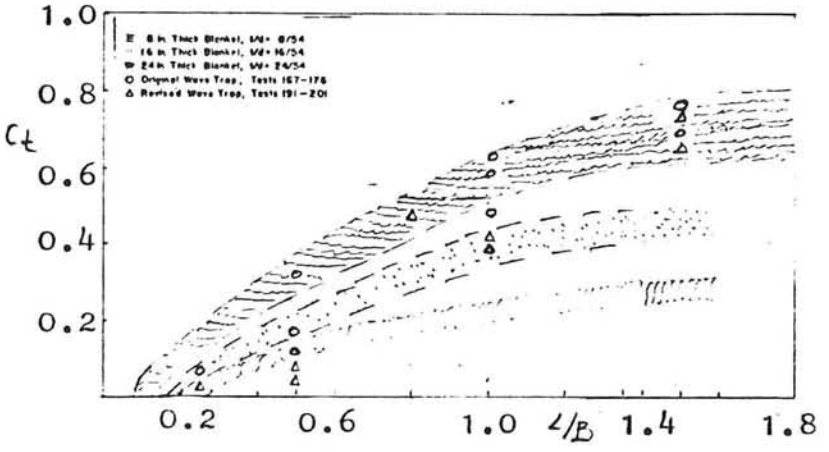

Figure 68: Wave blanket attenuation characteristics. (after Ripken, 1960).

14.3 MOORING CHARACTERISTICS

Mooring force data are only available for experimental studies carried out by Ripken. They are not contained in this report.

14.4 TRANSPORTABILITY

Since the structure attempts to retard the water movement, towing will be impractical.

Chapter XV

THE STEREO-GRID FLEXIBLE FLOATING BREAKWATER

15.1 INTRODUCTION

The Stereo-Grid breakwater is a flexible structure composed of plastic brocks and pipes. See figure 69 .

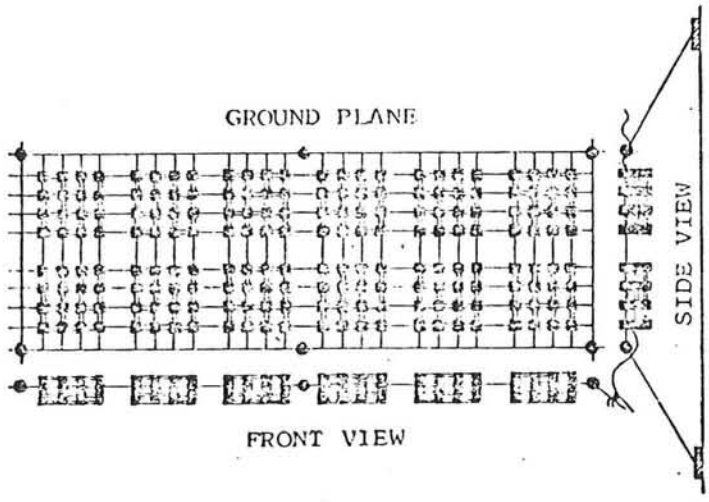

Figure 69: The stereo-grid breakwater.

The basic ideas which led to the design of the breakwater are summerized as follows:

1. Flexible and durable materials should be used to absorb wave energy.

2. The surface area should be as large as possible by constant weight and volume.

3. The structure ought to disperge waves.

4. The structure has to consist of units to facilitate erection and dismantling of the structure.

5. The structure must be economically feasible.

The authors state that the floating breakwater can be used to protect fish farms, harbors and marine constructions.

15.2 WAVE ATIENUATION PERFORMANCE

The design of the Stereo-Grid breakwater is such that wave energy is mainly attenuated by surface friction and wave reflection.

To investigate optimum damping performance two series of scale tests were carried out. The first serie of tests attempted to find out the optimal vertical position of the floating body. Using regular waves of lengths L=1.16m, L=0.69m and L=0.43m and a wave steepness ranging from 0.03-0.06m, optimum performance was found as h/(D+h)=0.2-0.3. The influence of the distance between the bodies was also investigated. A body distance between the structures of 1<l(b)<2*l, was recommended.

in which:

l : structure length
l(b): distance between the structures

This result seemed to be independent of the wave conditions. The second tests dealt with the form of the body. The attempt was to make clear how the volume, V, the weight, W, and surface area, S, contribute to the damping effect. Textile fibers, plastic materials and metals were used for various forms of the body. Figure 70 shows the damping effect related to W(r), V(r) and $S(r)^{2/3}$ .In which:

W(r) = W1/W2
V(r) = V1/V2
S(r) = S1/S2

W1: weight of the body
V1: volume of the body
S1: surface area of the body
W2: weight of displaced water
V2: volume of the displaced water
S2: area of the hull of the body

These parameters are dependent and therefore have similar characteristics.

To summarize the experiments tests results were compared with a formula derived by Kato:

$$C_t = \frac{H_t}{H_i} = \exp\left[-0.5\ a*b\right]$$

In which:

$a = 5\ W(r)+V(r)+0.5\ S(r)\exp(0.667)$ (a form factor)

$b = [1-\sinh 2k(h-d)/\sinh 2kh]*1/L$

The experimental results are in good agreement with the Kato formula. See figure 71 .

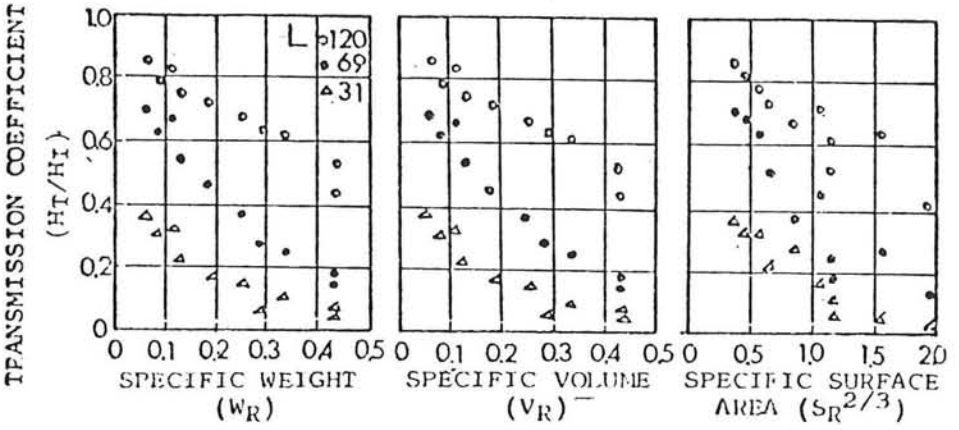

Figure 70: The damping effect related to W(r), V(r) and $[S(r)]^{2/3}$.

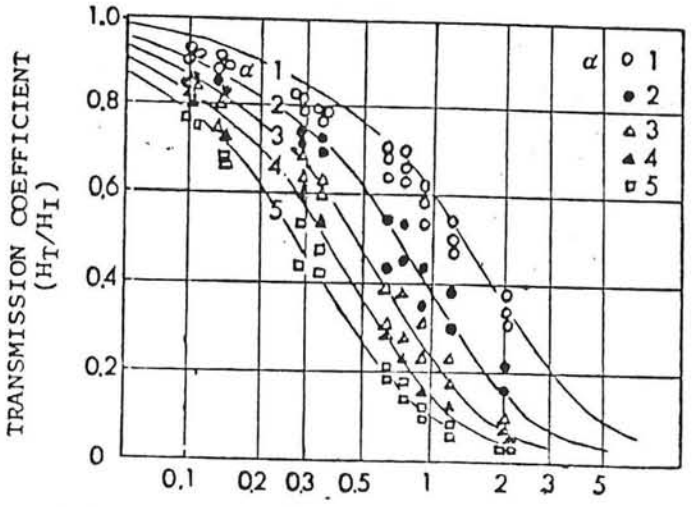

Figure 71: Kato curves for wave attenuation prediction.

15.3 MOORING CHARACTERISTICS

Mooring forces, F1 and F2, were studied under various wave conditions.
The relation between F and H is given in figure 72 . In irregular waves an interesting feature was observed. Large mooring forces were obtained by absorption of small steep waves. This performance needs further investigation.

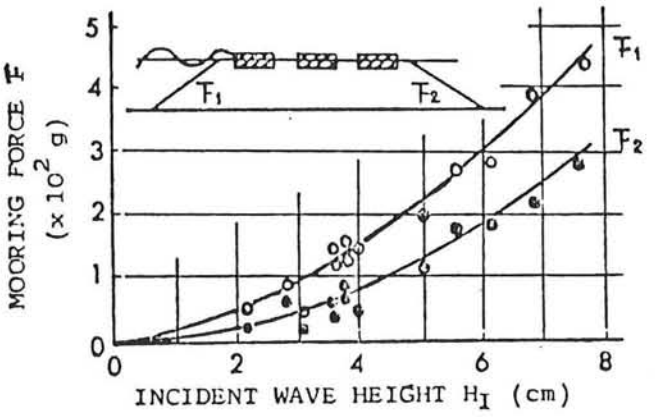

Figure 72: Mooring force characteristics.

15.4 TRANSPORTABILITY

No experiences are mentioned, but if the structure is build according the standards set out in the introduction, transportability will not be a major problem. A very important point in judging the transportability is the way how the coupling between the modules is realized. The designers, however, give no information about the coupling.

Chapter XVI

SALTER DUCK (ENERGY DEVICE)

16.1 INTRODUCTION

The Duck is invented by S.H. Salter and has been studied intensively at Edinburgh University. The original design of the Duck is that of an energy converter. The essential feature of such a duck is a very long common backbone on which the "ducks" are located. The design of the duck will facilitate if the duck is only mentioned to attenuate waves and conversion of the captured wave energy will not take place. Further work in the near future has to cover the testing of hinges and joints under cyclic loads. So more long term durability at sea can be judged. Still, many problems have to be solved before Salter Ducks can be operational. Structural criteria such as: survival-strength, fatigue-limit, corrosion and last but not least anchoring, will present very great problems. Other problems which have no engineering nature need also to be considered. These relate to fouling, wave-ownership and navigational hazards.

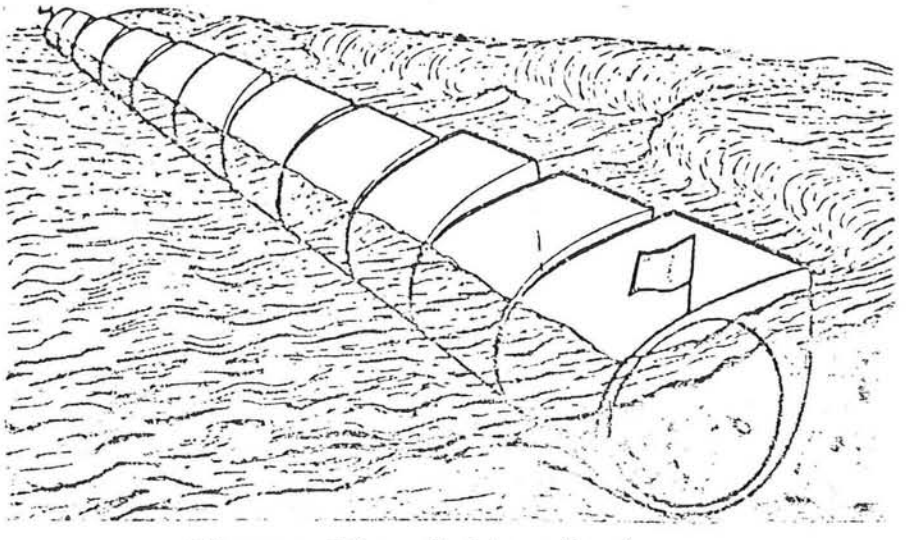

Figure 73: Salter Duck.

16.2 WAVE ATTENUATION PERFORMANCE AND ENERGY ABSORPTION

The natural "nodding" period is designed to coincide with the wave period where maximum efficiency and thus maximum wave attenuation is required.

Theoretically, if the restraining force applied to the ducks is chosen correctly, an inc dent wave is unable to distinguish between duck and adjacent water. It will transfer all of its energy to the duck. Laboratory tests on single units show very good efficiency for monochromatic and mixed spectrum waves. Directional properties of waves, however, have a significant bearing on the design of the ducks. To judge the efficiency of a duck we need directional spectra. Unfortunately, time instrumental measurements of wave directions are scarce. Directional spectra will be visualized using "K-space diagrams".

$$k = \frac{2\pi}{L}$$

Power is generated from motions of the duck relative to the spine. The front face of the duck is chosen such that the displacements match those of the water particles in a wave. The rear face of the duck is circular and therefore does not displace any water. Since the efficiency of the duck depends on the relative motion of the ducks to the spine, the net spine motion has to be small. Constructional problems arize if a spine is positioned with its ends on crests and its center over a trough. An advantage of a continuous backbone is that it allows collecting the power outputs of the ducks in a direct way. However, structural realization of a good design of a long spine is still a problem. If the Duck is only menticned to attenuate waves, the length of the long spine can be chosen independently.

figure 74 shows that there is a maximum distance between two wave crests in a mixed sea.

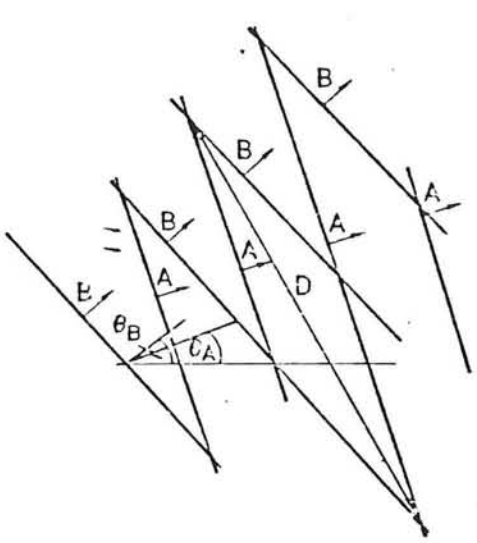

Figure 74: K-space diagrams.

16.3 MOORING

Mooring of the Ducks is one of the most difficult problems to be solved. Tests indicated very high peak forces in the mooring lines. Traditional mooring techniques are not apt to withstand these forces. A breakthrough in mooring engineering would be beneficial to the development of wave energy converters.

16.4 TRANSPORTABILITY

Transport of a string of ducks will be difficult. The ducks are intended to remain at the same site for a long period.

16.5 COSTS

Construction costs of a duck will be high. Especially if the duck is intended to convert wave energy.

Chapter XVII

HAGEN-COCKERELL RAFT (ENERGY DEVICE)

17.1 INTRODUCTION

The concept of the wave countering raft is developed by Cockerell (U.K. pat nr) and Hagen (U.S.A. pat nr 4,077,213). The raft converter consists of a string of pontoons, moored in line with the prevailing wave direction.

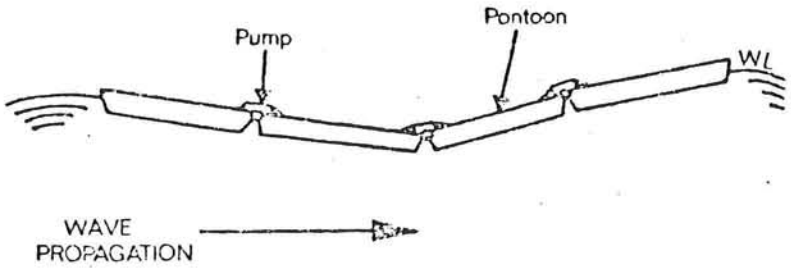

Figure 75: The Hagen-Cockerell raft.

Power is extracted from the relative angular movements of the adjoining rafts with the passage of waves underneath them.

17.2 WAVE ATTENUATION PERFORMANCE AND ENERGY ABSORPTION

The system can be made to operate effectively as a wide band oscillator. Model tests showed optimal performance for a string of three rafts. Haren came to the same conclusion using linear wave theory and shallow water conditions. Under laboratory conditions the optimal design, having dimensions of 100-50-9 meters, is capable of extracting energy from waves of periods from about 4-15 seconds. The fact that the efficiency falls rapidly for waves with periods over 15 sec-

onds can be regarded as an advantage from the power take-off point of view. From the damping point of view this feature limits the wave attenuation performance. Obviously the size of the converter depends on its operation range.

For the primary power take-off the relative angular motions about the hinges would be used to pressurize sea water in a hydraulic main which would lead to a turbine driven generator.

17.3 MOORING

Since energy is extracted from the relative angular motions of the adjacent rafts, no part of the raft need be rigidly moored. Because of the small draft, the instantanious horizontal wave force is relatively small. The moorings of both an individual raft and of adjacent rafts in relatively close proximity presents significant problems to which attention ought to be given.

17.4 TRANSPORTABILITY

If the rafts are designed to have small drafts and decoupling of the rafts is provided for, towing will be possible.

17.5 COST

Costs tend to be high, especially the construction of the hinges increases the costs a lot.

Chapter XVIII

FLOATING TIRE BREAKWATERS

18.1 INTRODUCTION

The floating tire breakwater (FTB) is a flexible breakwater, almost entirely constructed of scrap tires. The principal reason for considering FTB is their relatively low cost ($10 - $100/m). Users must be aware that FTB are less rugged and provide less protection than rigid breakwaters. Their extreme event survival should also be taken in consideration. Use of FTB should be limited to semiprotected sites, or short fetch applications e.g. F<10km, with H_s below 0.9m to 1.2m.

Two types of FTB presently exist as field installations:

1. The Wave-Maze, which is predominantly used on the West Coast of the U.S.A.

2. The Goodyear FTB, which predominates on the East Coast of the U.S.A.

A third type of FTB, the Pipe-Tire or Wave-Guard is introduced by Harms because it requires less space than an equivalent Goodyear FTB. Field installations of the Pipe-Tire do not yet exist, but experiments up to full scale have been performed at the laboratory.

The structures are shown in figure 76.

Field experiments with the Goodyear FTB have been examined to investigate the effects of the FTB. In the conclusion of the report by Adee it is stated that FTB designed and build according to the standards set by recent research have fared well and show promise of meeting their design goals. The weakest area of the present FTB-technology are flotation and anchoring systems.

18.1.1 Construction materials

The following recommendations concerning construction materials are made resulting from the experiences of the field experiments. The main construction material used is scrap tires. Connection materials for assembling the tires were thorougly tested. The recommended binding material is edged conveyor belting. This is a scrap product resulting from the trimming of new conveyor belts. Conveyor belting was found to have excellent abrasion resistance to chafing against tire casings and it showed no signs of delamination. In addition conveyor belting is inert in seawater. The belting distributes the loading troughout the whole system. To fas-

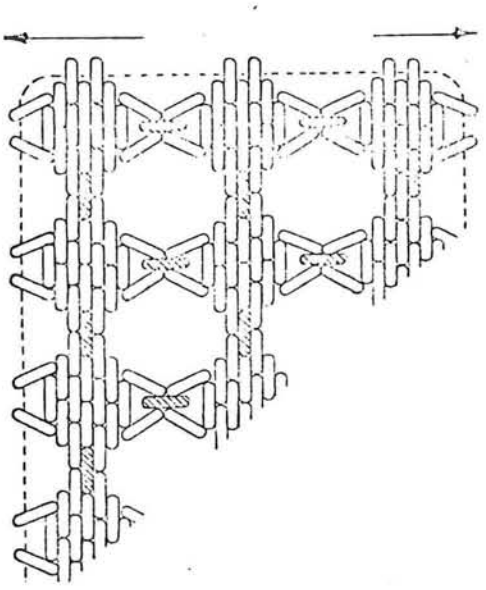

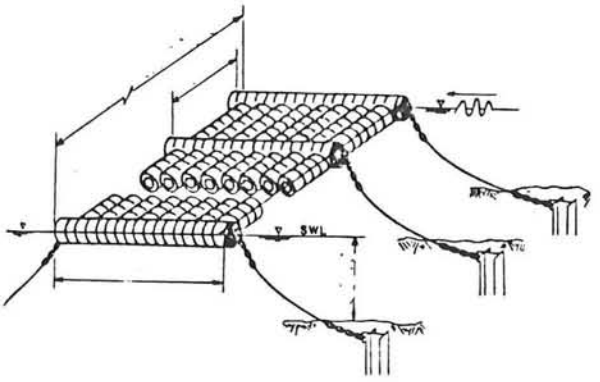

PIPE-TIRE BREAKWATER
NOT TO SCALE

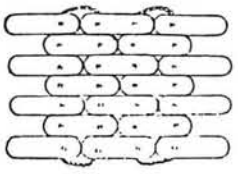

SIDE VIEW OF BUNDLE OF 18 TIRES IN WATER.

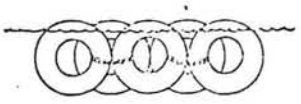

TOP VIEW OF BUNDLE AS IT IS CONSTRUCTED ON LAND.

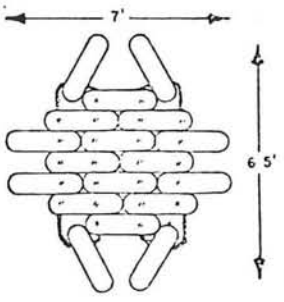

TOP VIEW OF BUNDLE PREPARATORY TO ATTACHMENT TO OTHER BUNDLES.

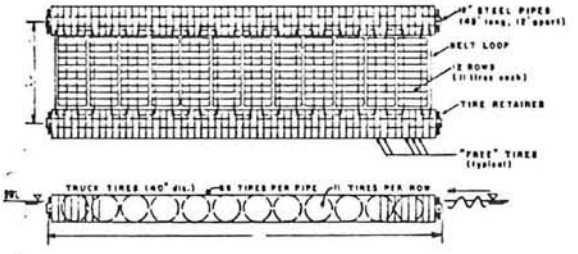

PIPE-TIRE BREAKWATER MODULE
NOT TO SCALE

Figure 76: Structures of scrap-tire floating breakwaters.

ten the belting the use of nylon bolts, nuts and washers is recommended. Heavy steel chain is regarded as a secondary choice. In the Wave-Maze hot dipped galvanized bolts and washers should be used to connect the tires. To ensure flotation for up to the estimated 10-year-life, liquid polyurethane foam has to be poured intc the tire crowns before assembling the modules.

18.2 WAVE ATTENUATION PERFORMANCE

A FTB differs not only structurally from other floating breakwaters. Because of its permeability the wave damping mechanism is dominated by dissipation. In contradiction to most other floating breakwaters reflection plays only a minor role in wave attenuation.
This feature is exhibited in figure 77 . On the ordinate the ratio of dissipated energy to reflected energy is plotted against the relative wave length on the horizontal axis. The reflected energy is only 7%-20% of the dissipated energy, depending upon the relative wave length L/B. This relationship is extracted from scale experiments on the Wave-Maze, but should apply as well to the Goodyear and Pipe-Tire FTB.

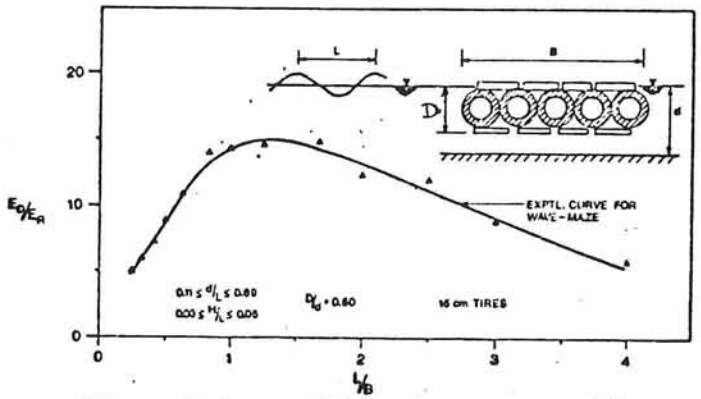

Figure 77: Attenuation by scrap-tires.

It is instructive to compare the wave-transmission characteristics of FTB to breakwaters who behave dominantly as wave reflectors. See figure 78 .
Experimental data for the Goodyear FTB indicated that a Goodyear FTB with a beam of B = 12D offers about the same wave attenuation as a fixed vertical plate of equal draft, D. Comparing the theoretical wave transmission characteristics of the horizontal plate with the Goodyear FTB indicates that the latter lies approximately midway between that of a fixed horizontal plate and a floating horizontal plate.

Wave attenuation by scrap tires is achieved in three ways:

1. Destruction of the orbital motion of the wave particles.

2. Turbulence of water particles caused by open casings of the tires.

3. Deformation of the tire casings.

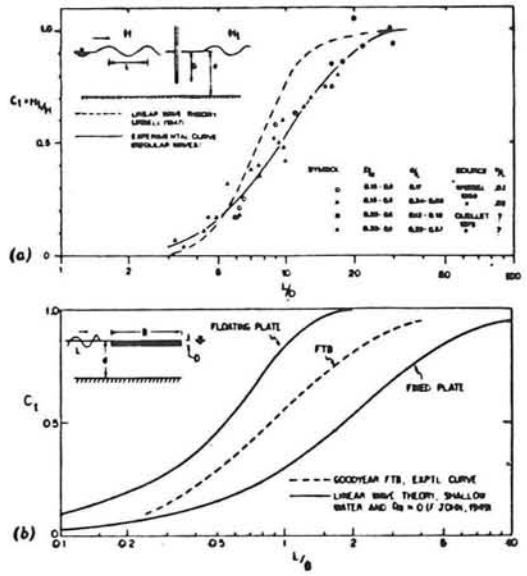

FIG. 2.—Wave Transmission: (a) Past Vertical Plate; (b) Past Horizontal Plate

Figure 78: Floating tire breakwater wave attenuation compared to that of a rigid horizontal plate and vertical plate, fixed and also floating.

Two prototype-scale Pipe-Tire floating breakwaters were tested using regular waves: The PT-1-Module constructed of truck tires and steel pipe buoyancy chambers and the smaller PT-2-Type constructed of automobile tires and telephone poles. Wave transmission characteristics and mooring load data were measured. The regular waves ranged in height from 0.15 to 1.78 meters and periods from 2.6 to 8.1 seconds; the water depth ranged from 2.0 to 4.6 meters. The modules were 12.2 meters wide in the direction of wave propagation and were held together with conveyor belt loops.

18.2.1 Comparing wave attenuation of three scrap-tire floating breakwaters

Wave transmission data for the PT-Breakwater are shown in figure 79 .
It can be seen that the shelter afforded by a PT-Breakwater is strongly dependent on the incident wave. Substantial protection is provided from waves which are shorter than the beam of the breakwater i.e. L<B, but very little from waves which are longer than three times the breakwater beam. As the water depth decreases, the wave attenuation performance improves. The wave damping generally improves with increasing wave steepness, especially for relatively long waves in shallow water e.g. L>3B and d<3D. From the figures it can be seen that the wave attenuation of the PT-1-Module was found to be superior to that of the PT-2-Module.
From figure 81, one can see that the PT-1-Breakwater provides substantially more wave protection than the Goodyear-Breakwater. This holds also for the PT-2-Module, but for shallower water the difference in wave attenuation is less pronounced. The influence of water depth is not of practical importance for the Goodyear-Breakwater if D/d<0.4. The importance of B/D is even smaller for the Goodyear-Breakwater.

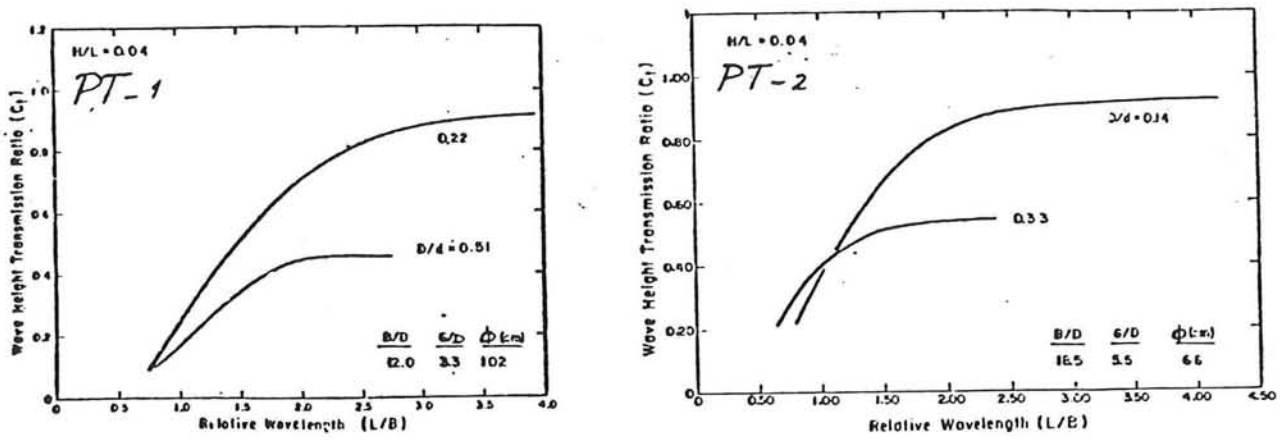

Figure 79: Wave attenuation characteristics for PT-Breakwaters.

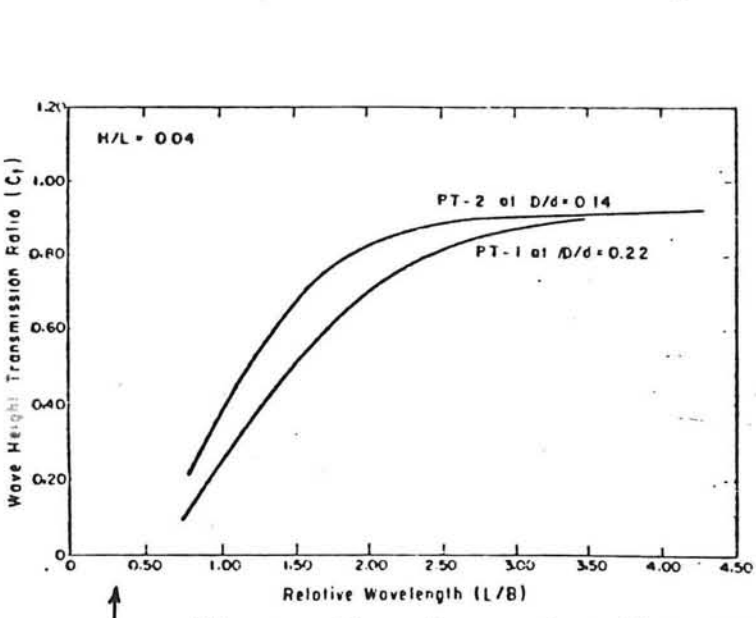

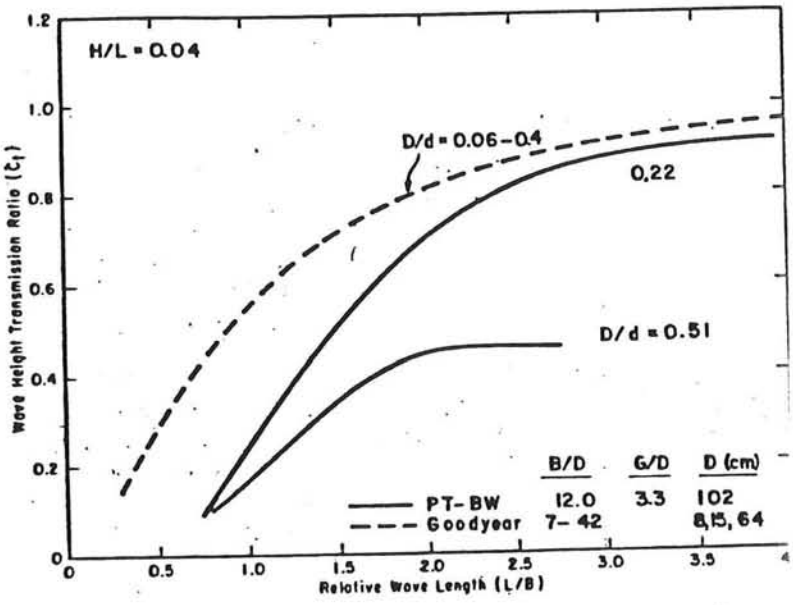

Figure 80: Comparing the wave attenuation performance of the PT-Modules.

Figure 81: Comparing the wave attenuation performance of the PT-Modules with the attenuation performance of the Goodyear.

18.3 MOORING CHARACTERISTICS

The influence of the stiffness of the mooring system was investigated using three types of mooring configurations listed in the following table.
For a given breakwater the peak mooring force F (on the seaward side, per unit length of the breakwater) was found to

Table 9.

Mooring configurations.

Compliance of mooring systems.

	Mooring system		
	MS-1	MS-2	MS-3
Type of mooring-line insert[1]	Tire (soft)	Belting (hard)	Belting (hard)
Type of breakwater connection	Pipe (hard)	Pipe (hard)	Tires on pipe (soft)
Mooring line stiffness (ranked)	3	1	2

[1] Inserts are 6 meters long; belting is in the form of a loop (used double strength) with elongation characteristics under load approximately equal to that of wire rope used.

depend primarily on the wave height, H, and the water depth, d. The wave length was only of secondary importance. The following relation was estimated by Harms:

$$F \sim H^n$$

n=1.5 for PT-1
n=2 for Pt-2 and Goodyear-Breakwater

18.3.1 Field experiences

Field experience with the Goodyear-Breakwater leads to the following recommendations. The mooring line should have a minimum length of approximately eight times the maximum water depth. The anchor should be positioned seven times the maximum water depth from the breakwater. Chain mooring should be attached to the breakwater in a manner that distributes the load between two or more modules.

18.4 TRANSPORTABILITY

Towing a scrap tire breakwater will be a difficult operation because of the great turbulence created by the tires. If the operator plans to lift modules of the structure problems at the connections, depending on weight and stiffness of the structure, may arise. One might conclude that transportation of a scrap tire is possible but not easy.

18.5 COST

The total cost of a scrap tire floating breakwater will depend to a high degree on the labor cost of accumulating and assembling the tires onsite and the types of binding and flotation materials used. Harms performed calculations based on "equal wave protection" since the wave attenuation performance of the three types are quite different even for the same beam. The cost of the mooring systems were not included since they are inherently site dependent. Harms calculated that PT-Breakwater cost is significantly smaller than those for the Goodyear and Wave-Maze for the same degree of wave protection. The Wave-Maze concept was found to be the most expensive. On the other hand, it has perhaps the longest life-time and the greatest extreme event survival capacity.

18.5.1 Wave-Maze Cost

The estimated construction cost for the Wave-Maze is about $\$48/m^2$. A royalty for the use of this patent adds about ten percent to the construction cost.

18.5.2 PT-Breakwater cost

Major construction components for the PT-Breakwater and their respective cost are listed in table 10 . Note that the steel pipe accounts for nearly 60% of the cost. The total components cost amounts up to \$19.60 per square meter breakwater.

Table 10.

Cost estimates of PT-Breakwater components.

Module dimensions:	3.7 by 12.2 m (B = 12.2 m)
Materials:	Truck tires (9.00-18 and 10.00-20) Steel pipe (41-cm-diameter steel-pile pipe) Conveyor-belt material (three-ply, 14 by 1.3 cm) Nylon bolts, washers, and nuts (13 mm)

Item	Quantity	Unit cost	Total cost	Cost/m^2
Steel pipe	12.2 m	\$43.00	\$524.60	\$11.60
Polyurethane foam (pipe plus 20 percent of tires)	2.4 m^3	75.00	180.00	4.00
Tying material (conveyor belt)	94 m	1.15	108.10	2.40
Tires (transportation cost)	176	0.25	44.00	1.00
Nylon bolts, washers, and nuts	80	0.35	28.00	0.60
Cost of breakwater (excluding mooring system and assembly)				\$19.60

18.5.3 Cost of the Goodyear-Breakwater

The cost of a Goodyear-Breakwater can vary substantially from site to site, depending on the coupling material used, the reserve flotation provided, the mooring system deployed and the labor available. However, some indications of relative cost per square meter of surface area are possible by seperately examining salt water and fresh water sites. For salt water sites total cost varied from $\$9.59/m^2$ to $\$44.50/m^2$ with an average cost of $\$26.87/m^2$. For fresh water locations total project cost varied from $\$6.01/m^2$ to $\$15.03/m^2$ with an average cost of $\$10.28/m^2$.

Table 11.

Goodyear breakwater cost.

COST [$/m²]	SALT	FRESH
MIN	9.59	6.01
MAX	44.50	15.03
AVERAGE	26.70	10.28

Additional considerations in the cost of a floating breakwater are the lead time required to obtain a permit for its installation and the design life of the structure.

Table 12.

Goodyear-Breakwater cost data (after Harms).

LEADTIME [months]	DESIGN-LIFE [years]	DISPOSAL COST [$/m² -1980]	MAINTENANCE COST [percent of total construction cost]
MIN	1	2.16	2.2
MAX	13	6.31	18.2
AVERAGE	5	4.88	

Chapter XIX

TETHERED-FLOAT BREAKWATER

19.1 INTRODUCTION

The tethered-float breakwater is constructed of a large number of very buoyant floats, each with a characteristic dimension about equal to the wave height. The floats are independently tethered at or below the water surface. Initially, the concept was developed for a water depth many times the float diameter; later a bottom-resting concept was developed for shallow water. The floats move as a result of the wave pressure gradient; the dominant attenuation mechanism is drag resulting from the buoy motion.

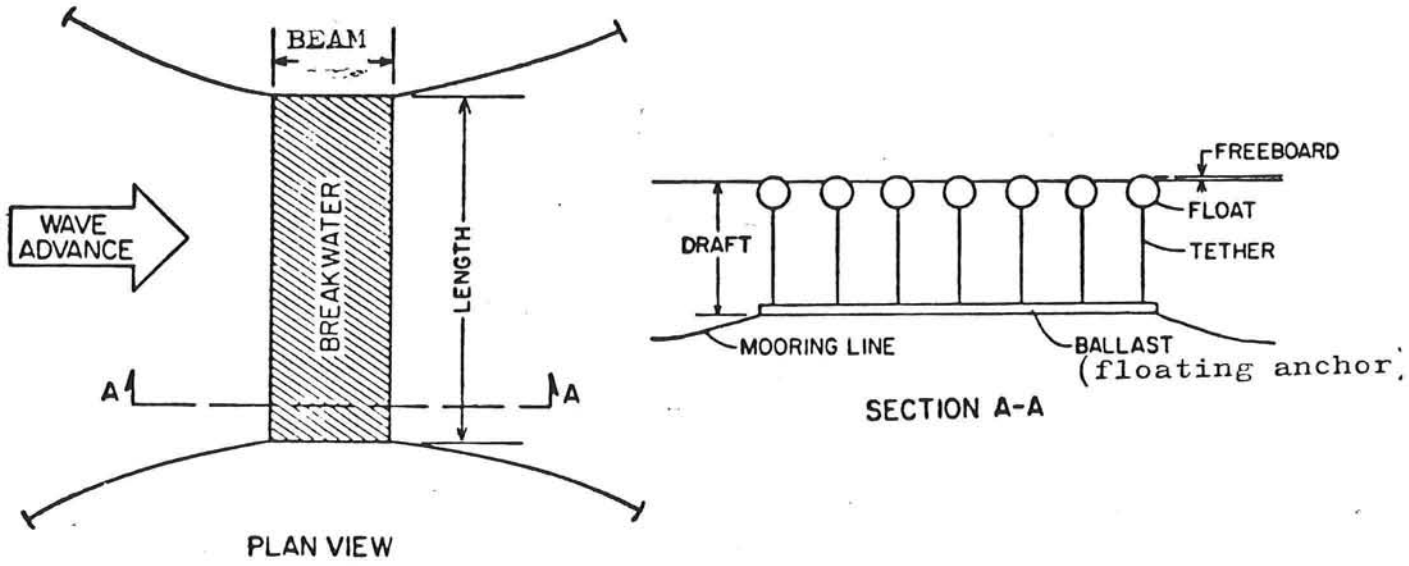

Figure 82: Definitive sketch of a tethered-float breakwater.

Many floating breakwaters rely on reflection or turbulence generation to disrupt the wave orbits and attenuate wave energy. The energy dissipated by friction (drag) is normally a small component of the total wave energy, since the relative velocities between the breakwater and the fluid particles are low. However, the drag power is proportional to the cube of these relative velocities. Hence, if a substantial increase in relative velocity can be achieved, the energy dissipation due to drag may become the most important mode. This constitutes the fundamental mechanism serving the TF-breakwater as a wave energy dissipator.

The materials which were used for the tethered float breakwater are:
For the floats: syntatic spheres or scrap tires filled with polyuretane foam.
For the tethers: "low-stretch single braid polyester rope" Ø 22mm (high modulus of elasticity: less than 3% elongation at design load) or steel torque-balanced Angel polyester jacket wire rope (Ø 12.5mm).
For the floating anchor: reinforced concrete, or steel (scrap railroad rails and cylindrical tanks, to regulate the weight).

There are essentially two scales of tethered-float breakwaters: the marina scale and the open sea scale. The primary difference between the two scales is the size and buoyancy of the floats to be used. Marina tethered float breakwaters are designed to use floats of about 0.30m diameter (130N buoyancy); the open sea scale uses floats up to 1.50m diameter (up to 17700N buoyancy).

The TF-system is not patented and is therefore available to commercial developers.

Some important design features are:

1. Optimum tether length in deep water is approximately 10% of the peak energy wave length of the spectrum.

2. Best performance in deep water is attained with floats totally submerged approximately one quarter diameter beneath the surface. Some floats must pierce the surface in order to provide reserve buoyancy.

3. Ballast frames must be flexibly interconnected and frames must be kept small with respect to the peak energy wave length. This is necessary in order that both frame and floats follow the sea surface and thus prevent emergence of floats in the wave trough (avoiding associated shock loading during resubmergence).

4. A flexible terminator or boot must be provided at the base of the tether, in order to reduce bending stresses and ensure reasonable life expectancy of the tether assembly.

5. Reasonable diameters of the TF-breakwater will be of the same order as the significant wave height.

19.2 WAVE ATTENUATION PERFORMANCE

To illustrate the performance characteristics, Seymour and Isaacs (1974) generalized the in section 2.12.1 described process by specifying an arbritary spectrum, the Pierson-Moskowitz model. The wave length at which the peak energy is found can be used to develcp two dimensionless ratios which define the breakwater configuration:

ϕ/L_p and d/L_p
where:

ϕ: floatdiameter.
L_p: the wave length in deep water according to the frequency at which the peak energy is found.
d : water depth.

A digital computer search of ϕ/L_p and d/L_p space will determine the required number of rows of floats to achieve a desired level of wave height reduction. For an assumed float density of 4 percent, with the anchor assumed on the bottom and for a float just below the surface, Seymour and Isaacs have presented performance estimations which determine the number of rows of floats to provide 75% and 50% wave height reduction. (See figure 83).

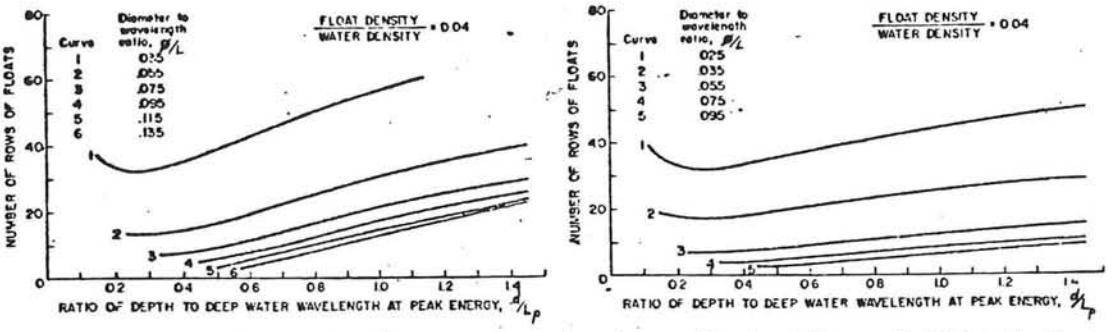

Figure 83: Relation number of floats and C_t.

Consideration of these results points to several interesting characteristics of the TF-breakwater:

1. Although it is a tuned **oscillator**, the performance of the breakwater is remarkably insensitive to tether length. For example, a spectrum with energy peaked at a period of 8 sec. gives L=100m and selecting $\phi/L=0.035$ gives a diameter of 3.5m.

Table 13.

Required number of rows in relation with C_t.

minimum depth height reduction	required number of rows		
	15 m	27 m	55 m
75%	37	32	37
50%	19	17	19
25%	8	7	8

Table 13 indicates the required number of rows at various water depths to achieve each of the three wave height reduction levels. Since the 27m depth is close to the optimum for this configuration, it can be seen that the number of rows (varying linear with costs) varies only 15% over the depth which ranged from 15 to 55m.

2. Performance improves with increasing diameter, but at decreasing rate. This is a result of the decay of the pressure gradient force as the center of the float is depressed with increasing diameter. Since the number of rows diminishes with increasing diameter only very slowly for large diameters, two distinct optima are suggested:

   a. The number of floats per unit length is proportional to 1/d. The total volume of the floats is therefore proportional to the number of rows times d^2. By establishing an approximate cost formula involving the float volume, it should be possible to estimate a diameter for which costs are minimized.

   b. The extent of the array normal to the shoreline is proportional to the number of rows that will produce the narrowest array.

3.

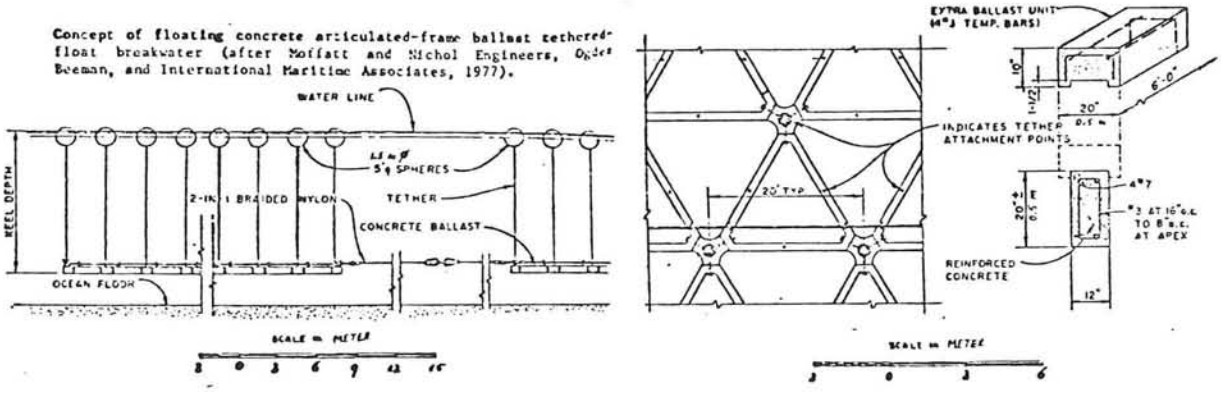

Figure 84: Concept of floating concrete articulated-frame balast TF-breakwater.

Optimum performance can be achieved for deep water conditions by utilizing a "floating anchor" as shown in fig. 84. Now the entire system is able to follow a slowly changing sea level such as tides, but is highly inertial damped so that it has negligible vertical response to the quick motion of waves. This arrangement makes it feasible to moor the breakwater in water of any depth.

Field experience indicated that the accuracy of the analytical model of Seymour and Hanes (section 2.12) is rather good.

Models of the TF-breakwater were tested in the large wind wave tank (109m * 4.5m * 1.5m) of the Hydraulic laboratory in Burlington, Ontario, Canada.

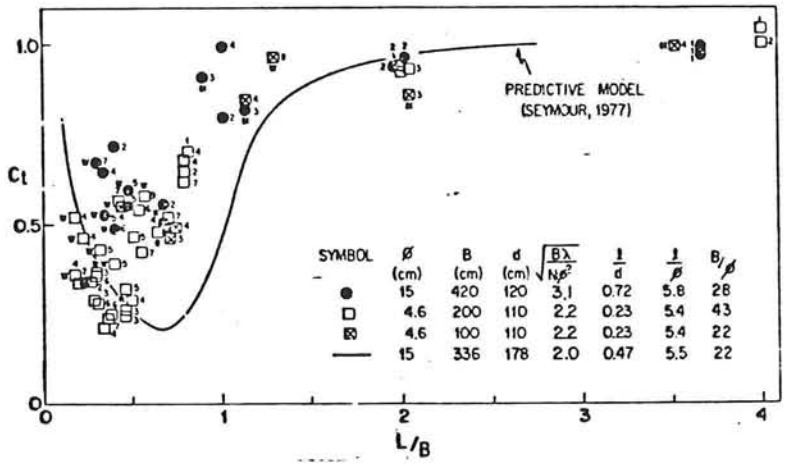

Figure 85: Wave-height transmission data for TF-breakwater.

In figure 85 the wave height reduction is plotted as a function of relative wave length, L/B, for three models of the TF-breakwater. These models were constructed according to the guidelines given by Seymour. An average wave height transmission curve representing Seymour's predictive model for several wave spectra with peak energies at L/B=0.6, 1.0 and 1.7 has been included for comparison. Agreement in base trends is evident. The measured C_t values are generally larger than the theoretical values. The TF-breakwater is a tuned filter that is most effective around L/B=0.7, and becomes increasingly less effective at wave lengths other than this (either shorter or longer).

19.3 MOORING FORCE

The mooring forces are not extreme high or low (comparable with a pole-tire breakwater with equal level of wave protection). The mooring force increases with increasing L/B. The increase is very large when $0 < L/B < 1$, but small when $L/B > 3$. See fig. 86. For example:

B=21 m, H=1.5 m, L=25 m (thus H/L=0.06, L/B=1.2)

$F_{peak} = 30 * 10^{-5} * 1020 * 9.8 * 21 * 21 = 1.32$ kN/m.

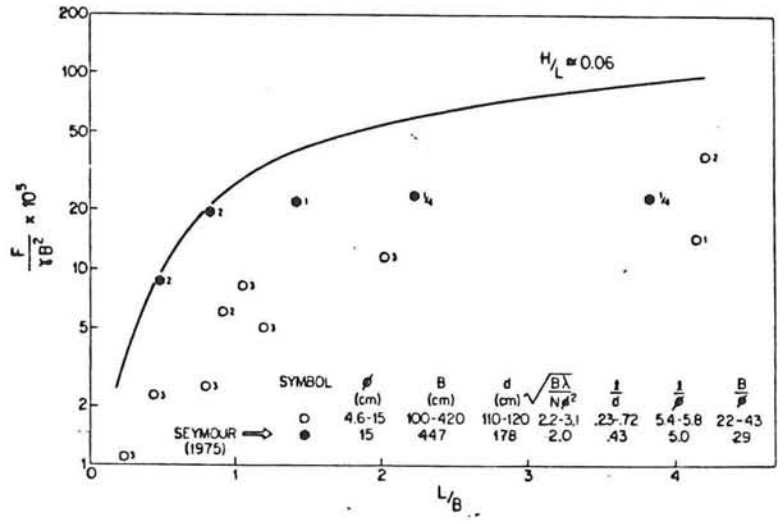

Figure 86: Peak mooring force data for the TF-breakwater and H/L<0.04 (curve for H/L=0.06).

19.4 TRANSPORTABILITY

If the anchors are designed to be hollow and floodable, they can be used as barges to transport the breakwater in sections from the fabrication facility to the site. Several such barge/anchors can be towed in a string and then floated to location. Blowing the water ballast allows the refloating of a breakwater section so that the entire system can be transported to a new location or individual sections can be inspected and maintained.

19.5 ECONOMIC FEASIBILITY

Economic evaluations of potential TF-breakwater installations have been prepared for site-specific locations by both private consulting firms and by the U.S. Navy. They concluded:

> In general, the feasibility varied widely with wave exposure and bottom characteristics at the various sites. The TF-breakwater shows potential use where:

1. conventional structural breakwaters cannot be build because of extreme water depth.
2. protection is needed only for a short period of time.
3. the protected area must shift with a transient marine operation.

For shallow water short-fetch sites, the feasibility of the TF-breakwater looks very promising (in those evaluations). And for shallow water, long fetch-sites, current research on

bottom-resting ballast frames and higher specific gravity floats may produce systems which will serve specific needs better than present alternatives. For deep water, long-fetch sites, the system appears feasible only for navel or military operations

To give an idea of the costs of a TF-breakwater: the estimated costs for the "concrete articulated-frame ballast TF-breakwater", having a size of 95m * 457m, with 555 rows are $7,600,000 (this is $13,694 per row).
Another example: TF-breakwater with B=21 m and spherical floats ⌀ = 38 cm, costs per meter $1377.90 (1980), excluding mooring system. See also chapter "comparison tethered-float and pole-tire breakwater".

Chapter XX

COMPARISON TETHERED-FLOAT AND POLE-TIRE BREAKWATER

20.1 WAVE ATTENUATION PERFORMANCE

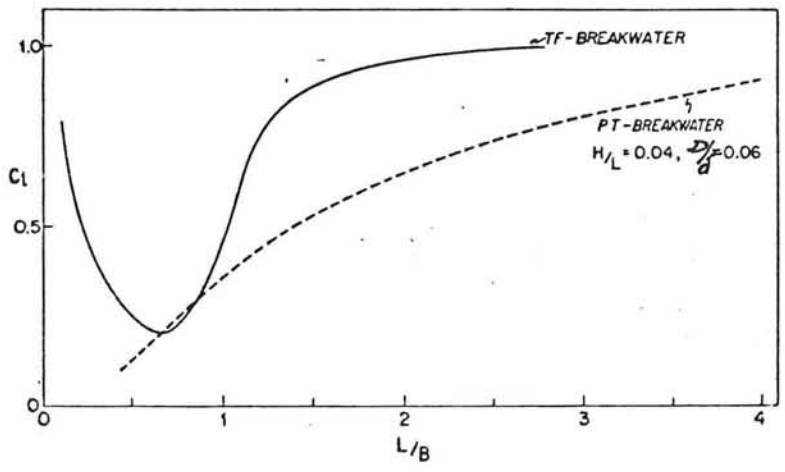

Figure 87: Wave transmission curves for TF and PT breakwaters of equal size.

In figure 87 the wave transmission curve for the PT-breakwater is shown as a dashed line. The PT wave attenuation increases monotonically as a function of L/B. This shown curve corresponds to H/L=0.04 and is based upon extensive data, from model and full scale tests. This curve was originally established using elements 8.4 cm in diameter, but has also been confirmed by full scale experiments with truck and automobile tires respectively 1.00m and 0.64m in diameter. A fundamental difference in the filtering characteristic of these structures is evident: The TF-breakwatwer is a tuned discrete filter that is most effective around L/B=0.7 and becomes increasingly less effective at a wave length other than this (either longer or shorter), whereas the PT-breakwater is a monotonic filter that becomes increasingly more effective as the wave length decreases. It is apparent that the PT-breakwater offers substantially more wave protection (lower C_t levels) than a TF-breakwater of equal size.

20.2 MOORING FORCES

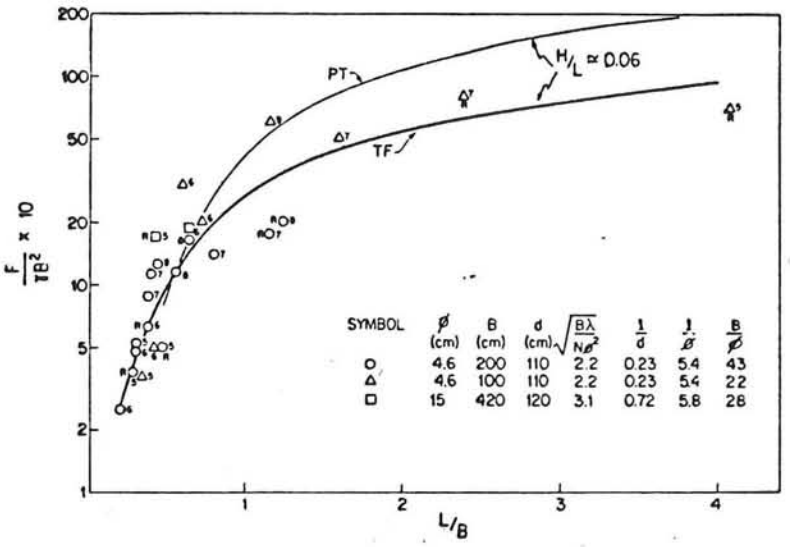

Figure 88: Peak mooring force data for TF and PT breakwaters.

Mooring force data of the TF-breakwater and the PT-breakwater are plotted in figure 88. It is evident that the peak mooring force for the PT-breakwater is larger than that of a TF-breakwater of equal size, but it should be recalled that such a PT-breakwater is also more effective. When the peak mooring forces of a larger TF-breakwater with "equal wave protection" as a PT-breakwater is compared with the PT-breakwater, they are approximately the same.

20.3 COSTS

The principle of "equal wave protection" has been utilized in order to arrive at comparable costs figures of those structures (see next table). Costs are given for major cost-contributing components of the structure, the mooring system not included. In a wave spectrum much broader than the cross-hatched region, it seems reasonable to compare a PT-breakwater with a TF-breakwater having a 50% larger planform area.

20.4 CONCLUSIONS

1. The tethered-float and the pole-tire breakwaters are technically feasible solutions to wave protection problems in short-fetch (say less than 10 km) or semi locations.

Table 14.

Cost estimates for TF and PT breakwaters.

COMPONENT COST ESTIMATES: TETHERED FLOAT (TF) BREAKWATER

Module Dimensions : B = 21.0 m, λ = 3.80 m

Materials : Spherical floats (D = 38 cm, γ = 0.04 gm cm^{-3}), Tethers and flexible tether terminals, Steel ballast frames with flexible couplings (3 frames 7.00 m × 3.00 m per module), Concrete ballast.

Item	Quantity	Unit Cost (US $)	Total (US $)	Cost per meter (US $)
Float unit (float, tether, flex. terminals)	135	24.30*	3279.30	863.00
Ballast frame (incl. flexible couplings)	3	465.90*	1397.60	367.80
Concrete ballast	4.2 m^3	113.10*	475.20	125.00
Assembly (labor only)	14 hrs	6.00	84.00	22.10

Cost per meter of breakwater = $1377.90 (excluding mooring system)

COMPONENT COST ESTIMATES: POLE-TIRE (PT) BREAKWATER

Module Dimensions : B = 14.0 m, λ = 4.00 m

Materials : Automobile tires (typically D = 64 cm), Telephone poles (4 m spacing), Conveyor belting (3ply, 14 cm wide, 5000 N cm^{-1} breaking strength), Nylon bolts, nuts, washers (13 mm or equivalent).

Item	Quantity	Unit cost (US $)	Total (US $)	Cost per meter (US $)
Tires	403	none	none	none
Tying material (conveyor belting)	180 m	0.90	162.40	40.60
Nylon bolts, nuts, washers	105	0.55	57.80	14.40
Telephone poles	1	50.00 (salvage @ 15% new)	50.00	12.50
Assembly (labor only)	18 hrs	6.00	108.00	27.00

Cost per meter of breakwater = $94.50 (excluding mooring system)

Note: The use of steel pipe (41 cm diam. 6 mm wall) and truck tires will increase the cost by approximately $130 per meter.

2. The pole-tire breakwater is a more effective wave energy filter than a tethered-float breakwater of equal size.

3. In a typical short fetch design case, a tethered-float and pole-tire breakwater were found to compare as follows (for equal levels of wave protection):

   a. The pole-tire breakwater costs less than one-tenth as much as the tethered-float breakwater.

   b. Peak mooring forces are approximately the same.

   c. The pole-tire breakwater requires less space.

Chapter XXI

CONCLUSIONS

First, some general features of floating breakwaters will be dicussed. Second, the feasibility of each breakwater will be discussed.

1. Influence of L/d
   If $L/d < 0.5$, nearly all the kinetic energy of the waves is concentrated in the upper third part of the water. It is obvious, that the damping will take place in this layer.
   Since $L/d = (L/B)(B/D)(D/d)$, the effect of L/d will be the same as L/B if B/D and D/d are constant. Or, if both L/B and B/D are constant, the effect of L/d will be the same as D/d.

2. Influence of the relative draft D/d
   For all types discussed, an increase of relative draft resulted in a better wave attenuation performance. This is not surprising, since an increase of the draft causes more reflection. For deep water waves, the influence of relative draft becomes negligible for $D/L > 0.30$. Generally, the mooring forces will increase with increasing relative draft.

3. Influence of relative wavelength L/B
   A decrease of relative wave length resulted in a decrease of the transmission coefficient. In some cases however, resonance gave rise to an increase of C_t with decreasing L/B.

4. Influence of the wave steepness
   The transmission coefficient will decrease with increasing wave steepness. In case of the A-frame, an increase of C_t instead of a decrease may occur.

5. Influence of the stiffness of the structure
   The stiffer the structure, the more it will perform like a reflector, and the higher the mooring forces will be. On the other hand, a flexible structure is able to absorb energy, which, generally, will lead to relative small mooring forces. However, the absorption may induce large internal stresses.

6. Influence of breakwater motions
   The larger the breakwater motions, the more wave energy will be transmitted. The surge motion (i.e.

horizontal motion in the direction of the wave propagation) was found to be the major energy transmittor.

7. Influence of the mooring
The mooring system plays an important role in the wave attenuation performance, by the mooring stiffness and the damping due to the line. It is impossible to give a general tendency.

8. Energy extraction
Energy conversion facilities complicate the construction of a floating breakwater a lot, thereby increasing construction costs enormously.

Protected sites

The different types discussed in this report are all applicable for protected sites (e.g. harbors). Under these conditions, the scrap-tire floating breakwater is problably the cheapest way to obtain a certain level of protection. The tethered-float requires more space than the scrap-tire and is much more expensive (up to ten times more). The offset breakwater has a good wave attenuation performance, but will probably be more expensive than the scrap-tire breakwater. The pontoon floating breakwaters have the advantage that they can be used as walkway, storage, boatmooring, and fishing pier. The wave attenuation of the pontoon breakwater is mainly achieved by the draft of the construction (reflection) and the beam of the construction is not very important. The parabolic beach and sloping float breakwaters can achieve a good wave attenuation, but they are still not put in practice. It is difficult to judge their feasibility. A good counterpart of the scrap tire is the A-frame breakwater. The costs are higher, but the required space is less, and it can be transported easier.

Now we can distinguish three cases (for protected sites):

1. Only costs are important: the best choice is a scrap-tire floating breakwater.

2. Costs are important, but possibilities for multiple use (walkways, piers, etc.) are also important: take a pontoon floating breakwater.

3. The area of the floating breakwater has to be small, or ease of transport over long distance is important: the A-frame is a good choise.

Open sea conditions

To judge the feasibility of floating breakwaters under open sea conditions, some wave data of "Hutton Field" (approximately midway between the Shetland Islands and Norway) are used. Since long waves cause a major nuisance and since they determine the dimensions of the breakwater, one of the longest wave periods is used to give an estimate of the dimensions.

With a recurrence interval of one year, prediction of the largest significant wave height in a 3 hour storm was found to be 12m and the maximum wave height was found to be 22.8m. The predictions for the maximum wave periods reached from 13.5 to 17.1 seconds (with 95% reliability). The following values are used:

H = 20 m
T = 16 s
L = 400 m
d = 200 m (L/d = 2, H/L = 0.05)

Use is made of the C_t curves in this report, to predict the dimensions of the breakwaters.

Assumed is:
- linear extrapolation may be carried out
- influence of the bottom is negligible for d/L > 0.5, thus two breakwaters in two different water depths (both larger than L/2) will have the same wave attenuation performance. (See appendix B).

	C_t = 0.50	C_t = 0.30
Type of breakwater:	Draft * Beam [m]	Draft * Beam [m]
Pontoon	?	30 * 225
Double Module	18 * 175	26 * 160
Twin Cylinder	55 * 150	?
Perforated Horizontal Plate Breakwater	75 * 360	?
A-Frame	46 * 242	46 * 286
Offset Breakwater	105 * 185	120 * 200
Wave Blanket	? * 400	? * 800
Salter Duck		40 * 40 1)
Cockerell Raft	? *(400?) 2)	?
Scrap-Tire:		
Goodyear	0.7 * 384 3)	0.7 * 667 3)
Pipe-tire	0.66 * 217 3)	0.66 * 377 3)
Tethered float	40 * 800	40 * (1000?)

1) Rough estimation, see point 7, pp 117
2) The wave attenuation level is not known, see point 8, pp 118
3) See the remark at point 9, pp 118

Considering the predicted dimensions, the following conclusions may be drawn:

1. Resulting from the scale module tests, the pontoon and the double module are some of the smallest breakwaters, concerning draft and beam. One must not forget that the total height of the structure (bottom to top) is twice, at C_t=0.3, to three times the draft. Although the draft and the beam are relatively small, transportation will be difficult, due to the large water displacement.

2. The twin cylinder exists of two cylinders: in this case the cylinders must have a diameter of 55m. Thus the twin cylinder will be very expensive. Besides, this type attenuates only steep waves and waves with a short wave length.

3. The perforated horizontal plate breakwater is not suited for the described location, because this type of breakwater with dimensions of 75 * 360 meter is very expensive and is extremely difficult to transport.

4. The A-frame breakwater with a beam of 242m may be very difficult to construct, since the two cylinders with a distance of more than 200m must have a strong and rigid connection. Another difficulty is the depth of the vertical rigid board (46m). Although the shape of the cross-section of the A-frame gives rise to good transport features, the large draft and large beam make easy transport impossible. It may be possible to construct a "fold in" A-frame breakwater.

5. The offset breakwater must have the largest draft of all. It may be possible that a better combination of offset length to draft ratio exists, but in the tests discussed in this report, this ratio was constantly 1.36. To calculate the beam, it is assumed to be 1.3 times the offset length. The predicted dimensions of the offset breakwater are very disappointing The very low wave attenuation level of C_t=0.10, which was achieved during the tests, would require dimensions of D*B=150*260. It is obvious that the transportability is not good at all.

6. The wave attenuation of the wave-blanket was found to depend primarily on the relative breakwater width and the blanket thickness. Towing of the structure will be very impractical.

7. The Salter Duck is a wave converter with an efficiency of approximately 50% . It is suited for both small and large scale applications. The predicted dimensions are a rough estimation, based upon designs for wave periods of T=5, 7 and 9 seconds, having a diameter of 6,10 and 16m. A disadventage of this type is that this type is very sensitive to the wave direction. This property has a significant bearing on the design. Problems

arise in the realization of the large backbone which has to withstand large bending moments. The mooring of the duck is also a problem that needs further investigation.

8. The Hagen-Cockerell raft is also a directional device but in contradiction with the Salter Duck, this imposes no engineering problems in the design, but it does affect the efficiency!. The efficiency of the raft is comparable to that of the duck, but the associated mooring forces are smaller. Problems may arise with regard to the available mooring space, since the rafts have to be spaced at intervals of a halve wave length to obtain maximal efficiency.
After Newman (section 2.15.2), the Cockerell raft must have a length of 400m in the direction of the wave propagation and about 60m parallel to the wave crests. The Cockerell rafts must have a distanceof 200m to each other. The wave attenuation was not predicted.
After Haren and Mei (section 2.15.4), the raft, having an efficiency of 89% (thus C_t<0.11), would have a length of 6400m.
More information about the wave attenuation perfomance is required.

9. Scrap-tire breakwaters have the smallest draft of all. It must be remarked that the extrapolation of the dimensions is not completely justified. The construction will be relatively thinner than the model, which will result in a higher C_t-value. On the other hand, the wave energy loss by turbulence per wave length is larger (more tires per wave length), this will result in a lower C_t-value. We do not know which effect will dominate. The required force for floating transport will be enormous because of the turbulence. For transport on barges the large sizes are a problem. Roll up seems to require a too large diameter.

10. The tethered-float breakwater was developed for deep water, but the required space is larger than for the scrap-tire, which will give problems with transport. A "floating-anchor" can make transport easier (floating-anchor = construction for attachement of the tethers). Starting from $\varnothing$=0.025L, the floats must have a diameter of 10m. The costs for the tethered float breakwater are relatively high.

Some points which need **further investigation**:

1. Possibilities to transport a scrap-tire breakwater, its wave attenuation performance under open sea conditions, and the magnitude of the forces needed for transport.

2. Possibilities of A-frame breakwaters with special modifications so that the draft can be restricted to, say 10 m. Magnitude of mooring forces, and forces needed for transport.

3. The relation between wave attenuation performance, and properties of a flexible membrane (beam, mass, height, bending modulus, tension modulus), the mooring characteristics, and the wave conditions (wave length, water depth, wave period, water depth).

BIBLIOGRAPHY

1. Adee, Bruce H., Operational Experience with Floating Breakwaters Marine Technology, Vol. 14, No. 4, Oct. 1977, pp. 379-386.

2. Adee, B.H./ Richey, A.P./ Christensen, D.R., Floating Breakwater Field Assesment Program, Friday Harbour, Washington. TP 76-17, U.S. Army, Corps of Engineers, Coastal Engineering Research Center, Fort Belvoir, Va., Oct. 1976.

3. Adee, B.H./ Martin, W., Thecretical Analysis of Floating Breakwater Performance. Proceedings of the Floating Breakwater Conference, University of Rhode Island, Kingston, R.I., 1974, pp. 21-40.

4. Arunacham, V.M./ Raman, H., Experimental Studies on a Perforated Horizontal Floating Breakwater. Ocean Engineering, 1982, pp. 35-45.

5. Baird, Andrew V./ Ross, Neil W., Field Experiences with Floating Breakwaters in the Eastern United States. MR 82-4, U.S. Army, Corps of Engineers, Coastal Engineering Research Center, July 1982.

6. Bishop, C.T., Floating Breakwater Design Comparison. Proceedings ASCE, Journal of the Waterway, Port, Coastal, and Ocean Division, Vol. 108, No WW3, Aug. 1981, pp. 421-426.

7. Candle, R.D., Goodyear Scrap Tire Floating Breakwater Concepts. Proceedings of the Floating Breakwater Conference, University of Rhode Island, Kingston, R.I., 1974, pp. 193-212.

8. Christensen, D.R./ Richey, E.P., Prototype Performance Characteristics of a Floating Breakwater. Proceedings of the Floating Breakwater Conference, University of Rhode Island, Kingston, R.I., 1974, pp. 159-180.

9. Dawson, J.K. (Energy Technology Support Unit), Wave Energy. Department of Energy (U.K.), Energy Paper Number 42, Londen, 1979.

10. Farley, F.J.M., Porpoise, the Buckling Resonant Raft. Second International Symposium Wave and Tidal Energy, Cambridge, Cranfield, BHRA Fluid Engineering, Sept. 1981, pp. 371-383.

11. Farley, F.J.M., Wave Energy Conversion by Flexible Resonant Rafts. Applied Ocean Research, Vol. 4, No 1, Jan. 1982, pp. 57-63.

12. Giles, Micheal L./ Sorensen, Robert M., Prototype Scale Mooring Load and Transmission Tests for a Floating Breakwater. TP 78-3, U.S. Army, Corps of Engineers, Coastal Engineering Research Center, April 1978.

13. Hales, Lyndell Z., Floating Breakwaters: State-of-the-Art. TR 81-1. U.S. Army, Corps of Engineers, Coastal Engineering Research Center, Oct. 1981.

14. Haren, Pierre/ Mei, Chiang C., An Array of Hagen-Cockerell Wave Power Absorbers in Head Seas. Applied Ocean Research, Vol. 4, No 1, Jan.1982, pp. 51-56.

15. Haren, Pierre/ Mei, Chiang C., Wave Power Extraction by a Train of Rafts: Hydrodynamic Theory and Optimum Design. Applied Ocean Research, Vol. 1, No. 3, 1979, pp. 147-157.

16. Harms, Volker W./ Westerink, Joannes J./ Sorensen, Robert M./ McTamany, James E., Wave Transmission and Mooring Force Characteristics of Pipe-Tire Floating Breakwater. TP 82-4, U.S. Army, Corps of Engineers, Coastal Engineering Research Center. 1982.

17. Harms, Volker W., Design Criteria for Floating Tire Breakwater. Journal of the Waterway, Port, Coastal, and Ocean Division, Vol. 105, No WW2, May 1979, pp. 149-170.

18. Harms, Volker W., Design Criteria for Floating Tire Breakwater. Journal of the Waterway, Port, Coastal, and Ocean Division, Vol. 107, No WW1, Febr. 1981, pp. 29-44 (disc.)

19. Harms, Volker W., Design Criteria for Floating Tire Breakwater. Journal of the Waterway, Port, Coastal, and Ocean Division, Vol. 107, No WW1, May 1980, pp. 296 (disc.)

20. Harms, Volker W., Floating Breakwater Performance Comparison. Lawrence Berkeley Performance Laboratory, University of California, Coastal Engineering, Vol. III, 1980, pp. 2137-2158.

21. Ippen, A.T., Estuary and Coastline Hydrodynamics. New York, Mc Graw-Hill, 1966.

22. Kickert, O., Inleiding Elektrische Energietechniek. Studiecommissie van de Electrotechnische Vereniging, 1980.

23. Kowalski, T., Scrap Tire Floating Breakwaters. Proceedings of the Floating Breakwater Conference, University of Rhode Island, Kingston, R.I., 1974, pp. 233-246.

24. Kobayashi, Kakuji/ Masuda, Yoshio, Wave Absorbing Effect of Net Type Movable Wave Absorber. Third International Ocean Development Conference, Tokyo, Aug. 1975.

25. Mei, C.C./ Newman, J.N., Wave Power Extraction by Floating Bodies. Proceedings First Symposium on Wave Energy Utilization, Gothenburg, Oct. 1979, Gothenburg, Chalmers University of Technology, 1979, pp. 36-76.

26. Miller, D.S., Materials and Construction Techniques for Floating Breakwaters. Proceedings of the Floating Breakwater Conference, University of Rhode Island, Kingston, R.I., 1974, pp. 247-262.

27. Miller, D.S., Practical Applications of Floating Breakwaters for Small Craft Harbors. Proceedings of the Floating Breakwater Conference, University of Rhode Island, Kingston, R.I., 1974, pp. 263-278.

28. Moore, Walter L./ Daily, James E. (University of Texas at Austin). A Stable Offshore Work Barge Using the Offset reflecting surface principle. Third International Ocean Development Conference, Tokyo, Aug. 1975.

29. Newman, J.N., Absorption of Wave Energy by Elongated Bodies. Applied Ocean Research, Vol. 1, No. 4, 1979, pp. 189-196.

30. Noyes, Robert, Offshore and Underground Power Plants. Noyes Data Corporation, New Jersey, U.S.A., 1977.

31. Ofuya, A.O., On Floating Breakwaters. Research Report No. CE-60, Queen's University, Kingston, Ontario, Canada, Nov. 1968.

32. Raichlen, F./ Lee, J.J., The Behavior of an Inclined Pontoon Breakwater. Report No. N62583/78M R552, U.S. Navy c.e.l., May 1978.

33. Richey, E.P., Floating Breakwater Field Experience, West Coast. MR 82-4, U.S. Army, Corps of Engineers, Coastal Engineering Research Center, July 1982.

34. Richey, E.P./ Nece, R.E., Floating Breakwaters: State-of-the-Art. Proceedings of the Floating Breakwater Conference, University of Rhode Island, Kingston, R.I., 1974, pp. 1-20.

35. Science Policy Research Division, Congressional Service, Library of Congress. Energy from the Ocean. U.S. Government Printing Office, Washington, 1978.

36. Sethness, E.D., Jr./ Moore, W.L., The Performance of an Offset Breakwater Configuration in Wind-Generated Waves. Technical Report HYD-18-7301, University of Texas, Austin, Tex., Feb. 1973.

37. Sethness, E.D., Jr./Moore, W.L./Sabathier, E., The performance of an Offset Breakwater Configuration in Wind-Generated Waves. Proceedings of the Floating Breakwater Conference, University of Rhode Island, Kingston, R.I., 1974, pp. 73-90.

38. Seymour, R.J., Tethered Float Breakwaters. Proceedings of the Floating Breakwater Conference, University of Rhode Island, Kingston, R.I., 1974, pp. 55-72.

39. Stoker, J.J., Water Waves. New York, Interscience Publishers, 1966.

40. Sutko, A.A./ Haden, E.L., The Effect of Surge, Heave, and Pitch on the Peformance of a floating Breakwater. Proceedings of the Floating Breakwater Conference, University of Rhode Island, Kingston, R.I., 1974, pp. 41-54.

41. Wiegel, R.L., Transmission of Waves Past a Rigid Vertical Thin Barrier. Journal of the Waterway, Harbours, and Coastal Engineering Division, Vol. 86, No. WW1, Part 1, Mar. 1960, pp. 1-12.

42. Wiegel, R.L., Oceanographical Engineering. Prentice-Hall, Inc., Englewood Clifs, N.J., 1964.

43. Yamashita, Shigeji/ Nakayama, Yoshifumi. (Toray Industries, Inc.). Development on Plastic Floating Breakwater. "Wave and Wind Directionality" International Conference, Paris, Sept./Oct. 1981.

Appendix A

SUMMARY OF WAVE POWERED GENERATORS BUILD AND TESTED THROUGH OCTOBER 1974.

WAVE POWERED GENERATORS - SUMMARY OF DEVICES BUILT AND TESTED UP TO OCTOBER 1974 [1]

	Year	System	Power	Location	Organisation / individual } concerned	Remarks
1	1910	Vertical bore hole in cliff oscillations in water level driving an air turbine	1 kW	Royan, nr Bordeaux, France	M Bochaux-Praceique	Supplied entire power and light for dwelling house
2	1911	Pier structure with floats using both vertical and horizontal motion	110 kW	Young's 'Million Dollar' Pier, Atlantic City, New Jersey, USA	US Wave Power Company	Power level claimed, but not substantiated on investigation
3	1920	Float system operating in a basin connected to sea	n.a.	Algiers, N Africa	M Fusenot	Feeble power level
4	1926	Not identified		Minou lighthouse, Brest, France	M Coyne	Discouraging results
5	Pre 1931	Savonius rotor	n.a.	Baltic Sea	J Savonius	Limited trials
6	Pre 1931	Savonius rotor operating pump	up to 7 kW	Musee Oceanographique Monaco	M Richards	Rotor driving double acting pumps lifting water to a height of 200 ft
7	1931	Heavy float rising and falling to operate pump		Musée Oceanographique Monaco	F Catlancao	Operated 10 years pumping water destroyed by heavy seas

n.a. = not available.

[1] J. M. Leishman and G. Scobie. The development of wave power: a techno-economic study. United Kingdom Department of Industry. National Engineering Laboratory. East Kilbride, Glasgow, Scotland. Report No. EAU M25. 1976. pp. 73-77.

A-2

	Year	System	Power	Location	Organisation / individual } concerned	Remarks
8	Pre 1944	Converging channels supplying a fore bay for a low head station	n.a.	i Pointe Pescade ii Sidi Ferruch Algeria	i Societe Mediterraneenne d'Energie Marine ii Societe Marocaine d'Etudes de la Houle et du Vent	Qualatative study with encouraging results
9	1944	Model of above	n.a.	-	Laboratoire Dauphinois Hydraulique	Technically successful concept but not economically viable
10	1947	Three float system	200 W	Japan	Y Masuda, Oceanographic Unit, Japanese Maritime Self-Defence Unit	Tests abandoned after device overturned by high wave.
11	1957-59	Hydraulic system	1 kW	Japan	Y Masuda	Test failed
12	1960-63	Air turbine-fixed system	500 W	i Kannonzaki, nr Yokosuka harbour, Japan ii Institute test tank	Masuda supported by R & D HQ of Japan Defence Agency	
13	1962	Submerged buoy with diaphragm activated generator	0.25 W	Buzzard's Bay, Massachusetts	AVCO Corporation (RAD) Division	Tests carried in sheltered location with no effective swell. Diaphragm ruptured in hurricane

n.a. = not available.

	Year	System	Power	Location	Organisation / individual concerned	Remarks
14	1963	Air turbine system in fixed pipe	n.a.	Nakaminato Rock, Pacific Ocean, Japan	Y Masuda supported by R & D HQ of Japan Defence Agency	Test safety of fixed air-turbine system in high waves
15	1963-65	Pendulum-type buoy	2-3 W	Japan	Nichiro Kogyo Kaisha Ltd Ryokuseisha Corporation funded by Foundation New Technique Development Corporation	Based on a suggestion and research of Y Masuda, was developed as a navigation buoy. Rejected because of sway effect on light
16	1964	'Ocean motion harness' operating on principle of self winding watch	n.a.	USA	Hamilton Watch Company Industrial and Military Products Division	Prototype weight 1 lb 3 in dia x 3 in high
17	1965-present	Air-turbine buoys	100 W	Japan, USA, UK	Invented by Y Masuda Patented and manufactured by Ryokuseisha Corporation UK agents: Sumitomi Shaji Kaisha Ltd	Over 300 buoys now in operation off Japan, USA, Canada, Persian Gulf, and British Isles, Tested by Irish Lights 1970
18	1966	Air turbine fixed system adapted to power lighthouse		Ashika-Jima Lighthouse, Tokyo Bay, Japan	Customers: Japan Maritime Safety Board Suppliers: Ryokuseisha	
19	1967	Wave-powered device to move sand	n.a.	USA	Coastal Engineering Research Centre	Device found to be unsatisfactory
20	1970	Air turbine generator	500 W	Expo 1970, Osaka, Japan	Y Masuda	

n.a. = not available.

	Year	System	Power	Location	Organisation / individual concerned	Remarks
21	1970	Hydraulic pumping over pliable strips in concrete trough	n.a.	USA	Power Systems Company, Boston, Mass, USA	Small scale tests successfully made
22	1970	Bobbing buoy with direct generation of electricity from linear generator	Less than 1 W	UK exhibited at 1970 Lighthouse Conference	Invented and patented by University College of N Wales.	Manufacturers dropped development after tests gave very low output
23	1971-2	Investigation of new construction method for air-turbine fixed method	n.a.	Japan	Y Masuda. Japan Electric Machine Association	
24	1970 - present	Wave pump device fitted to ship R V Ellen B Scripps	60 W (no turbine)	Tested off Point Conception, California, USA	i David Castell/Scripps Institute of Oceanography, La Jolla, California, USA ii Glosten Associates	First experiment July 1972 terminated because of pipe failure. Latest experiment reported July 1973 plagued by calm seas
25	1972 - present	Float with propellors on shaft	n.a.	Sweden	Fagersta A B, Sweden M Gustaffson, K J Loqvist	Experiments carried out on ½-m dia float
26	1973 - present	Oscillating vane device	Model	UK	S Salter, Department of Mechanical Engineering, Edinburgh University	Model tests have shown that 90 per cent conversion efficiency is possible
27	1973 - 1974	Model wave energy converter		USA	A D Little Inc. Test under contract for US firm	Device found to be of low efficiency

n.a. = not available.

	Year	System	Power	Location	Organisation / Individual concerned	Remarks	Ref
28	1974	Float with impeller on shaft	n.a.	UK	National Physical Laboratory	Subject of patent application through NRDC	-
29	1974	Various float devices	n.a.	UK	Wave Power Ltd		-
30	1972-present	Autobailer wave-powered bilge pump	0.025 gal/min	Sweden	Imported by Yachtex, Westcliffe-on-Sea	Commercially available	100

n.a. = not available.

Appendix B

INFLUENCE OF WATER DEPTH IN DEEP WATER

With the formula of Ippen (formula 2.22), which describes the kinetic energy distribution as a function of water depth, the influence of the water depth on the kinetic energy distribution in the upper 40m (influence area of floating breakwaters) is investigated:

d	% kin. energy in upper 40m	
45 m	100 %	
75	91.8	
100	72.1	-------
200	71.5	|L=400 m|
300	71.5	-------
500	71.5	
1000	71.5	

As can be seen in the table, the absolute water depth is unimportant for the kinetic energy distribution if d/L>0.5 (deep water). So the information "deep water" is sufficient to estimate the kinetic energy distribution in the area influenced by the breakwater. Then, the water depth will not effect the wave attenuation performance.